

**UNIVERSITY OF SOUTHAMPTON**

Faculty of Engineering and Physical **Science**  
School of Electronics and Computer Science

# **Energy Budgeting for Intermittently-Powered Systems**

*by*

**Jie Zhan**

*A thesis for the degree of  
Doctor of Philosophy*

December 2021



University of Southampton

Abstract

Faculty of Engineering and Physical Science  
School of Electronics and Computer Science

Doctor of Philosophy


**Energy Budgeting for Intermittently-Powered Systems**

by Jie Zhan


Abstract to be done



# Contents

<b>List of Figures</b>	<b>ix</b>
<b>List of Tables</b>	<b>xi</b>
<b>Declaration of Authorship</b>	<b>xiii</b>
<b>Acknowledgements</b>	<b>xv</b>
<b>1 Introduction</b>	<b>1</b>
1.1 Energy-Harvesting Intermittently-Powered Systems . . . . .	2
 1.1.1 Applications of Energy-Harvesting IPSs . . . . .	4
1.2 Research Justification . . . . .	7
1.3 Research Questions . . . . .	8
1.4 Research Contributions . . . . .	9
1.5 Publications . . . . .	9
1.6 Thesis Structure . . . . .	10
<b>2 Energy-Harvesting Intermittent Systems</b>	<b>11</b>
2.1 Energy Harvesting Techniques . . . . .	11
2.1.1 Light Energy Harvesting . . . . .	12
2.1.2 Radio Frequency Energy Harvesting . . . . .	15
2.1.3 Flow Energy Harvesting . . . . .	15
2.2 Energy Storage for Sensor Nodes . . . . .	16
2.2.1 Rechargeable Batteries . . . . .	17
2.2.2 Capacitors . . . . .	18
2.2.3 Discussion . . . . .	19
2.3 Energy-Neutral Computing . . . . .	20
2.4 Intermittent Computing . . . . .	22
2.4.1 Checkpointing IC . . . . .	22
2.4.2 Reactive IC . . . . .	24
2.4.3 Harvest-Store-Use IC . . . . .	26
2.4.4 Task-based IC . . . . .	27
2.4.5 Non-Volatile Processors . . . . .	28
2.5 Power-Neutral Computing . . . . .	29
2.5.1 Principles of Operations . . . . .	29
2.5.2 Recent Approaches . . . . .	30
2.6 Summary . . . . .	32

<b>3</b>	<b>Effect of Energy Storage Sizing on IPS Performance</b>	<b>35</b>
3.1	Reactive IPS Modelling . . . . .	36
3.1.1	Operating Modes of Reactive IPS . . . . .	37
3.1.2	Formulating Forward Progress . . . . .	38
3.1.3	Dynamic process . . . . .	40
3.2	Exploration of Energy Storage Sizing . . . . .	40
3.2.1	Model Configuration . . . . .	41
3.2.1.1	Energy Storage . . . . .	41
3.2.1.2	Intermittent Computing Load . . . . .	41
3.2.2	Sizing Energy Storage to Improve Forward Progress . . . . .	42
3.2.2.1	Impact of Supply Current . . . . .	42
3.2.2.2	Impact of Volatile State Size . . . . .	44
3.3	Experimental Validation . . . . .	46
3.3.1	Experiment Setup . . . . .	46
3.3.2	Model Validation . . . . .	46
3.3.3	Validation of Sizing Effects . . . . .	48
3.4	Summary . . . . .	48
<b>4</b>	<b>Energy Storage Sizing Approach for Deploying IPSs</b>	<b>49</b>
4.1	Related Work . . . . .	50
4.2	Energy Storage Sizing Approach . . . . .	51
4.2.1	Input . . . . .	51
4.2.2	System Model . . . . .	51
4.2.3	Trade-off . . . . .	53
4.3	Sizing under Real-World Energy Conditions . . . . .	53
4.3.1	Simulation Configuration . . . . .	53
4.3.2	Exploration with Real-World Energy Source Conditions . . . . .	54
4.3.2.1	Sizing the Energy Harvester . . . . .	54
4.3.2.2	Sizing the Energy Storage . . . . .	55
4.3.2.3	Interruption Period . . . . .	55
4.3.3	Trading Forward Progress, Dimensions, and Interruption Period . . . . .	57
4.3.3.1	Metric of Dimensions . . . . .	57
4.3.3.2	Metric of Interruption Periods . . . . .	58
4.3.3.3	Cost Function . . . . .	58
4.3.3.4	Results . . . . .	59
4.4	Summary . . . . .	61
<b>5</b>	<b>Runtime Energy Profiling and Adaptation for IPSs</b>	<b>63</b>
5.1	Related Work . . . . .	65
5.2	Design Exploration . . . . .	66
5.2.1	Variability in Intermittent Systems . . . . .	66
5.2.1.1	Variable Data Sizes . . . . .	66
5.2.1.2	Variability in Peripheral Configurations . . . . .	67
5.2.1.3	Device Variability . . . . .	67
5.2.1.4	Capacitor Ageing and Tolerance . . . . .	68
5.2.2	Performance Improvement with Adaptive Thresholds . . . . .	68
5.2.2.1	Power Analysis . . . . .	68

5.2.2.2	Runtime Control Models . . . . .	69
5.2.2.3	Simulation Setup . . . . .	70
5.2.2.4	Results . . . . .	70
5.3	OPTIC Runtime Energy Profiling . . . . .	73
5.3.1	A disconnecting-supply approach . . . . .	73
5.3.2	Principles . . . . .	74
5.3.3	Minimising and Compensating Theoretical Profiling Error . . . .	76
5.3.4	Effect of Volatile Supply Current . . . . .	76
5.4	OPTIC Runtime Energy Adaptation . . . . .	77
5.4.1	Adaptation Routine . . . . .	78
5.4.2	Linear Adaptation . . . . .	80
5.5	Implementation . . . . .	81
5.5.1	External Voltage Monitor . . . . .	82
5.5.2	Software . . . . .	83
5.6	Experimental Evaluation . . . . .	83
5.6.1	Experimental Setup and Benchmarks . . . . .	83
5.6.2	Profiling Accuracy . . . . .	84
5.6.3	Reliability with Dynamic Energy Consumption . . . . .	85
5.6.3.1	Changing once . . . . .	85
5.6.3.2	Changing infrequently . . . . .	86
5.6.3.3	Changing frequently . . . . .	88
5.7	Summary . . . . .	89
<b>6</b>	<b>Conclusions and Future Work</b>	<b>91</b>
6.1	Future Work . . . . .	93
	<b>References</b>	<b>95</b>





# List of Figures

1.1	A conceptual architecture of an IPS. . . . .	4
1.2	Application Suitability of Energy-Harvesting IPSs. . . . .	5
2.1	Typical current-voltage curve of a solar module (monocrystalline, adapted from [40]) . . . . .	13
2.2	Daily global horizontal solar energy available in Los Angeles 2012-2014 [47].	14
2.3	One-day dynamics of global horizontal solar irradiance in Los Angeles 29 April 2016 [48]. . . . .	14
2.4	Dynamics of a micro wind harvester (reproduced from [53]). . . . .	16
2.5	Voltage trace with hibernation and restoration points in Hibernus (taken from [34]). . . . .	25
2.6	Harvest-Store-Use execution (taken from [75]). . . . .	26
2.7	Memory architectures of traditional processors and NVPs (taken from [79]).	28
2.8	Architecture of an example power neutral system based on TI MSP430FR platform (taken from [53]). . . . .	31
2.9	Board power consumption of ODROID XU4 vs operating frequency and core configurations, running CPU intensive application Raytrace (taken from [87]). . . . .	32
3.1	Operating modes of reactive IPSs, and achieved forward progress against supply current. . . . .	37
3.2	Operating cycles in the <i>Intermittent</i> mode. . . . .	38
3.3	Forward progress against energy storage capacitance at different levels of constant supply current. Error bars around $C_{\alpha\_max}$ denote the impact of typical $\pm 20\%$ capacitance tolerance. The 30–150 $\mu\text{F}$ range is omitted as forward progress in that range increases monotonically. . . . .	43
3.4	Maximum forward progress improvement by sizing energy storage given a spectrum of supply current (normalised by the minimum capacitance case), with the corresponding capacitance for maximum and sub-maximum (95% of maximum) forward progress improvement. . . . .	44
3.5	Impact of RAM usage (linear to restore/save overheads) on sizing energy storage with 0.4 mA current supply. Improvement and reduction are normalised by the minimum capacitance case. . . . .	45
3.6	Model validation with experimental and modelled forward progress. .	47
3.7	The relationship between energy storage capacitance and IPS forward progress, for various supply currents. . . . .	47
4.1	Structure of the proposed system model and sizing approach. . . . .	52
4.2	System model of a PV-based IPS. . . . .	53

4.3	Improvement of average forward progress by sizing energy storage given different PV panel areas under real-world energy source conditions. The model is able to find the PV panel area required for achieving the target mean forward progress. . . . .	56
4.4	Time percentiles of forward progress by sizing energy storage with target $\alpha_{\text{exe}} = 0.1$ and the corresponding PV panel area listed in Figure 4.3. The percentiles start from the 60th as the system is off for around 55 % of time due to insufficient energy source. . . . .	57
4.5	Distribution of interruption periods. . . . .	58
4.6	Tantalum capacitor volume against capacitance for the six series of capacitors analysed. . . . .	59
4.7	The sizing approach trades off forward progress, capacitor volume, and interruption periods. The results are plotted against a range of PV panel area, given Denver 2018 energy source dataset. . . . .	60
5.1	$\Delta V_{\text{task}}$ varying linearly with the data size in AES 128-bit encryption. . . .	67
5.2	An I-V curve of a glass-type amorphous PV panel (Sanyo AM-1417CA, 35 mm $\times$ 13.9 mm) under a white LED lighting condition. . . . .	69
5.3	Numbers of completed and failed operations of DEBS Low, Samoyed, DEBS High, and Adaptive given random data sizes and configurations and a PV supply in a 10 s simulation. . . . .	71
5.4	An instance of supply voltage traces in simulation. . . . .	72
5.5	Number of completed operations of Samoyed, DEBS High, and the Adaptive scheme with capacitance reduction. . . . .	72
5.6	Experimental schematic. . . . .	74
5.7	An illustrative supply voltage trace for explaining OPTIC's runtime energy profiling method. . . . .	75
5.8	Flowchart of OPTIC's runtime energy adaptation routine. The blue blocks represent a configurable control logic to decide when to perform energy profiling. The dashed purple blocks are only run when the profiling is enabled, and represent OPTIC's energy profiling with the last block updating $V_{\text{th}}$ with the new $\Delta V_{\text{task}}$ . . . . .	79
5.9	OPTIC system schematic. . . . .	81
5.10	Error Distribution of OPTIC's Runtime Energy Profiling given a PV supply, compared to the "Naive" disconnecting-supply method. . . . .	84
5.11	A voltage trace of OPTIC adapting to a new operation on a new device. . . . .	86
5.12	Effect of Capacitor Degradation on OPTIC and DEBS. . . . .	87
5.13	Relative Completion Rates of Samoyed, DEBS, and OPTIC with variable data sizes and a PV supply. . . . .	88

# List of Tables

2.1	Classification of energy sources and energy harvesters in IoT. . . . .	12
2.2	Comparison between commercial NiMH and Li-ion rechargeable batteries. . . . .	18
3.1	Model parameters of reactive IPS . . . . .	36
3.2	Profiled MCU parameters . . . . .	42
3.3	Linear scaling range of volatile state size and restore/save time overheads . . . . .	45
4.1	PV cell properties under a 1000 W/cm <sup>2</sup> , AM-1.5 light source . . . . .	54
5.1	$\Delta V_{\text{task}}$ Varying with Configurations in AES 4KB Encryption . . . . .	67
5.2	$\Delta V_{\text{task}}$ Varying among Devices in AES 128-bit 4KB Encryption . . . . .	68
5.3	Definitions of Mathematical Symbols . . . . .	74



## Declaration of Authorship

I declare that this thesis and the work presented in it is my own and has been generated by me as the result of my own original research.

I confirm that:

1. This work was done wholly or mainly while in candidature for a research degree at this University;
2. Where any part of this thesis has previously been submitted for a degree or any other qualification at this University or any other institution, this has been clearly stated;
3. Where I have consulted the published work of others, this is always clearly attributed;
4. Where I have quoted from the work of others, the source is always given. With the exception of such quotations, this thesis is entirely my own work;
5. I have acknowledged all main sources of help;
6. Where the thesis is based on work done by myself jointly with others, I have made clear exactly what was done by others and what I have contributed myself;
7. Parts of this work have been published as:  
 Jie Zhan, Geoff V. Merrett, and Alex S. Weddell. Exploring the effect of energy storage sizing on intermittent computing system performance. *IEEE Transactions on Computer-Aided Design of Integrated Circuits and Systems*, pages 1–10, 2021  
 Jie Zhan, Alex S. Weddell, and Geoff V. Merrett. Adaptive energy budgeting for atomic operations in intermittently-powered systems. In *Proceedings of the 8th International Workshop on Energy Harvesting and Energy-Neutral Sensing Systems*, ENSys '20, page 82–83, New York, NY, USA, 2020. Association for Computing Machinery

Signed:.....

Date:.....



## **Acknowledgements**

Thanks to ...





*To ...*



# Chapter 1

## Introduction

The promising expansion of the Internet of Things (IoT) has drawn research interests on new design paradigms for deploying tens of billions of electronic devices over a wide geographical range and probably in hard-to-reach places [3, 4]. Such a scenario generates considerations on how to enable the devices in networks to operate independently and effectively and how to construct a long-life, maintenance-free, environmentally friendly, and low-cost IoT.

One of the most significant concerns in deploying IoT devices is how to power numerous low-power devices (tens of billions expected [3, 5, 6]). Traditional wired electricity limits flexibility of deployment and involve expensive wiring costs [7]. Traditional primary batteries (i.e. non-rechargeable batteries) are not suitable for such a large number of devices. A widespread use of primary batteries can cause tedious work of battery replacement due to the limited battery lifetime, and also pose pollution concerns as these batteries are typically made of non-disposable heavy-metal materials [Reference needed]. Therefore, it is necessary to find an alternative powering solution.

A potential power alternative is energy harvesters. Energy harvesters scavenge energy from environmental sources (e.g. solar irradiation, wind flow, radio frequency (RF) signals, and kinetic energy) [8].

Some more information on energy harvesters? e.g. a table of power density of common energy harvesting sources.

Devices powered by energy harvesters can get rid of power wires and surpass the lifetime limit of primary batteries, enabling a scalable IoT. However, the power generated by energy harvesters in real-world deployment is variable, uncontrollable, and in many cases insufficient for continuous workload operation [9]. Hence, directly using energy harvesters as the power supply without energy buffering may cause a device to keep booting up and shutting down, making little application progress.

Initially, large energy storage, in forms of rechargeable batteries (also known as secondary batteries) or supercapacitors, is allocated with energy harvesters to buffer the temporal variations of energy input and provide reliable power supply. Motivated by such a scenario, energy-neutral (EN) operation was proposed to balance energy input and energy consumption so as to prevent a system from power failures [10]. EN operation intends to sustain systems over a long period of time (e.g. a few days [11] or a year [12]) by adapting system runtime schedules (e.g. duty cycles [11–13] or task schedules [14, 15]) according to the available energy amount.

Rechargeable batteries and supercapacitors are two main choices of energy storage in EN operation. Rechargeable batteries are historically used as energy storage in energy harvesting embedded systems because of their high energy density [16] and stable discharging profile [10]. However, due to electrolyte deterioration, the limited charge-discharge cycles of rechargeable batteries constrain the operating lifetime, causing heavy battery replacement work as well as environmental issues as primary batteries do [17]. To alleviate the problems of rechargeable batteries, supercapacitors are then explored in research. Although the energy density of supercapacitors is several orders of magnitude lower than the energy density of batteries [18], supercapacitors outperform rechargeable batteries in terms of lifetime (e.g. up to 10-20 years for supercapacitors compared to 3-5 years for rechargeable batteries [19]). However, to achieve a comparable energy capacity as batteries, supercapacitors should be designed to tens of farads or one hundred farads [20, 21]. Supercapacitors in such a scale occupy large volume in contrast to small IoT devices.

Numbers?

## 1.1 Energy-Harvesting Intermittently-Powered Systems

To circumvent the lifetime, pollution, and volume problems in rechargeable batteries and supercapacitors, a research trend in energy-harvesting sensor nodes moved towards eliminating the demand for energy storage and adopting only a minimum amount of energy storage, where the energy storage is only enough for ensuring the most energy-expensive atomic operation<sup>1</sup>, typically in the form of a  $\mu\text{F}$ -level capacitor.

Capacitors have longer lifetime, smaller volume, blabla... Reference for lifetime of electrolytic capacitors. Seems a bit contradictory to contribution 3.

<sup>1</sup>In this context, an operation is atomic if it should be completed in one consecutive period without power interrupts; otherwise, if interrupted, it should be re-executed from the beginning. Example atomic operations in IoT devices can be peripheral operations and nonvolatile memory read/write operations.

Despite the benefits of small capacitors over batteries and supercapacitors, they considerably limit the buffering capacity for varying harvested power. Thus, the variable harvesting power is almost directly connected to the load, e.g. with only a decoupling capacitor. This violates the demand for stable power supply in conventional computing systems. Without any modifications, a conventional system can only work when input power is higher than system power consumption (which is rare for an energy-harvesting supply), and cannot boot up when input power is lower than system power consumption. Hence, it becomes a major concern that how to guarantee forward execution and functionality of such systems with only minimum energy storage.

Ensuring and improving local processing ability of sensor nodes is crucial for a few reasons. First, to reduce network traffic volume and energy consumption, sensor nodes should be able to process sensing data on-site and transmit only the useful information, typically when the number of sensor nodes increases in orders of magnitude [6]. Second, advanced communications techniques, such as scheduling, routing, coding, and decoding, require local computing ability to ensure timeliness and efficiency in networking [22]. Third, IoT devices are also expected to be able to trigger actions in reaction to the physical world by either receiving commands from other nodes and servers or making a decision based on locally acquired data [23].

Need many citations in the next paragraph.

With an energy-harvesting supply and small energy buffering capacitance, a system is powered up *intermittently* once a small amount of energy is accumulated in the capacitor. The system has to utilise these intermittent power-on cycles to make application progress. To this end, many approaches for energy-harvesting Intermittently-Powered Systems (IPS) have been proposed in the past few years. The majority of these approaches have been addressing how to sustain computational progress throughout intermittent power-on cycles by correctly and efficiently saving and restoring volatile computing state. The volatile computing state includes CPU registers, Static RAM (SRAM) data, and perhaps peripheral configurations and data, i.e. the volatile part that cannot sustain after a power failure. The volatile state is saved into and restored from non-volatile memory (NVM), where most published approaches use Ferroelectric RAM (FRAM). According to the style of saving and restoring state, approaches in IPSs can be categorised as *proactive* and *reactive*. Proactive approaches save and restore state at design-time or compile-time defined points, whilst reactive approaches do that upon an imminent power failure when supply falls below a low threshold ( $V_{cc} < V_L$ ). Details of these approaches are illustrated in Chapter 2.

A bit unnecessary to show the details of Harvester and Source in Figure 1.

A conceptual architecture of an typical energy-harvesting IPS is shown in Figure 1.1. The power frontend is an energy harvester, which transduces an ambient energy source

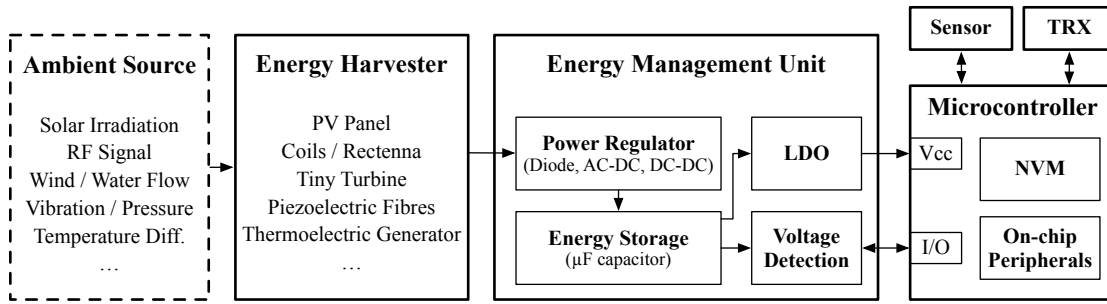


FIGURE 1.1: A conceptual architecture of an IPS.

into electric power. Then, a power regulator converts the harvested power to a suitable voltage that charges up the energy storage. The type of the power regulator depends on the pattern of the power input, which can be an AC-DC converter for AC input (e.g. a rectenna), or a DC-DC converter or a diode for DC input (e.g. a PV panel). The energy storage is in the form of a  $\mu\text{F}$ -level capacitor, which buffers a small amount of energy for the load to operate intermittently in short active cycles. The power given to the load is usually conditioned through a low-dropout regulator (LDO) to lower down supply voltage, and hence current consumption. IPSs are usually equipped with a voltage detection circuit so as to wake up or power up the load when the voltage of the energy storage reaches a threshold. In IPSs, the load is typically a microcontroller (MCU) with NVM to sustain computing state, and with many on-chip or external peripherals, e.g. sensors and wireless transceivers (TRX).

### 1.1.1 Applications of Energy-Harvesting IPSs

This part intends to illustrate the key performance metric of IPSs through example applications, but it doesn't seem to directly make the point yet.

An inherent limitation of IPSs is that the system can only execute when there is available power, as opposed to an EN system where it can still executes with buffered energy if ambient power is not available. This limitation thereby indicates that *application operation periods and power availability should be compatible in time*. While there are various needs of operation periods for various application scenarios, the power availability is constrained and determined by the availability of the target energy source in the deployed environment. Hence, the applications of IPSs should suit, or be adapted to suit, the power availability. Under this consideration, there are two typical categories of application scenarios as seen in recent publications.

To summarise the application suitability of IPSs, a diagram is shown in Figure 1.2. An example unsuitable application can be a periodic sensing task without periodically available power or the period of the energy source does not match the sensing period (left bottom circle in Figure 1.2).

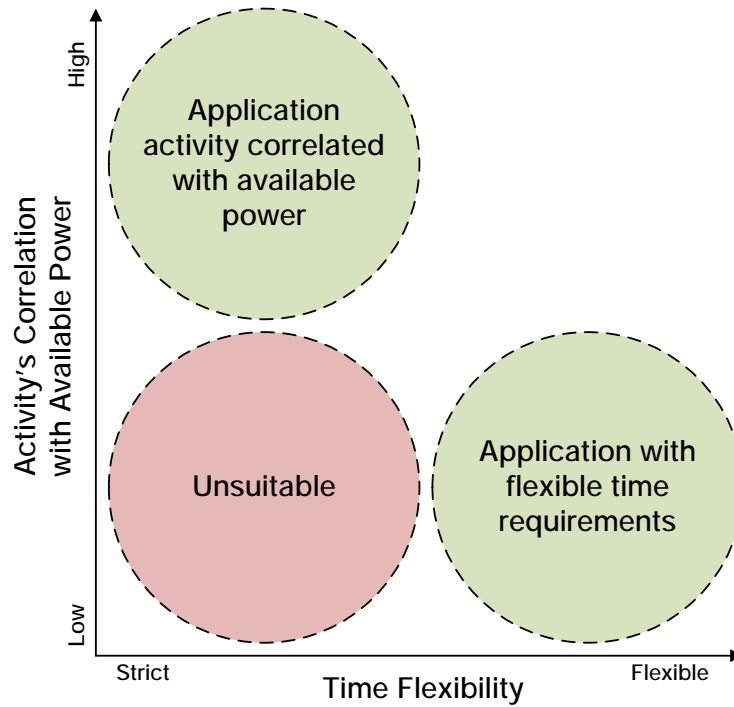


FIGURE 1.2: Application Suitability of Energy-Harvesting IPSS.

- **Category 1: Applications with flexible time requirements.**

Applications with flexible requirements on operating periods tolerate the intermittency of energy sources. In such applications, devices are allowed to wait for power-on periods to execute.

**Application 1: Kitchen event detection**

This application intends to capture kitchen events, such as dishwasher working, fan on, and refrigerator cooling, to record equipment usage. As such events usually last for tens of seconds to a few hours, the device does not need to operate immediately after the event occurs or disappears. An implementation of this application is shown by Maeng *et al.* [24]. The device iterates the following tasks in turn during power-on periods: sampling acoustic information from a microphone, classifying kitchen events with a pre-trained model, and transmitting the results in Bluetooth Low-Energy (BLE) packets to an always-on server. The device harvests RF energy from a dedicated RFID reader, and the packets are transmitted every a few seconds as reported. This application is to complete program iterations as frequently as possible so as to improve the accuracy of event records.

**Application 2: Temperature monitor for air conditioning**

This application intends to monitor indoor temperature for air conditioning. As the room temperature does not usually change over a few minutes, the temperature monitor does not need to wake up frequently or periodically. An implementation of this application is shown by Colin *et al.* [25]. During power-on periods,

the device samples temperature by an external analog sensor. If the temperature is detected to be out of a pre-defined range, the device sends a BLE packet to **alarm** the server. **The device is also powered by a dedicated RFID reader.** Similar to Application 1, the device is expected to maximise sampling frequency in order to capture out-of-range temperature as soon as possible.

- **Category 2: Application activity in correlation with available power.**

In such applications, the required operation periods correlate with power-on periods. This correlation is typically linked by an event that comes with harvestable power. When the event occurs, the device is activated by harvesting the power of the event at the same time to start operating. Therefore, the application operation periods and the power availability are inherently simultaneous in such applications.

### **Application 3: Bicycle trip counter**

The bicycle trip counter intends to read cycling speeds and calculate total travelled distances. The wheel rotation brings energy for the device to sense the cycling speed; the device does not need to operate without cycle movement. The trip counter is designed as a nail-sized board installed on the frame of a bicycle, with a magnet on the wheel that brings electromagnetic energy to the system [26]. Every round of wheel rotation activates the trip counter to calculate the current speed and log the traveled distance. After collecting enough energy over a few **cycling rounds**, the trip counter transmits the logged information. This application is also expected to report results as frequently as possible.



### **Application 4: Power meter**

The power meter measures the power flow of a main load wire. The AC power in the wire can be harvested by a coil to activate the power meter. A design is shown in Monjolo [27], where the power meter transmits a plain packet to a server once it collects a preset amount of energy. The server then calculates the elapsed time between the recent two packets to estimate the main load power.



As shown in the above **application**, a common **application specification of IPSs is to do as much 'work' as possible under the same energy conditions, e.g. completing program iterations as frequently as possible**, because the energy cannot be saved for later use. Other types of 'work' could include improving sensing accuracy or processing offloaded tasks received from other devices. To generally describe the 'work', in IPSs, *forward progress* denotes the effective application progress, excluding lost progress due to power failures and the progress on saving and restoring state [28]. **As indicated by the above applications, an IPS should maximise forward progress using the limited energy.**



## 1.2 Research Justification

As illustrated with the previous background and application examples, a major target for many IPS approaches is to **maximise forward progress given restricted energy condition**. Various **approaches have been proposed** for the load to efficiently sustain computing state across power failures, so as to leave more energy for forward progress. However, energy efficiency can not only be explored from the load side, but can also be explored from a system perspective, where the energy allocation of IPSs has not yet been widely studied. **The energy allocation of IPSs are mainly represented in two specifications – the system energy storage size and the voltage threshold to wake up the load**. Together, they determine the energy budget of one power-on cycle (but they do not change the energy input). This thesis will focus on how to improve the energy allocation of IPSs in order to increase forward progress, where it can be further discussed on three issues.

1. With the goal of minimising device dimensions and interruption periods, most IPS approaches adopt a minimum amount of energy storage [29–33]. This is typically just sufficient for the most energy-expensive atomic operation, e.g. saving and restoring a complete state [34]. However, a system with minimum energy storage may frequently go through a cycle of: wake up, restore state, execute program, save state, and halt. Provisioning more energy storage can prolong the power-on cycles, reduce the overheads, and hence increase forward progress, but can also increase system leakage and decrease forward progress. The sizing effect of energy storage on forward progress has not been studied. Therefore, a focus of this thesis will be studying the relationship between energy storage capacitance and forward progress in IPSs.
2. Extending the above ~~sizing effect~~, to determine a size of energy storage of IPSs in deployment, developers **may consider**, along with forward progress, other design factors, e.g. devices' physical volume and interruption periods. An approach for **exploring the sizing effect of energy storage** on multiple design factors has not been proposed yet. Also, there is not a method of determining an energy storage size that balances different design factors. Hence, another focus of this thesis will be exploring an energy storage sizing approach for IPSs that balances multiple design factors in deployment.
3. Apart from the energy storage size, the voltage threshold that wakes up an IPS also determines the energy budget of one power-on cycle. Existing approaches use one or a few fixed voltage thresholds, which are calibrated at design time. Some approaches (e.g. [35]) minimise the threshold for each task, but the fixed threshold can be violated at runtime due to variability in energy consumption, **leaving the system in non-termination**. The variable energy consumption can

come from many reasons, which include, but not limited to, variability in data amounts, peripheral configurations, **devices**, and capacitance degradation. In contrast, some approaches (e.g. [24]) set a universal high threshold, such that the energy budget should be **mostly enough** for all tasks. However, waiting for a high voltage threshold can be energy-inefficient because, typically, current input reduces with higher voltage and a high operating voltage also increases system quiescent current consumption. Hence, the final focus of this thesis will be the scheme of voltage threshold settings that avoids non-termination under runtime variable energy consumption while **maintains** system energy efficiency.

### 1.3 Research Questions

Motivated by the previous discussion, the following three research questions are derived:

1. What is the effect of sizing the energy storage capacity on the performance of IPSs?



Specifically, the energy storage capacity in IPSs is presented as the capacitance between  $V_{cc}$  and ground. The **forward progressing rate** directly determines application performance, e.g. program iteration rate or task completion time, and hence is regarded as the performance metric in this study. The goal is to explore whether sizing the energy storage capacity can change the forward progressing rate in IPSs, and if so, to study and quantify the relationship between them.

2. How may the energy storage of IPSs be sized to trade off forward progress against **device dimensions and interruption periods**?

While the last question explores the energy storage sizing effect on computational performance, this question encompasses more design factors in IPSs that a capacitor size can affect. Increasing energy storage capacity may benefit forward progress, but may also **exhibit side effects**. A larger capacitor typically has larger physical dimensions, which are a key design factor that IPSs should minimise in some application scenarios, e.g. wearable and implantable sensors. Also, a larger capacitor ~~also~~ leads to longer charge-discharge cycles, and thus prolongs interruption periods and undermines system reactivity to external events. The goal is to study the trade-off and to propose an approach that recommends an energy storage size for practical deployment.

3. How can an IPS run safely and efficiently with **runtime variable** energy consumption of tasks?

Energy consumption of tasks can change at runtime with regards to many factors, where **we consider, but not** limited to, the variability in data amounts to


process, peripheral configurations, devices, and capacitor degradation. A design concept is to allocate just enough energy for each task. This design concept can further break into two aspects – safety and efficiency. The safety aspect means that the IPS should intend to avoid **non-termination** by allocating enough energy for tasks. The efficiency aspect means that, while meeting the safety aim, the IPS should minimise the energy budget, such that the system **can wait for the least** possible energy threshold, maintaining energy efficiency and forward progress. The goal is to devise an approach that can enable IPSs to run with variable energy consumption of tasks, following the above design concept.

## 1.4 Research Contributions

Need more explanation



The contributions done to address the research questions in this thesis are:

1. Exploration and analysis of the energy storage sizing effect on reactive intermittent computing system, where we quantify and explain the relationship between energy storage capacity and forward progress.
2. A method and a simulation tool for sizing energy storage in deploying IPSs, where forward progress, dimension  and interruption periods are traded off in a cost function.
3. A runtime energy profiling and voltage threshold adaptation approach for efficiently performing atomic operations in cases of variable runtime energy consumption.



## 1.5 Publications

The research presented in this thesis were published in the following papers:

- J. Zhan, G. V. Merrett, and A. S. Weddell. "Exploring the Effect of Energy Storage Sizing on Intermittent Computing System Performance." *IEEE Transactions on Computer-Aided Design of Integrated Circuits and Systems*, 2021. [1]
- J. Zhan, A. S. Weddell, and G. V. Merrett. "Adaptive Energy Budgeting for Atomic Operations in Intermittently-Powered Systems." In *Proceedings of the 8th International Workshop on Energy Harvesting and Energy-Neutral Sensing Systems (ENSys '20)*, pp.82-83, 2020. [2]



## 1.6 Thesis Structure

The remaining part of this thesis is organised as follows. Chapter 2 provides background on energy harvesting, energy storage and energy-neutral computing, as well as reviews recent IPS techniques following a taxonomy based on their fundamental mechanisms and focusses. Chapter 3 analyses the sizing effect of energy storage on IPS performance. **Extending Chapter 3**, Chapter 4 explores a wider energy storage sizing effect on IPSs considering multiple design factors and real-world energy conditions. Apart from sizing energy storage, Chapter 5 focusses on runtime energy profiling and adaptation through adaptive voltage thresholding, so as to maintain system performance despite runtime variability. Chapter 6 concludes this thesis and discusses potential directions of future research.

## Chapter 2

# Energy-Harvesting Intermittent Systems

The emerging of energy harvesters provides diversified prospects for design paradigms of energy harvesting sensor nodes in IoT applications [23]. This chapter first provides a review on various energy harvesting sources and corresponding energy harvesters in Section 2.1, followed by energy storage techniques that used in energy harvesting computing in Section 2.2. Energy-neutral computing, an early paradigm in energy harvesting computing, is reviewed in Section 2.3. Finally, two recent research topics towards storage-less energy harvesting computing, i.e. intermittent computing and power-neutral computing, are reviewed in Section 2.4 and Section 2.5 respectively with an illustration of proposed methodologies.

### 2.1 Energy Harvesting Techniques

For all kinds of energy harvesters, although there is only one basic concept — to extract energy from ambient sources, various energy sources and harvesters lead to miscellaneous output characteristics in the amount and wave forms of harvested power, voltage, and current. To select a energy harvester for powering sensor nodes, one important concern is whether the supply power level matches the consumption of the load [36]. For one certain type of energy harvesters, the amount of energy harvesting supply can be scaled within an extent by the amount of energy sources or scaling the energy harvesters. The amount of energy sources is determined by the deploying environment, which cannot be controlled by the harvesting devices, but the size of energy harvesters can be decided at design-time with considerations on systems requirements, such as energy utilization, form factors, performance, etc.

In order to appropriately size and designate energy harvesters for sensor nodes, the power features of different energy harvesters are widely considered by researchers and engineers [37]. A classification of common energy harvesting sources and corresponding energy harvesters used in IoT is presented in Table 2.1. The voltage and current features of different energy harvesters largely differ from each other, due to the intrinsic differences in temporal distributions of the available amount of different energy sources and the physical principles of power conversion. The following part of this section introduces each kind of energy sources and energy harvesting techniques listed in Table 2.1.

Energy source	Energy harvester
Light (solar, artificial)	Photovoltaic cells
Radio waves	Radio frequency harvester (antenna)
Flow (air, liquid)	Wind turbine, hydrogenerator
Mechanical (vibrations, pressure, stress-strain)	Electromagnetic, electrostatic, piezoelectric harvester
Heat	Theomo electric generator

TABLE 2.1: Classification of energy sources and energy harvesters in IoT.



### 2.1.1 Light Energy Harvesting

Due to the abundant energy amount of light, whether from outdoor sunlight or indoor artificial light, light energy becomes a feasible source to powering sensor nodes and is historically treated as a substitute for battery supplies [38, 39]. Light energy can be converted to DC power by photovoltaic (PV) cells, which consist of semiconducting materials, e.g. silicon. When PV cells absorb light, electrons are excited by the photovoltaic effect, producing an electric potential by the separation of electrons and holes.

Given a fixed intensity of light, the output current from PV cells manifests an inverse relationship with the output voltage, as there is a semiconducting bypass within the PV cells. Although the power conversion efficiency may vary among different PV cell techniques (such as monocrystalline, polycrystalline, thin film), the curve shapes of current-voltage relationships are similar. Obviously, higher irradiance leads to higher current output when the output voltage is fixed, because there is more intensive light sources provided. More importantly, the output feature of PV cells can be summarised like “an inverse semiconductor” — when the terminal voltage is low, the output

current is almost constant and close to short-circuit current; when the terminal voltage gets close to open-circuit voltage, the output current significantly decreases and finally terminates at the open-circuit voltage.

Typical current-voltage curves of PV cells are shown in Figure 2.1, with an example of a monocrystalline cell given five values of illumination intensity from  $200 \text{ W/m}^2$  to  $1000 \text{ W/m}^2$ . When the voltage is under 15V, the PV cell is similar to a current generator (so when the voltage increases, the power increases almost linearly). When the output voltage increases above 15V, the output current drops significantly and reaches zero at around 22V. According to this phenomenon, there is a voltage point where the cell produces the maximum power, which is named Maximum Power Point (MPP) as indicated by black dots in Figure 2.1.

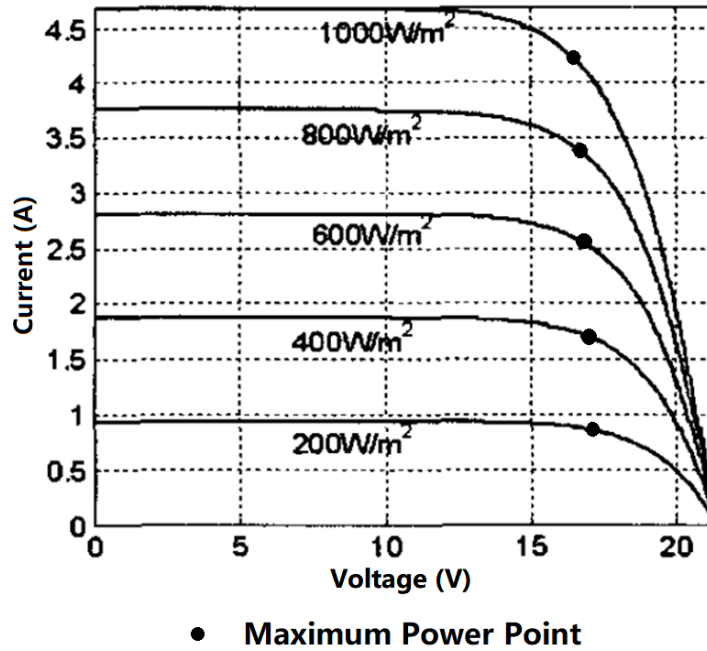


FIGURE 2.1: Typical current-voltage curve of a solar module (monocrystalline, adapted from [40])

In order to extract as much power as possible out of PV panels, most energy harvesting systems with PV modules adopts maximum power point tracking (MPPT) techniques [41–43]. MPPT is achieved by dynamically controlling the output voltage of PV cells around the maximum power point (MPP).

Outdoor sunlight and indoor artificial light are two main sources for light energy harvesting. The illumination intensity of direct sunlight on the earth's surface is typically  $1000 \text{ W/m}^2$  [44], while the typical indoor illumination intensity is  $10 \text{ W/m}^2$  [36]. Due to this large difference in the power density of these two circumstances, PV modules are more prospective in outdoor applications for harvesting solar energy. Conversion efficiency of PV cells is typically 15% to 25% in outdoor conditions [45].

Solar energy is an uncontrollable but partially predictable source [12, 46]. Solar irradiance demonstrates daily and annual periodicity due to the regularity of celestial movements, as well as irregular variations due to cloud movements, air mass, etc. A 3-year trace of diurnal global horizontal solar energy available measured in Los Angeles from 2012 to 2014 is presented in Figure 2.2, and an example of daily dynamics of global horizontal solar irradiance of the same location is presented in Figure 2.3. As shown in both figures, the predictability is reflected from the roughly annual and daily periodicity, and the uncontrollability and randomness relates to the irregular variations, which include both daily variations in an annual scale and variations over a few seconds and minutes on a daily scale.

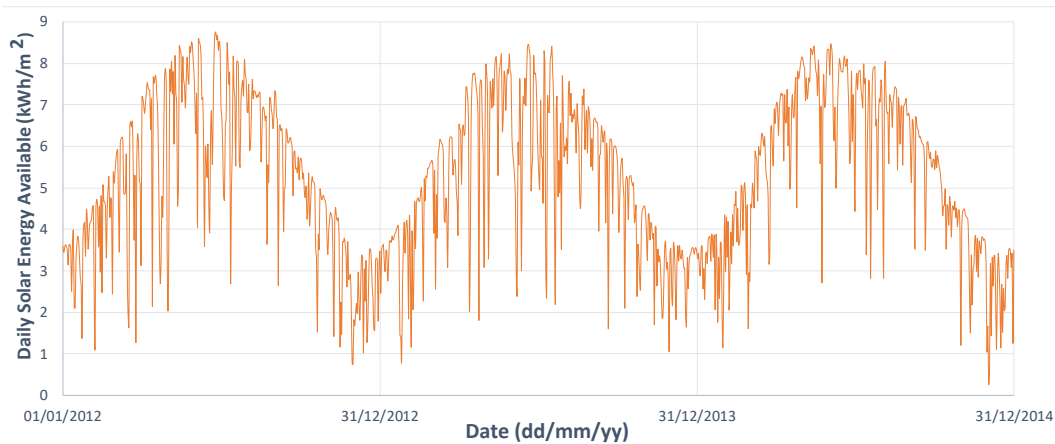


FIGURE 2.2: Daily global horizontal solar energy available in Los Angeles 2012-2014 [47].

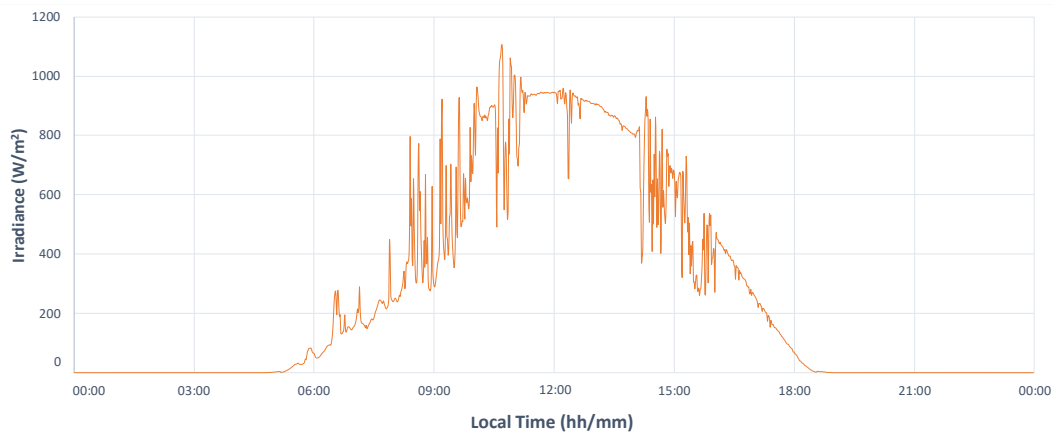


FIGURE 2.3: One-day dynamics of global horizontal solar irradiance in Los Angeles 29 April 2016 [48].

In order to make full use of solar energy, substantial efforts have been made to develop and improve energy harvesting sensor nodes with solar panels [38, 39]. Generally, solar energy harvesting approaches adopt large energy storage, e.g. a rechargeable battery, to smooth out the daily and annual variations. Examples of solar-powered sensor nodes are presented in [11, 38, 49], and a comprehensive review on solar-powered sensor nodes is published in [10].



### 2.1.2 Radio Frequency Energy Harvesting

Radio Frequency (RF) energy exists in time-varying electromagnetic fields, which widely spread in our environment now due to the propagation of wireless networks, such as Wi-Fi and cellular phone signals [50]. When radio waves pass through an antenna, due to electromagnetic induction, AC voltage is generated. This AC voltage can be rectified and regulated to DC power for sensor nodes. The received RF power is reciprocal to the square of distance from the source to the destination. The maximum conversion efficiency from RF waves to DC power is typically 50-75% given a transmission distance of 100 metres [36].

Due to the widespread deployment of telecommunication networks, RF energy harvesting becomes available in a wide range of locations, both outdoors and indoors. Compared to light energy harvesting, RF harvesting shows its strength in indoor applications as there is often low or no light intensity inside buildings.

A basic and common example of RF harvesting is RF Identification (RFID). In a passive RFID application, an RFID reader transmits RF signals to an RFID tag for asking its tag information. The tag absorbs the signals and energy through its antenna, and then responds the reader with its information. Up to now, Wireless Identification and Sensing Platform (WISP) [51, 52] is presented to show the possibility of the integration of RF energy harvesting in IoT applications.

### 2.1.3 Flow Energy Harvesting

Flow-based energy harvesting utilises turbines and rotors to collect the kinetic energy in air flow or liquid flow. Air flow is converted by wind turbines and liquid flow is converted by hydrogenerators. Wind turbines and hydrogenerators are normally in different mechanical structures (shapes), but the fundamental principles of them are the same.

Wind turbines are manufactured in a wide spectrum in terms of dimensions, from a large-scale wind farm (arrays of large turbines) to a portable micro wind turbine. Micro wind turbines are suitable for battery charging and powering autonomous electronic devices.

A raw voltage output trace of a micro wind turbine given a blast of wind is presented in Figure 2.4. Given a constant blow, a wind turbine should produce a sinusoidal voltage signal. Its voltage output vibrates from the positive domain to the negative domain with time, so a rectifier is normally required in order to utilise this AC power for DC load.

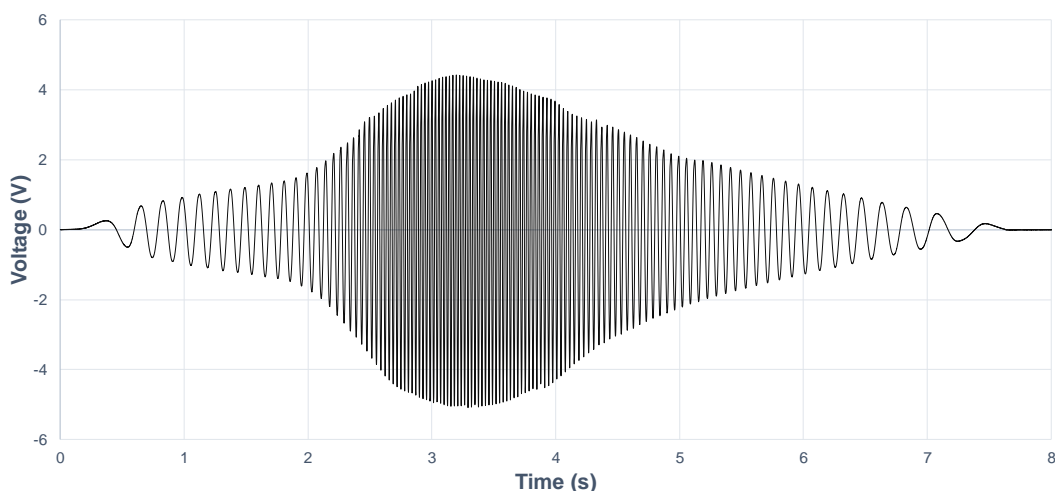


FIGURE 2.4: Dynamics of a micro wind harvester (reproduced from [53]).

Similar to solar energy, wind energy is uncontrollable but partially predictable. Sharma *et al.* [54] introduce a system that achieves available wind energy predictions based on downloaded weather forecast information within recent 3 days. Also, Cammarano *et al.* [55] present a wind and solar energy predicting method which dynamically adjusts its time horizon of prediction in order to achieve higher accuracy than its prior methods.

Hydrogenerators harness the energy in moving liquids, such as water or a mix of different liquids. Traditionally, hydrogenerators are used for generating large-scale electricity from rivers and streams. However, since the possible underwater applications in IoT, hydrogenerators can be a suitable alternative for powering sensor nodes. For example, Morais *et al.* [56] incorporate a small-sized hydrogenerator as a part of energy harvesting supply for sensor nodes.

## 2.2 Energy Storage for Sensor Nodes

Energy harvesting supply is variable and intermittent over time, causing disparity between power supply and power consumption. In order to deliver stable power output from a varying source, a critical component in an energy harvesting power unit is energy storage, which buffers the harvested energy and powers the load when needed. Besides its ability to buffer energy and its effect on overall efficiency, energy storage has a dominant effect on the size, cost, and lifetime of sensor nodes [16]. Therefore, how to design energy storage is a critical concern in deploying energy harvesting sensor nodes.

Technologies of energy storage used in sensor nodes are generally divided into two categories: rechargeable batteries and capacitors, which are different from each other in

terms of energy density, power density, lifetime, discharging features, leakage, etc. In general, batteries have higher energy density (containing more energy with the same volume/weight), lower leakage, and a more stable discharging curve (a stable voltage output while discharging), while capacitors have higher power density (higher limits for charging/discharging current), and longer lifetime in terms of charge-discharge cycles [16, 38]. The choice of these two forms of energy storage depends on application requirements. These two technologies and their implementations will be briefly reviewed in the following subsections.

### 2.2.1 Rechargeable Batteries

Batteries are more energy-dense than capacitors and manifest a stable voltage output when discharging. Rechargeable batteries have been widely adopted in mobile devices. Rechargeable batteries are generally made in the following techniques: Sealed Lead Acid (SLA), Nickel Cadmium (NiCd), Nickel Metal Hydride (NiMH), Lithium Ion (Li-ion), and Lithium ion Polymer (Li-Po). Due to the similar techniques and features of Li-ion and Li-Po batteries, Li-ion will be used to represent Li-ion and Li-Po batteries in this subsection. SLA and NiCd batteries are less likely to be implemented in energy harvesting sensor nodes [16, 38]. SLA batteries suffer from low energy density and are normally bulky and heavy, which is unfavorable for sensor nodes. NiCd batteries involve memory effect, i.e. decrease of energy capacity after repeated partially discharging and recharging, which is a common situation in energy harvesting implementations.

Compared to SLA and NiCd batteries, NiMH and Li-ion batteries show a strength in energy density in both weight and volume, and hence, are more suitable for energy harvesting applications [16, 38, 57, 58]. A comparison of two commercial NiMH and Li-ion batteries is listed in Table 2.2 with a variety of perspectives and features. Li-ion batteries are typically lighter than NiMH batteries, with weight energy density 2-3x and volume energy density 1-2x to NiMH batteries. Also, Li-ion batteries significantly outperform NiMH batteries in terms of charging efficiency and self-discharge rate. However, Li-ion batteries are normally more expensive than NiMH batteries, and require more complicated pulse charging circuits [38]. NiMH batteries also provide a relatively constant voltage supply during discharging [11].

NiMH and Li-ion batteries have been widely implemented in energy harvesting sensor nodes. Heliomote [38] uses two NiMH batteries in series to match the charging voltage (2.2-2.8V) with the MPP of the solar panel. HydroSolar [57] also adopts two NiMH batteries to avoid the Li-ion charging hardware. Jiang *et al.* [20] design a hybrid storage system including a lithium based rechargeable battery as the secondary buffer, due to its high efficiency and charge density.

	NiMH (Panasonic BK150AA)	Li-ion (EEMB LIR14500)
Nominal voltage	1.2 V	3.7 V
Charge capacity	1500 mAh	750 mAh
Energy capacity	1.80 Wh	2.775 Wh
Weight	26 g	20 g
Dimensions	∅14.5mm × 50.5mm	∅14.1mm × 48.5mm
Weight energy density	69 Wh/Kg	139 Wh/Kg
Volume energy density	216 Wh/L	366 Wh/L
Operating temperature	-20°C to 65°C	-20°C to 60°C
Charging cycles (until 80% capacity)	>500	>300
Reference price	£2.91	£3.25
Charging efficiency [58]	66%	99.9%
Self-discharge [58]	30% per month	10% per month
Charging Method [58]	Trickle	Pulse

TABLE 2.2: Comparison between commercial NiMH and Li-ion rechargeable batteries.

Despite the high energy density and stable discharging voltage, batteries still show a typical drawback at short lifetime (less than 5 years [19]), which involves manual replacement of batteries or devices after the battery lifetime expires. Also, batteries raise environmental concerns due to the heavy metals and toxic chemicals within. If not properly charged, Li-ion batteries can cause safety issues, i.e. explosion and fire, which are problematic when deployed in distant and wild places. In addition, rechargeable batteries are susceptible to temperature. Most batteries only exhibit their rated characteristics around 20°C, and lose their efficiency and capacity when operating at extreme temperatures (around their rated limits) [58].

### 2.2.2 Capacitors

Due to the lifetime limits and pollution issues of batteries, capacitors, typically supercapacitors, are considered as an alternative to replace rechargeable batteries as energy storage. Supercapacitor (also known as ultracapacitors or electrostatic double-layer capacitors) are capacitors with higher energy density than electrolytic capacitors. Unlike conventional capacitors, where charges are stored and separated by solid dielectric, supercapacitors maintain charges based on double-layer or pseudo-capacitive charging phenomena [59]. Supercapacitors are still much less energy-dense than batteries, but act as a transition from capacitors to batteries.

Compared to rechargeable batteries, supercapacitors exhibit strengths in a large number of charge/discharge cycles, long lifetime (20 years), high charge/discharge efficiency (98%). The self-discharge rate of supercapacitors is higher than batteries, with 5.9-11% of maximum capacity per day [60, 61], but this leakage is insignificant compared to the small capacity and the total energy gained per day. The main constraint

of supercapacitors is still the low energy density, which results in large storage dimensions if the aim were to achieve a comparable capacity with batteries. In order to maintain the same form factors of sensor nodes, designers have to adapt system architecture to a small storage (compared to batteries).

Prometheus [20] introduces supercapacitors into energy storage for sensor nodes whereby two 22F supercapacitors are used in combine with a Li-Po battery. AmbiMax [62] also proposes a hybrid storage design similar to Prometheus, but with two more 10F supercapacitors for wind energy harvesters. To achieve longer lifetime than battery-based sensor nodes, Everlast [21] demonstrates the feasibility of replacing batteries with supercapacitors in energy harvesting sensor nodes, designing a power system that adopts a 100F supercapacitor as the only energy reservoir.

However, farad-level supercapacitors occupy a significant part of device volume. The advent of energy-driven computing [63] introduces the application and design scenario where execution happens only if there is energy available. Within this scenario, energy storage using millifarad-level supercapacitors are investigated in energy harvesting sensing applications [35, 52]. Furthermore, intermittent computing, which will be illustrated in the next section, enables computation given intermittent power, making progress with electrolytic capacitors or even without dedicated storage (only microfarad-level parasitic capacitance).

### 2.2.3 Discussion


To summarise, due to the requirements on lifetime, environmental-friendliness, and form factors in energy harvesting sensor nodes, the energy storage designs have transformed from batteries to supercapacitors, and eventually eliminated the need for dedicated storage.

Batteries have been the preferable choice for buffering harvested energy and powering sensor nodes because they make sensor nodes easy to program and operate reliably until the battery lifetime expires. However, the environmental issues and short lifetime of batteries limit the deployment of ubiquitous sensors. Supercapacitors avoid the problems of batteries and have been used to replace batteries, but the low energy density of supercapacitors also makes sensor nodes bulky and heavy in order to achieve sufficient capacity for uninterrupted operations. Recent development of intermittent computing enables forward execution over power outages and encourages storage-less designs in energy harvesting sensor nodes.

Although the minimum need for storage capacity to operate sensor nodes decreases with the evolution of computing techniques, decreased storage does limit the flexibility of energy usage. A storage-less system has to consume the incoming power immediately, otherwise the energy is wasted. This fact consequently restricts the application

scenarios of storage-less systems to energy-driven applications, where execution needs to run only when there is available energy sources to harvest. However, energy-driven applications do not cover all the demands in IoT, so simply reducing the storage need is not always desirable. A wider spectrum of storage designs should be explored to suit and optimise for different application scenarios.

## 2.3 Energy-Neutral Computing

Energy-neutral (EN) computing aims to  operate sensor nodes with at least a certain performance level over a period of time. Energy-neutrality can be described as the following equation:

$$E_{min} \leq E_{t_0} + \int_{t_0}^{t_0+\Delta t} [P_h(t) - P_c(t)]dt \leq E_{max} \quad (2.1)$$

where  $P_h(t)$  and  $P_c(t)$  are the harvested and consumed power at time  $t$ ,  $t_0$  is the time when EN computing is meant to start,  $\Delta t$  is the length of period during which EN conditions are achieved,  $E_{t_0}$  is the initial available energy in energy storage at time  $t_0$ ,  $E_{min}$  is the minimum amount of stored energy below which the system cannot sustain (typically due to insufficient supply voltage), and  $E_{max}$  is the maximum capacity of energy storage beyond which the harvested energy is wasted.  $P_c(t)$  includes the power consumption of the whole system, such as the MCU, peripherals, power conversion circuit, and the power leakage of energy storage.  $P_h(t)$  is the harvested power after conversion.

EN devices are typically powered by solar cells [64], and  $\Delta t$  is typically 24 hours or one year to suit the period of the solar energy source. In order to achieve energy neutrality over such a long term, sufficient amount of energy storage, typically in the form of rechargeable batteries, is required to smooth out the large temporal variations of harvested power. The capacity of the energy storage is determined by how long the system tries to maintain a stable performance as larger energy storage tolerates more energy differences. In general, the length of  $\Delta t$  and the difference between  $P_h$  and  $P_c$  determine how much storage is required, and on the other hand, the capacity of energy storage limits how long  $\Delta t$  can be.

In order to ensure that the system works uninterruptedly by managing the stored energy (the middle term in Equation 2.1) between  $E_{min}$  and  $E_{max}$ , EN computing dynamically adapts system performance and power consumption over the period  $\Delta t$ . Typical adapting techniques include adjusting workload duty cycles and participation in network activity [63].

Kansal *et al.* [11] illustrate a preliminary power management algorithm by which the incoming energy is estimated by an Exponentially Weighted Moving Average (EWMA) of the past recorded slots of harvested energy, and the system tries to exploit the harvested energy by scaling its duty cycles. Vigorito *et al.* [65] introduce a Linear-Quadratic Tracking (LQT) approach to scale duty cycles based on the current battery level, and as evaluated in its datasets, mean duty cycle is improved by 6-32% and duty-cycle variation is reduced by 6-69% compared to [11], which means the system works with a more stable performance. In [13], a Proportional-Integral-Derivative (PID) controller is used for monitoring and stabilizing the voltage of a supercapacitor-based energy storage, and hence, the storage level of this system. While these approaches achieve satisfactory energy neutrality for the magnitude of hours, they all show a latency when responding to the harvested power, and high variance of duty cycles when adapting to a new power trace. Additionally, approaches in [65] and [11] rely on an accurate estimating algorithm to detect the remaining battery energy, which is vulnerable to deployed time and temperature.

In [66], a prediction algorithm for solar energy named Weather-Conditioned Moving Average (WCMA) is presented, in which both the current and the past weather data are taken into account to achieve higher accuracy than EWMA methods. It is reported by the authors that the average prediction error is improved from 28.6% in EWMA to 9.8% in WCMA over a test duration of 45 days, but it is unclear in the article that how to harness this prediction to improve the system performance. Similarly, weather forecast is adopted in [54], by which the authors build a model to approximate the available solar and wind energy. Although these two methods based on weather data provide high prediction accuracy, the network overheads for receiving these data are not presented, and how to fully utilise this daily prediction is still a problem.

Different from the aforementioned daily EN operations, a long-term annual power management based on duty-cycling is presented in [12] to achieve annual energy neutrality. The authors use an adjustment factor, which is dynamically calculated from the historical windows, to modify the design-time energy prediction model to a more realistic model, and determine its performance level accordingly. However, this algorithm is only tested in simulation instead of practical experiments. Moreover, for such a long-term EN operation, a large battery is required, but the battery deterioration is ignored in their analysis.

In [14], a task scheduling algorithm for optimising the performance of an energy harvesting system (typically based on PV harvesters) is exhibited. Given a predicted power trace, storage bounds, energy consumption of tasks and quality of tasks, the proposed scheduling algorithm is proved to be able to find the optimal scheduling in a pseudo-polynomial time which leads to the maximum sensing quality. While this algorithm provides an ideal solution for power management, it requires that the energy source should be predictable with high accuracy, and the energy cost and quality



of each task should be defined at design time. The first requirement almost constrains this algorithm within the cooperation of solar energy. The second requirement is hard to achieve since a) in practice the energy consumption of tasks may change due to temperature and dynamic data amount [67] and b) the energy cost of a system includes many elements other than the energy consumption of computing tasks.

EN computing efficiently utilises energy and maintains system performance, ensure reliability and periodic task execution despite variable harvesting power input. However, in almost all energy neutral approaches reviewed above, a large energy storage, i.e. a rechargeable battery, is in need in order to buffer temporal energy variations. The usage of batteries poses sustainability challenges due to the limited lifetime and pollution issues. Recent research develops intermittent computing and power-neutral computing, which minimise the need for energy storage. The next two sections (Section 2.4 and Section 2.5) review the methodologies of these two research topics.

## 2.4 Intermittent Computing

Energy harvesting provides an autonomous power supply for wireless sensor nodes as an alternative of battery power. However, with small storage, energy harvesting systems inevitably suffer from frequent power outages, which affect forward execution of programs. Intermittent computing (IC, also known as transient computing) aims to maintain forward execution and computation correctness through power failures [68]. Intermittent execution spans its execution and intermittently computes over power outages, while conventional execution restarts after power **interrupts**. A typical characteristic of an IC system is that it starts executing whenever there is power available and suspends during power outages; after power recovery, it can continue its prior task correctly instead of restarting from the beginning of a program.

Due to different design considerations, the methodologies in IC varies in a wide spectrum [69]. These methodologies include saving snapshots of system state to non-volatile memory (NVM), breaking down execution into small tasks, hardware circuits for suspend and restore operations, etc. The existing IC approaches can be classified into four types: checkpointing, reactive IC, task-based IC, and non-volatile processors (NVP). The following part of this section explains the each methodology one by one, as well as their works and current research progress.

### 2.4.1 Checkpointing IC

Checkpointing IC inserts checkpoints into code at compile time. When a checkpoint is called, the system checks the current available energy amount. If this amount is less



than a predefined threshold, which indicates the available energy may not be enough to sustain execution, a snapshot saving function is called at this checkpoint. To save a snapshot of the system computing state, the system copy current stacks and heaps, local and global variables, general registers, the stack pointer, and the program counter, into the NVM. A checkpointing system continuously operates until it encounters power outages, where the supply voltage is less than the minimum operating voltage of the systems. After the supply voltage recovers, the system restore its state from the last checkpoint, and hence, continue its execution from that checkpoint.

Mementos [68] first provides a checkpointing solution in which checkpoints are planned at compile time. Mementos includes three strategies of placing checkpoints, which are placing at every loop, placing at every function call, and an auxiliary timer delay to determine the minimum cycle between two adjacent checkpoints. Additionally, programmers can also insert or delete checkpoints manually as a custom option. Two NVM blocks are used and snapshots are saved to the two blocks alternately, so there is always at least one available and complete snapshot even if the energy is depleted during saving a new snapshot. One significant shortcoming of Mementos is the instrumenting strategy: with the different sizes of loops and functions, the granularity of checkpoints can be either too small, which introduces high run-time overheads, or too large, which leads to non-termination where the execution can never get to the next checkpoint. It is a concern in Mementos that how to set the voltage threshold which triggers saving snapshot. Setting this too high leads to redundant snapshots, while setting this too low leads to the failure of saving snapshots and cannot guarantee forward progress.

HarvOS [70] is proposed to improve the strategies of inserting checkpoints in Mementos. HarvOS analyses the control-flow graph of a program and splits it into sub-graphs with a checkpoint inserted for each sub-graph. To reduce the number of checkpoints compared to Mementos, the size of sub-graphs is set close to the worst-case number of useful cycles the MCU can execute until the next checkpoint. To reduce the size of snapshots, the RAM usage in each sub-graph is analysed and the checkpoint is placed at the point with the least RAM usage. HarvOS claims to reduce 68% checkpoints on average compared to Mementos.

Chinchilla [71] proposes a checkpointing tool which automatically overprovisions checkpoints at compile time and adaptively eliminates unnecessary checkpoints at run time. Compared to Mementos and HarvOS, Chinchilla relieves the programming efforts on manually inserting checkpoints while still achieves an efficient number of checkpoints at run time.

An advantage of the checkpointing method is the size of a specific snapshot can be estimated from the program execution flow to find a smaller snapshot [70]. However,

there are still two significant challenges remaining unsolved in checkpointing methods: idempotency violation and non-termination.

An execution is idempotent if it can be repeated while maintaining the same result [72]. Non-idempotent actions include I/O operations and NVM writes, which are fairly common in IC applications. Repeating non-idempotent actions can lead to undesired results, so these non-idempotent actions should be executed only once. Checkpointing systems repeat executing the code between two adjacent checkpoints, and hence, cause non-idempotency. Current compile-time checkpointing methods as listed above are not able to ensure idempotency.

Non-termination in checkpointing systems exhibits when the energy consumption of execution between two checkpoints is **too much that** the system energy buffer and harvested supply **cannot** sustain. Non-termination typically happens when the instrumentation strategy of checkpoints ignores the size of the energy buffer, as in Mementos. HarvOS and Chinchilla manage to mitigate non-termination, but they cannot eliminate this problem as they cannot dynamically insert checkpoints at run time according to varying environmental sources.

## 2.4.2 Reactive IC

Instead of instrumenting checkpoints at compile time, reactive IC does not set predefined checkpoints but save snapshots at run time when the supply voltage is detected to be lower than a threshold that indicates an imminent power failure. Therefore, the snapshot saving operations is only invoked when there is an indication of an imminent power outage, i.e. a low supply voltage. Also, after saving a snapshot, a reactive IC system suspends its execution and enter a low-power mode, rather than continues execution until a power outage as checkpointing systems do. When the voltage supply recovers above a restore threshold, the system either restores the last snapshot if the system reboots, or just continues execution if the system comes back from the low-power mode.

Hibernus [34] saves only one snapshot before a power interruption and then enter the sleep mode. Two fixed voltage thresholds,  $V_H$  and  $V_R$ , are predefined for hibernation (save a snapshot and sleep) and restoring a snapshot. An on-chip voltage comparator and an on-chip voltage reference generator are used for monitoring the supply voltage and triggering hibernation when the supply voltage drops to  $V_H$  or restoration when the supply voltage recovers to  $V_R$ . A voltage trace is shown in Figure 2.5 to explain Hibernus behaviours, and this trace is representative for a reactive IC system behaviours. To adapt thresholds to variable energy sources, Hibernus++ [29] implements dynamic self-calibration for suspend and restore thresholds by executing a hibernation test. By using adaptive thresholds instead of fixed thresholds as in Hibernus,

Hibernus++ makes itself compatible with a variety of energy sources. Compared to Hibernus, Hibernus++ improves application execution time by reducing the overheads of suspend and restore operations.

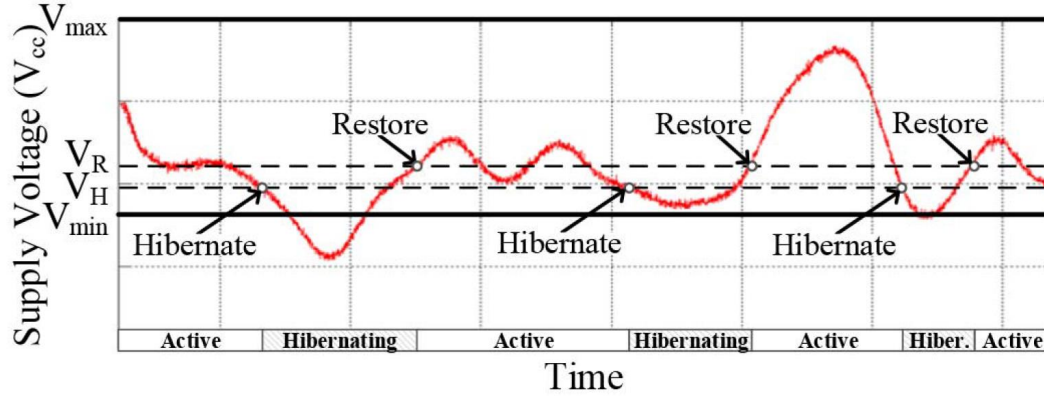


FIGURE 2.5: Voltage trace with hibernation and restoration points in Hibernus (taken from [34]).

Quickrecall [73] is a similar approach to Hibernus except replacing RAM with NVM, so that all the run-time volatile data become non-volatile and only registers are necessary to be saved in a snapshot. An external voltage comparator detects a triggering voltage  $V_{trig}$  to back up only peripherals and registers. Compared to the voltage thresholds in Mementos and Hibernus,  $V_{trig}$  in Quickrecall is lower since the reduced energy and time overheads for saving and restoring a snapshot. However, using NVM as RAM may lead to the higher cost of NVM accesses. A comparison between Hibernus and Quickrecall is presented in [74], showing that Quickrecall performs worse when the frequency of power interrupts is low as the NVM consumes more than volatile RAM, and performs better when the frequency of power interrupts is high as the overheads of saving snapshots are much lower.

Reactive IC methods only save snapshots when power failure is imminent, and hence, reduce the number of snapshots compared to checkpointing methods. Also, reactive IC avoids code re-execution by suspending execution after saving a snapshot, and hence, ensures idempotency.

The RAM usage varies at run time, so the size of snapshots in reactive IC also varies throughout code execution. To circumvent this issue, Hibernus saves the entire RAM in each snapshot while Quickrecall does not use RAM at all. Comparing Hibernus to checkpointing methods, the overheads of saving snapshots in Hibernus is larger as checkpointing methods can avoid saving large snapshots by analysing the program. Such high saving overheads becomes significant when the frequency of power outages increases. Increasing the size of energy storage in reactive IC should be helpful to mitigate frequent snapshot taking because the increased energy storage can filter the variations of supply voltage and avoid frequent voltage drops.

### 2.4.3 Harvest-Store-Use IC

Harvest-store-use IC systems perform a complete task in one consecutive period when the harvested energy in energy storage is enough. A complete task typically includes sensing, processing, and transmitting actions. In order to sustain a successful task execution, the required capacity of energy storage is larger than the minimum required storage in other IC methodologies. Harvest-store-use systems need to calibrate the energy consumption of the task at design time and set an energy threshold to trigger execution based on that energy consumption. When the threshold is reached, which means there is enough energy for a task, the system performs one task and sleeps until the next threshold trigger. As shown in Figure 2.6, the behaviours of the amount of stored energy can be seen as alternating in turn between two states: the collecting state and the executing state.

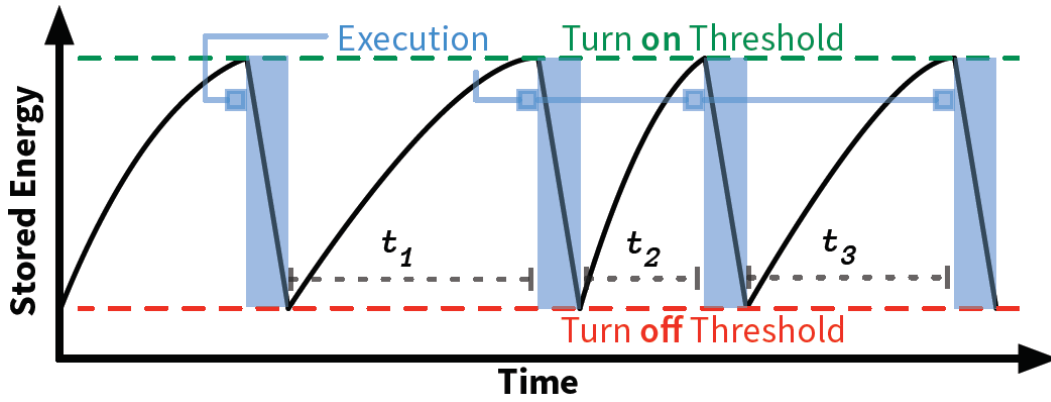


FIGURE 2.6: Harvest-Store-Use execution (taken from [75]).

Monjolo [27] is an early design following the harvest-store-use pattern. Monjolo presents a home power meter, whereby a current transformer is installed around the main power cable and provides the energy for this metering system. When the energy stored in a  $500\mu\text{F}$  capacitor reaches a predefined amount, the system transmits a data packet. Another wireless receiver keeps collecting these packets and approximates the power of the main cable based on the receiving frequency of packets. Such a system contains little sensing and processing work on the transmitting node, and instead, it treats the intensity of energy sources as the sensing data, and processes this translation of data on the receiving node which is powered stably.

WISPCam [52] is a wireless camera that obtains energy from an RF harvester. The harvested energy is stored in a  $6\text{mF}$  supercapacitor and the data (photos) are saved in NVM. Once the energy is sufficient for taking one photo, the system starts execution and depletes the energy for taking a picture and data transmission.

Similarly, Dynamic Energy Burst Scaling (DEBS) [35] also wakes up and executes tasks when there is enough energy in the  $80\mu\text{F}$  capacitor. The major difference between DEBS and the above two approaches is DEBS can adjust the energy thresholds dynamically

for a set of different tasks and generates energy bursts according to which task is in need.

Harvest-store-use paradigms are suitable for occasions where the harvested power is too weak to support the power consumption of any normal execution (other IC methodologies may quickly deplete energy storage and make little progress). Also, harvest-store-use methods circumvent the idempotency issues by complete tasks in one burst. However, this pattern is task-based, which means its operation is limited to one or several fixed energy-defined tasks and also relies on high-quality design-time profiling of tasks.

#### 2.4.4 Task-based IC

Task-based IC decomposes a program into a series of atomic tasks, which only deliver non-volatile results after all operations in a task are completed [72]. Task-based IC is achieved by programming and execution models, which aim to ensure NVM consistency and idempotency. In such models, accesses to NVM and I/O operations are carefully managed to prevent idempotent violations. To ensure idempotency, the program control flow is divided by task boundaries, and the communication between tasks is enabled by reading or writing NVM data on those boundaries. To avoid non-termination, the maximum size of one task is limited by the capacity of energy storage. Therefore, task-based IC can be seen as a rigorously-organized and fine-grained checkpointing method, which eliminates the non-termination and idempotency problems in checkpointing IC. Task-based systems feature with fast suspend and restore operations because only the runtime and the current task should be versioned and restored through power outages [69].

DINO [72] proposes the first task-based IC programming and execution model, illustrating the task-based idea and providing a basic groundwork. DINO implements the programming and execution model on the LLVM compiler for C code, with program libraries and compiler passes. Chain [76] improves DINO data flows with "Channels", which is dedicated to manage non-volatile data, guaranteeing the correctness on applications with both idempotent and non-idempotent code. Alpaca [77] introduces data privatization which reduces memory usage compared to Chain.

A main drawback of DINO, Chain, and Alpaca is they require great programming efforts for programmers to understand the implemented libraries and redesign a program according to the task-based concept. A recent work, CleanCut [78], proposes an auxiliary tool to check and automatically decompose the non-terminating tasks (the energy consumption of which exceeds the capacity of system energy storage).

Also, like checkpointing IC, task-based IC inevitably involves re-execution. Alpaca, the state-of-the-art task-based approach, reports a run time overhead of 1.3-3.6x compared to plain C code given constant power supply.

### 2.4.5 Non-Volatile Processors

Non-Volatile Processors (NVPs) incorporate automatic backup and restore hardware within the chips. A comparison of memory architecture between traditional processors and NVPs is shown in Figure 2.7. The traditional volatile elements are replaced with non-volatile elements to achieve efficient backup and restore operations with a faster speed and lower energy consumption than the conventional memory architecture. To be specific, the registers and cache are equipped with built-in additional non-volatile backup and restore circuits, so that when the supply power is going to disappear, the computing state can be saved locally just beside the elements, rather than being copied out into an external NVM. It is reported that the backup and restore speed of NVPs can be 2-4 $\times$  magnitudes faster than the state-of-the-art NVM based commercial processors [79].

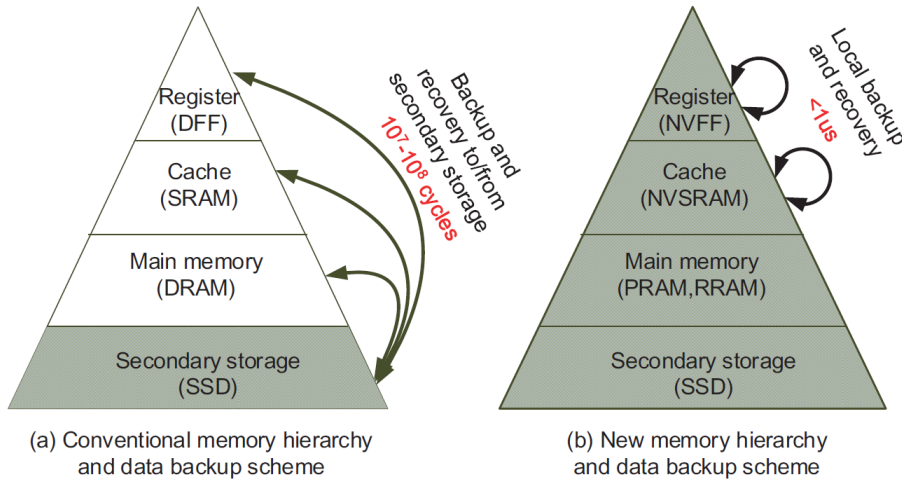


FIGURE 2.7: Memory architectures of traditional processors and NVPs (taken from [79]).

Wang *et al.* [80] present a preliminary NVP with 3 $\mu$ s backup time and 7 $\mu$ s restore time, which enables the processor to operate safely under a 20 kHz square wave of power. As a comparison, the existing MCUs in TI MSP430 family can only achieve 212 $\mu$ s and 310 $\mu$ s for saving and restoring states respectively. Su *et al.* [81] extend the backup and restore time overheads to a system level, presenting a NVP with 46 $\mu$ s system-level wake-up time and 14 $\mu$ s system-level sleep time. Liu *et al.* [82] integrate a NVP into a system-on-chip with independent backup and restore circuits for peripherals.



NVP-based research follows with the development of NVP hardware. Ma *et al.* [83] examine the performance and energy consumption of several types of NVPs with different ambient sources, providing a guideline for NVPs selection. The concept of “Incidental Computing” based on NVPs is proposed in [84] to improve the forward progress under unstable power supply, and also provides an evaluation of performance on NVPs. Essentially, it pays more attention to processing forward data in need than the buffered historical data from recovery, but an incidental recomputing on the historical data is performed when there is abundant energy. It is reported that this approach outperforms the existing save-and-use computing scheme by  $2.2\text{-}5\times$  in the simulation with respect to an image processing speed, and also the forward progress is improved by  $4.28\times$  on average over a basic NVP.

NVPs perform well in terms of the response to power intermittency, but the research on how to deliver better forward progress with NVPs is limited. Dynamic Voltage and Frequency Scaling (DVFS) can be a potentially applicable solution [85]. In a traditional NVP, the small buffering capacitor tends to be either charged to be full or depleted rapidly and frequently [86]. This behaviour accounts for a large part of backup and recovery overheads, so power management based on NVP is in need.

## 2.5 Power-Neutral Computing

While IC aims to ensure forward execution despite frequent power outages, energy harvesters may also generate more power than systems can consume when ambient sources are sufficient. Such excessive energy is wasted if not stored for later usage or consumed immediately.

### 2.5.1 Principles of Operations

Power-neutral (PN) computing aims to manage power without additional storage or with only a very limited amount of storage which can only sustain its system for milliseconds. In principle, power-neutral computing is a special case of energy neutral computing when  $\Delta t$  in Equation 2.1 is equal (or close) to zero. Technically, PN computing scales the instantaneous system power consumption to match the instantaneous harvested power with theoretically zero storage (in other words, energy neutrality is met instantaneously). PN operations can be translated into the following expressions:

$$P_h(t) = P_c(t) \quad (2.2)$$

$$\text{where } t \in \{t | V_{cc}(t) \geq V_{min}\} \quad (2.3)$$

where  $V_{cc}$  is the input voltage of the computing load, and  $V_{min}$  is the minimum voltage required for the system to operate. Equation 2.2 describes the methodology of power neutrality (dynamic and instantaneous power adaptation). Equation 2.3 limits the requirement for power neutrality that the system should be powered and active to make reactions of performance scaling. This requirement may change according to different system designs, but for contemporary computing and sensing loads, this is determined by the supply voltage.

Given a very limited amount of storage and a range of scalable performance and power consumption, PN computing scales down performance if  $P_h$  is lower than  $P_c$ , such that  $V_{cc}$  remains stable, which extends execution time and avoids suspend and restore operations. On the other hand, PN computing scales up performance if  $P_h$  is higher than  $P_c$ , such that the excessive harvested energy is immediately consumed on useful work rather than wasted.

In practice, however, there does not exist a system that can adjust its power consumption instantaneously to the harvested power without any overheads. Any performance scaling costs a small amount of time and energy overheads, which a system cannot afford without any energy storage. Therefore, a minimum storage is still required, normally in the form of decoupling or parasitic capacitance, to provide a small but sufficient amount of energy for scaling performance and adapting power consumption.

In order to achieve power neutrality, a system has to adapt its performance and hence power consumption. Performance scaling can be achieved by hardware controlling, such as Dynamic Frequency Scaling (DFS) [53], Dynamic Voltage and Frequency Scaling (DVFS) [87], or switching on/off load elements [87, 88] (also known as Dynamic Power Management, DPM [89] or hot-plugging). Apart from these achieved methods, duty-cycle scaling and task scheduling are also choices for changing performance and consumption, though they have not been implemented in current research yet.

## 2.5.2 Recent Approaches

The concept of PN computing is proposed in [53] and implemented on a Texas Instrument MSP430FR5739 MCU without an external energy buffer. As shown in Figure 2.8, the executing load is directly connected to a regulated energy harvesting source. The control scheme in [53] utilises DFS with a voltage feedback. Specifically, two voltage thresholds,  $V_{dec}$  and  $V_{inc}$ , are set for detecting voltage variance caused by power inequality and then scaling performance accordingly. In order to respond fast to power difference, the capacitance is reduced to  $19\mu\text{F}$ , which is only the parasitic and on-board decoupling capacitance. When  $P_h(t) > P_c(t)$  and the operating voltage  $V_{cc}$  increases rapidly due to the small capacitance and reaches  $V_{inc}$ , the MCU increases its operating frequency resulting in faster computing speed and higher power consumption, and



also increases the thresholds between which the new voltage value is contained; and vice versa, a reverse procedure is executed for  $P_h(t) < P_c(t)$ . In a word, this control scheme is trying to make the operating voltage stable around a desired value so that  $P_h(t)$  equals  $P_c(t)$  approximately.

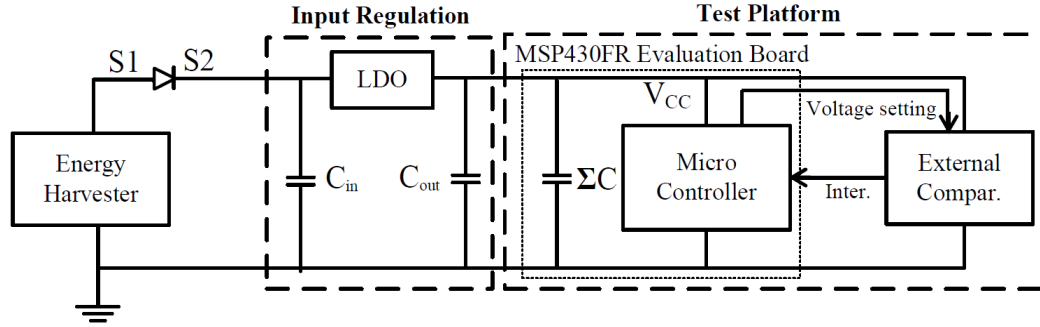


FIGURE 2.8: Architecture of an example power neutral system based on TI MSP430FR platform (taken from [53]).

A similar control scheme is adopted in [87] where the platform is an MP-SoC adopting DVFS and DPM, which leads to higher performance, higher power consumption, and more operating points than the MCU in [53]. A 47mF supercapacitor is used for safely overcoming performance switching where the power consumption of the board is normally above 2W. As an illustration for how to scale performance by DVFS and DPM, Figure 2.9 presents an example application profile of ‘power consumption vs performance’ when DVFS and DPM applied on a heterogeneous multi-processor system-on-chip (MP-SoC) platform. The SoC used in this platform is the Samsung Exynos5422 big.LITTLE SoC with four ‘big’ high-performance A15 cores and four ‘LITTLE’ low-power A7 cores. In this case, the performance refers to the speed of executing this application for one time and is proportional to the operating frequency under a certain core configuration. As shown in the figure, each performance level (a pair of frequency and core status, also named as an operating point) requires a certain power consumption. At run-time, the system dynamically switch its performance among these operating points so as to timely match  $P_c(t)$  with  $P_h(t)$ .

There are three advantages in this kind of PN control scheme. First, the voltage is stabilized so it can offset ephemeral power drops which cause insufficient voltage supply and power failures, and therefore the lifetime increases (e.g. reported by 4-88% in [53]). Second, as power neutral computing eliminates many elements that required in EN systems, such as large energy storage, power converters and MPPT units, the size and cost of devices is reduced and the number of power consumption components also decreases. Third, if powered by a solar panel and the operating voltage range encompasses the MPP of the given solar panel, the system embraces an intrinsic MPPT characteristic as it can stabilize the voltage around a target value.

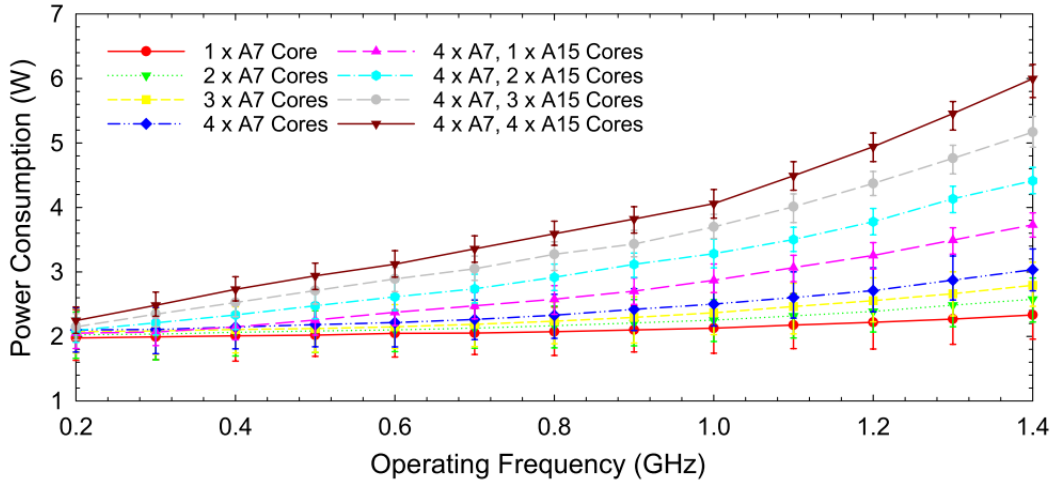


FIGURE 2.9: Board power consumption of ODROID XU4 vs operating frequency and core configurations, running CPU intensive application Raytrace (taken from [87]).

Similarly, Wang *et al.* [88] propose a storage-less and converter-less approach which can be classified as a power neutral system. In this design, a  $47\mu\text{F}$  bulk capacitor is equipped with a  $3.29\text{mW}$  non-volatile MCU and up to  $16.5\text{mW}$  peripherals. This capacitor is also small enough compared to the  $19\mu\text{F}$  capacitance operating with an up to  $3\text{mW}$  MCU in [53]. An external MPPT controlling element dynamically adjusts the power duty-cycle for the non-volatile load in order to match the harvested current and the consumed current, and hence power neutrality is met.

One disadvantage of power neutral computing is that it has to passively scale its power consumption as well as its performance, causing large variations in performance. However, this might not be good in terms of the overall forward progress. In the next chapter, a preliminary analyse is explained about how the forward progress is improved when the capacitor size is increased, while not violating the merits of PN computing.

## 2.6 Summary

This chapter introduces a background of energy harvesting techniques, summarises the evolution of energy storage used in energy harvesting computing, and reviews the existing methodologies of battery-less energy harvesting computing.

EN computing emphasizes the continuous activity of devices over a long-term duration (e.g. several days, one year) by buffering harvested energy in large energy storage and adapting energy consumption "reluctantly". However, large energy buffers, usually in the form of batteries or large supercapacitors, are demanded for EN operations, whereas such large energy storage limits device lifespans, increases the cost, mass, dimensions of devices, and bring pollution and maintenance issues. This contradicts the design requirements of ubiquitous sensor deployments.

To circumvent the limitations in EN computing, intermittent computing is recently developed. Intermittent computing continues computation after the supply fails rather than restarts from the beginning of programs. Hence, intermittent computing devices can achieve forward execution despite frequent power failures with only minimum storage (e.g. a decoupling capacitor) to secure successful saving and restoring operations of computing states between volatile and non-volatile components. Based on intermittent computing, PN computing introduces run-time performance adaptation to match power consumption with harvested power, such that the number of saving and restoring operations can be reduced and application execution speed is increased.

However, with minimised storage, an intermittent computing device has to frequently wake up, execute **shortly**, and halt when the harvested power is less than the load power consumption, consuming much energy in managing system states. As for PN computing, volatile power from environment results in significant performance variations, which then cause performance loss. The remaining part of this thesis reports a study on how to mitigate these two problems and improve system execution speed by adding a small amount of energy storage without significantly affect device dimensions.



## Chapter 3

# Effect of Energy Storage Sizing on IPS Performance

With the goal of minimising device dimensions and interruption periods, most IPS approaches adopt only a minimum amount of energy storage [29–32, 32, 33, 90], e.g. a decoupling capacitor. This is typically just sufficient for the most energy-expensive atomic operation. However, our assertion is that this can be *inherently inefficient in terms of time and energy*. We show that a system with minimum energy storage frequently goes through a cycle of: wake up, restore state, execute program, save state, and halt. We propose that provisioning *slightly more* energy storage can prolong the operating cycles, reduce the frequency of interruptions, and hence improve forward progress.

However, the relationship between IPS energy storage capacitance and forward progress has not previously been defined. Due to the computational speedup of reactive IPSs over proactive IPSs as discussed in Section 2, we focus on reactive IPSs in this chapter. We develop an experimentally-validated model of reactive IPSs to estimate forward progress. Taking advantage of the model, we explore the effect of energy storage capacitance on forward progress with respect to supply current and volatile state size. The main contributions in this chapter can be summarised as:



- A reactive IPS model which accurately estimates forward progress; experimental validation based on a TI MSP430FR6989 MCU shows a 0.5% mean absolute percentage error across a range of current inputs and energy storage capacitance.
- An exploration based on the model, where **we analyse** the energy storage sizing effect on forward progress with respect to supply current and volatile state size, showing up to 65% forward progress improvement.

As discussed in Chapter 1, *forward progress* denotes the computation beneficial to the progress of the active application, excluding lost progress due to power failures and

TABLE 3.1: Model parameters of reactive IPS

Input Parameters	
$I_{\text{harv}}$	Energy harvester current supply
$C$	Energy storage capacitance
Configuration Parameters	
$I_{\text{exe}}$	Execution current draw
$I_{\text{lpm}}$	Low-power mode current draw
$I_r$	Restore current draw
$I_s$	Save current draw
$I_{\text{leak}}$	Leakage current draw
$V_r$	Restore voltage threshold
$V_s$	Save voltage threshold
$T_r$	Restore time overhead
$T_s$	Save time overhead
Output Parameter	
$\alpha_{\text{exe}}$	Normalised forward progress

state-saving and -restoring operations [28]. The amount of forward progress directly determines application performance, e.g. program iteration rate or task completion time. In this chapter, to allow fair comparison, we define normalised forward progress as the ratio of the effective execution time to the total elapsed time, without being restricted to a specific workload.

The rest of this chapter is organised as follows. The reactive IPS model is proposed in Section 3.1. The exploration on the energy storage sizing effect is presented in Section 3.2. Section 3.3 validates the proposed model and the energy storage sizing effect. Finally, Section 3.4 summarises this chapter.

### 3.1 Reactive IPS Modelling

To facilitate the understanding and exploration of reactive IPSs, we present a model which outputs the normalised forward progress  $\alpha_{\text{exe}}$ . Parameters of this model are listed in Table 3.1. The model assumes that all configuration parameters remain constant. We assume that all input and configuration parameters remain constant in this model derivation, but later provide a dynamic process for cases where parameters change dynamically.

For brevity,  $I_{\text{in}}$  denotes the usable input current as expressed in Equation 3.1. The effect of capacitor leakage current,  $I_{\text{leak}}$ , is discussed at the end of Section 3.1.2.

$$I_{\text{in}} = I_{\text{harv}} - I_{\text{leak}} \quad (3.1)$$

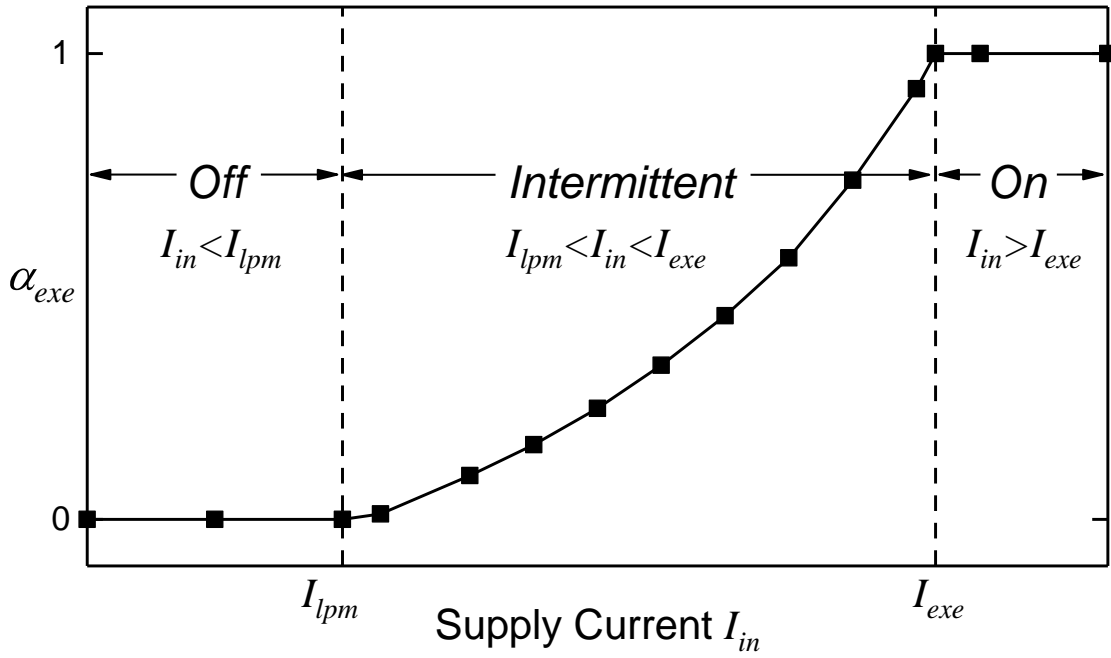
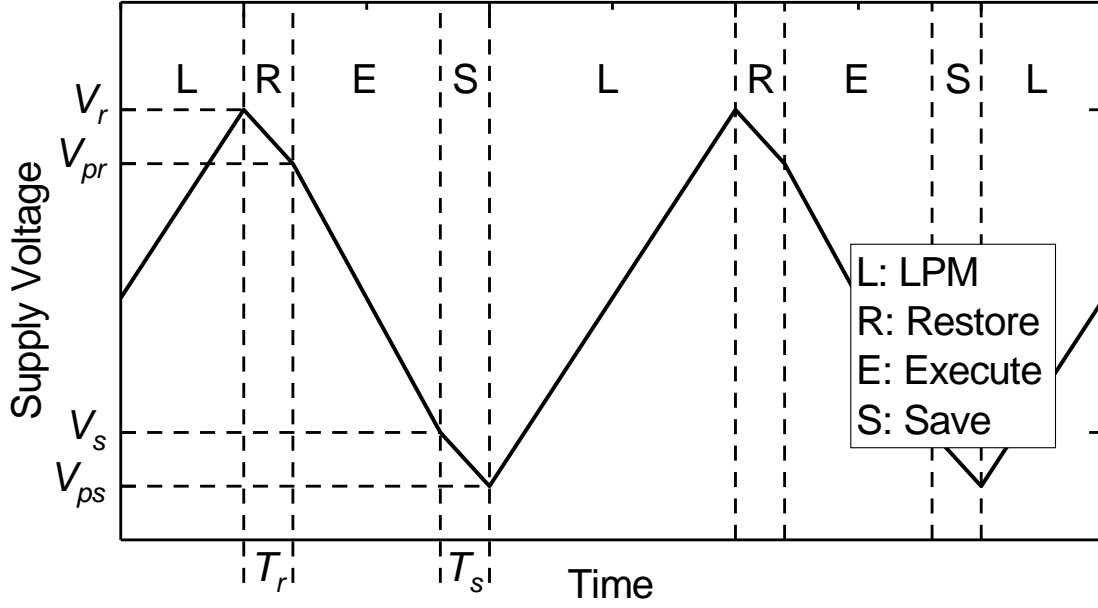


FIGURE 3.1: Operating modes of reactive IPSs, and achieved forward progress against supply current.

### 3.1.1 Operating Modes of Reactive IPS

The behaviour of reactive IPSs can be classified into three operating modes depending on the supply current, as shown in Figure 3.1. These are differentiated by the relationship between input current  $I_{in}$  and the system's current draw in its low-power mode (LPM) or active modes, i.e.  $I_{lpm}$  and  $I_{exe}$ . We define the three modes as:

- *Off* mode: When  $I_{in} < I_{lpm}$ , the system stays inactive. The supply voltage  $V_{cc}$  cannot rise above the restore threshold  $V_r$  to wake the system and start execution. The LPM current  $I_{lpm}$  includes the consumption of voltage monitoring circuits and system idle current.
- *On* mode: When  $I_{in} > I_{exe}$ , the system executes constantly as the supply voltage  $V_{cc}$  never drops below  $V_s$ .  $V_{cc}$  grows until  $I_{in}$  and  $I_{exe}$  are in equilibrium, which may result from  $I_{in}$  decreasing due to poor impedance matching, or  $I_{exe}$  increasing due to either greater current draw at higher voltage or dissipation through overvoltage protection circuits.
- *Intermittent* mode: When  $I_{lpm} < I_{in} < I_{exe}$ , the system executes intermittently after  $V_{cc} > V_r$  and before  $V_{cc} < V_s$ .  $V_{cc}$  can rise above  $V_r$  and the system starts execution. However, the stored energy is then consumed by the load as  $I_{in} < I_{exe}$ , causing  $V_{cc}$  to eventually drop below the save threshold  $V_s$ , where the system saves its state and enters LPM. The system stays in LPM until  $V_{cc}$  rises to  $V_r$

FIGURE 3.2: Operating cycles in the *Intermittent* mode.

again and then resumes execution. In general, a higher  $I_{in}$  leads to more forward progress in this mode, but the exact relationship between  $I_{in}$  and forward progress requires further analysis.

### 3.1.2 Formulating Forward Progress

Next, we derive formulations to calculate  $\alpha_{exe}$  from  $I_{in}$  and energy storage capacitance  $C$ . We then explore the effect of capacitor leakage on maximum forward progress.

In the *On* and *Off* modes, the normalised forward progress is trivial to find (simply 1 and 0 respectively). In the *Intermittent* mode, as shown in Figure 3.2, the system goes through four intervals in turn, i.e. charging, restoring, executing, and saving, with current consumption of  $I_{lpm}$ ,  $I_r$ ,  $I_{exe}$ , and  $I_s$  in each interval respectively. The normalised forward progress, i.e. effective execution time ratio, is indicated as  $T_{exe}/T_{cycle}$ , where  $T_{exe}$  is the time spent on effective execution in one operating cycle and  $T_{cycle}$  is the period of operating cycles. Hence, the forward progress given all supply levels is expressed as:

$$\alpha_{exe} = \begin{cases} 0 & , \text{ Off } (I_{in} < I_{lpm}) \\ \frac{T_{exe}}{T_{cycle}} & , \text{ Intermittent } (I_{lpm} < I_{in} < I_{exe}) \\ 1 & , \text{ On } (I_{in} > I_{exe}) \end{cases} \quad (3.2)$$

In the following analysis, we focus on deriving  $T_{exe}/T_{cycle}$  in the *Intermittent* mode. Let  $V_{pr}$  (post-restore) and  $V_{ps}$  (post-save) denote the voltage after restoring and saving



operations. Referring to Table 3.1 and Figure 3.2,  $V_{pr}$  and  $V_{ps}$  can be calculated as:

$$V_{pr} = V_r + \frac{T_r(I_{in} - I_r)}{C} \quad (3.3)$$

$$V_{ps} = V_s + \frac{T_s(I_{in} - I_s)}{C} \quad (3.4)$$

With Equation 3.3, the time spent on effective execution  $T_{exe}$  in one operating cycle can be expressed as:

$$\begin{aligned} T_{exe} &= \frac{C(V_{pr} - V_s)}{I_{exe} - I_{in}} \\ &= \frac{C(V_r - V_s) + T_r(I_{in} - I_r)}{I_{exe} - I_{in}} \end{aligned} \quad (3.5)$$

Analogously, with Equation 3.4, the charging interval can be described as:

$$\begin{aligned} T_{charge} &= \frac{C(V_r - V_{ps})}{I_{in} - I_{lpm}} \\ &= \frac{C(V_r - V_s) - T_s(I_{in} - I_s)}{I_{in} - I_{lpm}} \end{aligned} \quad (3.6)$$

With Equation 3.5 and Equation 3.6, the period of an operating cycle is:

$$\begin{aligned} T_{cycle} &= T_{charge} + T_r + T_{exe} + T_s \\ &= \frac{C(V_r - V_s) + T_s(I_s - I_{lpm})}{I_{in} - I_{lpm}} + \frac{C(V_r - V_s) + T_r(I_{exe} - I_r)}{I_{exe} - I_{in}} \end{aligned} \quad (3.7)$$

Finally, combining Equation 3.3 to Equation 3.7, we obtain normalised forward progress  $\alpha_{exe}$  in the *Intermittent* mode ( $I_{lpm} < I_{in} < I_{exe}$ ) as:

$$\begin{aligned} \alpha_{exe} &= \frac{T_{exe}}{T_{cycle}} \\ &= \left[ \frac{C(V_r - V_s) + T_r(I_{in} - I_r)}{I_{exe} - I_{in}} \right] / \\ &\quad \left[ \frac{C(V_r - V_s) + T_s(I_s - I_{lpm})}{I_{in} - I_{lpm}} + \frac{C(V_r - V_s) + T_r(I_{exe} - I_r)}{I_{exe} - I_{in}} \right] \end{aligned} \quad (3.8)$$

In the numerator  $T_{exe}$ ,  $C(V_r - V_s)$  represents the amount of charge in the capacitor available for restoring and executing.  $T_r(I_{in} - I_r)$  represents the charge used by a restore operation.  $I_{exe} - I_{in}$  is the rate of charge consumption from the energy storage during execution.

Also, the ratio of the time overhead on state-saving and -restoring operations to the total elapsed time  $T_{rs\%}$  can be deduced as:

$$T_{rs\%} = \frac{T_r + T_s}{T_{cycle}} \quad (3.9)$$

$$= (T_r + T_s) / \left[ \frac{C(V_r - V_s) + T_s(I_s - I_{lpm})}{I_{in} - I_{lpm}} + \frac{C(V_r - V_s) + T_r(I_{exe} - I_r)}{I_{exe} - I_{in}} \right]$$

Equation 3.9 can describe the impact of state-saving and -restoring overhead with respect to  $C$  and  $I_{in}$ .

To explore the effect of energy storage on forward progress, we need to analyse  $d\alpha_{exe}/dC$ . Here, if we assume that  $I_{leak}$  remains constant,  $\alpha_{exe}$  keeps increasing and approaches  $(I_{in} - I_{lpm})/(I_{exe} - I_{lpm})$  when energy storage capacitance  $C$  increases. Defining  $(I_{in} - I_{lpm})/(I_{exe} - I_{lpm})$  as  $\alpha_{exe\_ideal}$ ,  $\alpha_{exe} = \alpha_{exe\_ideal}$  is an ideal case, where state-saving and -restoring overheads are absent.

In an electrolytic capacitor, however,  $I_{leak}$  typically increases with  $C$  with the following relationship [91]:

$$I_{leak} = kCV_{cc} \quad (3.10)$$

where  $k$  is a constant normally in a range of 0.01–0.03 A/(FV). Combining Equation 3.10 with Equation 3.1,  $dI_{in}/dC$  is  $-kV_{cc}$ , meaning  $I_{in}$  decreases linearly as  $C$  increases. Thus, when  $C$  increases,  $\alpha_{exe}$  keeps approaching  $\alpha_{exe\_ideal}$  while  $\alpha_{exe\_ideal}$  decreases. Hence, we believe that there is a capacitance value that leads to the maximum  $\alpha_{exe}$  considering  $I_{leak}$  increases with  $C$ .

### 3.1.3 Dynamic process

The above model assumes all parameters are constant, which is useful for fast exploration in cases where this can be considered to approximately hold true (this is used for the analysis of principal sizing effects presented in Section 3.2). For dynamically-varying parameters (e.g. a dynamic harvesting profile), we also implement a dynamic process, where the supply voltage is calculated with system's current flows and energy storage capacitance across small time steps, hence updating system state accurately. This is used for the exploration of real-world energy conditions in Section 4.3.

## 3.2 Exploration of Energy Storage Sizing

In this section, we configure the reactive IPS model presented in Section 3.1 to approximate a real IPS platform, and then present an exploration of the relationship between  $\alpha_{exe}$  and  $C$  with respect to supply current  $I_{harv}$  and volatile state size.

### 3.2.1 Model Configuration

We configured the model with an empirical capacitor model and experimentally measured load characteristics.

#### 3.2.1.1 Energy Storage

The energy storage is represented as an ideal capacitor with empirically defined leakage current. Its terminal voltage is directly applied to the load, so is modelled as:

$$C \frac{dV_{cc}}{dt} = I_{harv} - I_{load} - I_{leak} \quad (3.11)$$

where  $I_{load}$  is the current consumption of the load. In this exploration, we refer to the empirical  $I_{leak}$  of AVX TAJ low-profile series tantalum capacitors, which depends on capacitance  $C$ , rated voltage  $V_{rated}$ , and terminal voltage  $V_{cc}$  [91]:

$$I_{leak} = 0.01\lambda C V_{rated} \quad (A) \quad (3.12)$$

where  $\lambda$  denotes the ratio of the actual current leakage at  $V_{cc}$  to the current leakage at  $V_{rated}$ , and  $\lambda$  is approximated as:

$$\lambda = 0.05 \times 20^{\frac{V_{cc}}{V_{rated}}} \quad (3.13)$$

We assume a typical load of  $< 4.0$  V so, to minimise leakage, we select a device with  $V_{rated} = 10$  V so as to operate between 25-40% of its rated voltage [91].

#### 3.2.1.2 Intermittent Computing Load

We configured the load with experimentally measured current draws and time overheads. We only consider computational loads in this study, as handling of peripherals in intermittent systems is still an ongoing research topic [92, 93].

We implemented and parameterised a reactive IPS [34] on a TI MSP430FR6989-based development board. The load parameters were profiled with the MCU running a Dijkstra path finding algorithm with 1696 B RAM usage at 8 MHz. The supply voltage monitoring circuits use the MCU's internal comparator and an external  $3\text{ M}\Omega$  voltage divider. The restore and save voltage thresholds are set as  $V_r = 2.4$  V and  $V_s = 2.1$  V respectively. The MCU shutdown voltage  $V_{off}$  is 1.8 V.

The measured current draws and time overheads are listed in Table 3.2. The current draw was profiled with experimental measurements at a range of supply voltages. The variation of  $I_{lpm}$  between  $V_{off}$  (1.8 V) and  $V_r$  (2.4 V) is 2%, and for  $I_{exe}$  between  $V_s$  (2.1 V)

TABLE 3.2: Profiled MCU parameters

Parameter	Value
$I_{\text{exe}}$	887 $\mu\text{A}$
$I_{\text{ipm}}$	26 $\mu\text{A}$
$I_r$	971 $\mu\text{A}$
$I_s$	811 $\mu\text{A}$
$T_r$	1.903 ms
$T_s$	1.880 ms

and 3.3 V is 1.5%.  $I_{\text{exe}}$  also has a run-time variation of 2.8% due to a variable memory access rate. As these variations of  $I_{\text{exe}}$  and  $I_{\text{ipm}}$  in their effecting voltage range are minor, we therefore omit the variations and use the mean of  $I_{\text{exe}}$  and  $I_{\text{ipm}}$  in the model.  $I_r$  and  $I_s$  are measured at  $V_r$  and  $V_s$  respectively.

Given the voltage thresholds and the current consumption, the minimum energy storage capacitance is 6.2  $\mu\text{F}$ . This guarantees that a save and restore operation can complete even if the incoming supply current drops instantaneously to zero. Moreover, the model parameters in Table 3.2 are given as an example, and can be changed for different load characteristics. For example,  $T_r$  and  $T_s$  can be tuned for different volatile state sizes.

### 3.2.2 Sizing Energy Storage to Improve Forward Progress

#### 3.2.2.1 Impact of Supply Current

Increasing energy storage capacitance beyond the minimum one can improve forward progress by reducing the frequency of power interruptions, but this improvement may be offset by increased leakage. Figure 3.3 shows the relationship between forward progress and energy storage capacitance for a range of constant supply currents. In this section, we denote the capacitance that leads to the maximum forward progress  $\alpha_{\text{exe}}$  as  $C_{\alpha_{\text{max}}}$ .  $C_{\alpha_{\text{max}}}$  for each current value is also shown in Figure 3.3.

The minimum capacitance (dashed line in Figure 3.3) is calculated to deliver correct operation even if the supply current instantaneously drops to zero. If it does not drop to zero, this means that correct operation could have continued even with a smaller capacitance given that the current supply keeps providing energy during execution, though designing a system in this way would be inadvisable owing to unpredictability of the supply. This property is illustrated in Figure 3.3, in the area on the left of the dashed line. It may be observed that, for each of the current values, there is a sudden drop-off towards zero forward progress. This illustrates the hazard of setting the capacitance too small: the stored energy is too low to allow a restore and save to be

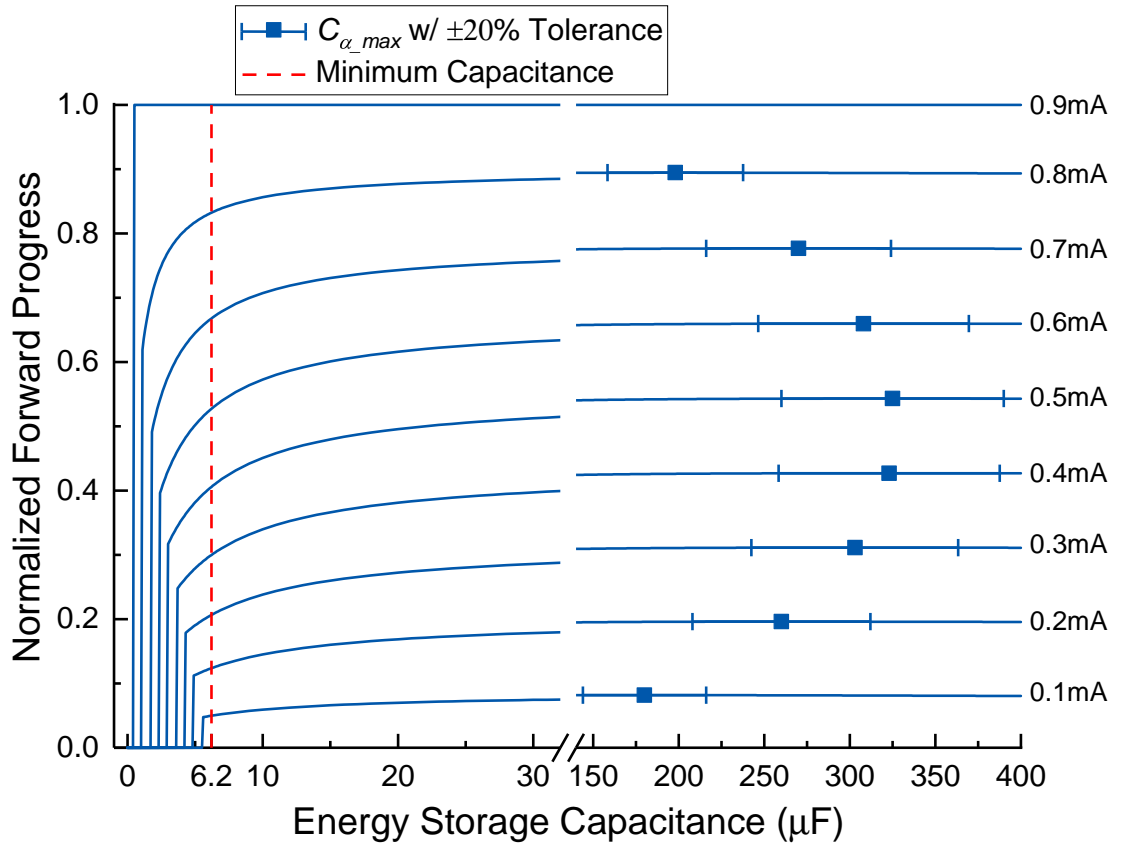


FIGURE 3.3: Forward progress against energy storage capacitance at different levels of constant supply current. Error bars around  $C_{\alpha_{\max}}$  denote the impact of typical  $\pm 20\%$  capacitance tolerance. The 30–150  $\mu\text{F}$  range is omitted as forward progress in that range increases monotonically.

undertaken. The reason for this step change rather than a continuous change is that the implemented IPS only performs one restore operation in the first execution cycle after a reboot and enters a low-power mode with volatile state retained after a save operation. Hence the energy used for restoring state is then used for effective execution in the following operating cycles as long as the supply voltage recovers to the restore threshold without a power interruption.

Typically, commercially-available capacitors have a  $\pm 20\%$  tolerance. The effect of this variation on maximum forward progress is shown to be negligible ( $< 0.23\%$ ) in Figure 3.3. However, it must be pointed out that the effect would be much more pronounced if operating at the minimum capacitance as the variation of forward progress is larger with smaller capacitance values. Thus, it is recommended that a tolerance is considered when designing IPSs with minimum capacitance.

Figure 3.4 shows that an improvement in forward progress of up to 65% can be achieved when using  $C_{\alpha_{\max}}$  instead of the minimum. However, it may not be desirable to set the capacitance solely for maximising forward progress, because there are often trade-offs

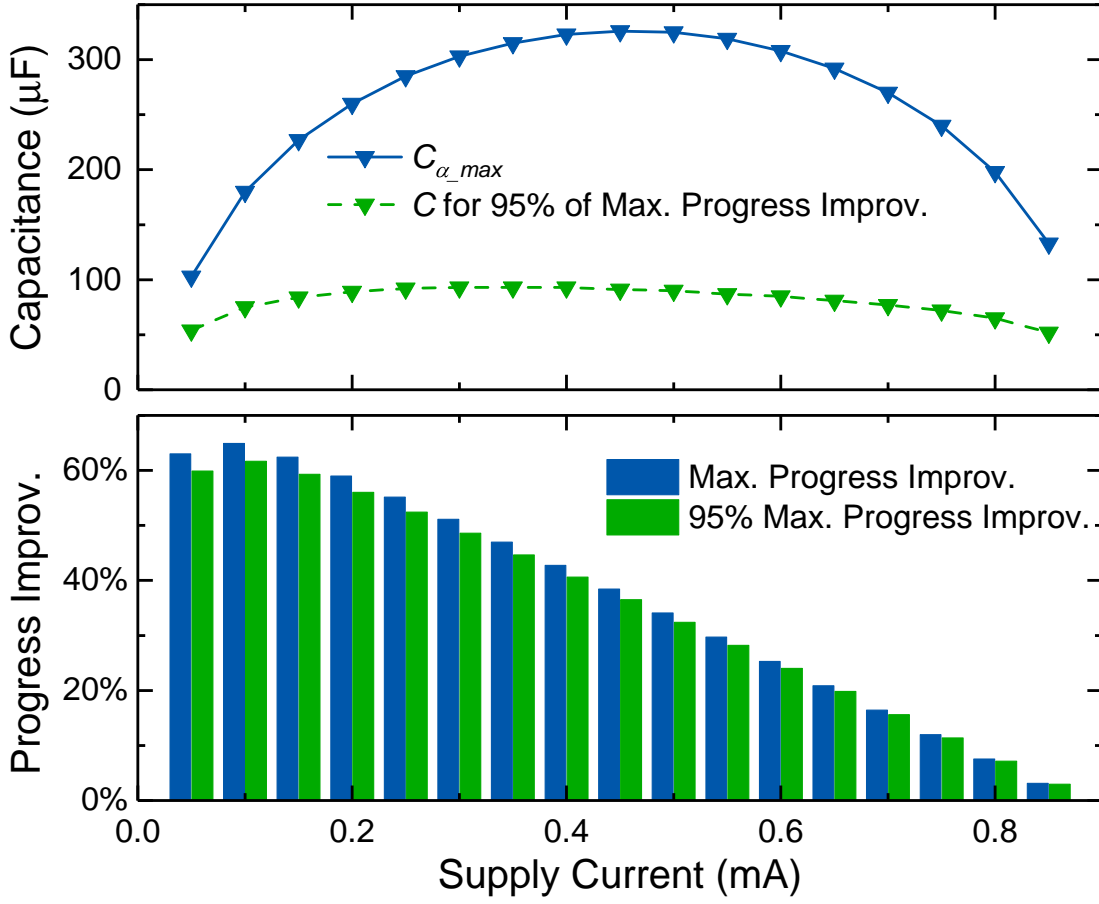


FIGURE 3.4: Maximum forward progress improvement by sizing energy storage given a spectrum of supply current (normalised by the minimum capacitance case), with the corresponding capacitance for maximum and sub-maximum (95% of maximum) forward progress improvement.

with other factors including increased interruption periods and dimensions (later explored in Section 4.3.3). In real-world energy source conditions, the supply current varies across this spectrum, and hence leads to an overall progress improvement based on its supply distribution. This improvement exists only when the device operates in the *Intermittent* mode, since the device keeps either inactive in the *Off* mode or active in the *On* mode without the need for restoring and saving state. Correspondingly,  $C_{\alpha\_max}$  is also plotted against supply current. While a large improvement can be delivered with  $C_{\alpha\_max}$ , as shown in Figure 3.4, 95% of this gain can still be obtained with significantly smaller capacitances (mean 31% of  $C_{\alpha\_max}$ ). For example, reducing from 325  $\mu\text{F}$  to 90  $\mu\text{F}$  gives 95% of the maximum improvement with a 0.5 mA supply.

### 3.2.2.2 Impact of Volatile State Size

The size of volatile state differs across applications with different amounts of RAM usage, and hence incurs varying time and energy overheads for restore and save operations. We measured time overheads of restore and save operations in the minimum

TABLE 3.3: Linear scaling range of volatile state size and restore/save time overheads

State Size (Registers + SRAM)	Restore Time	Save Time
64B + 160B (lower bound)	232 $\mu$ s	208 $\mu$ s
64B + 2048B (upper bound)	2.298 ms	2.274 ms

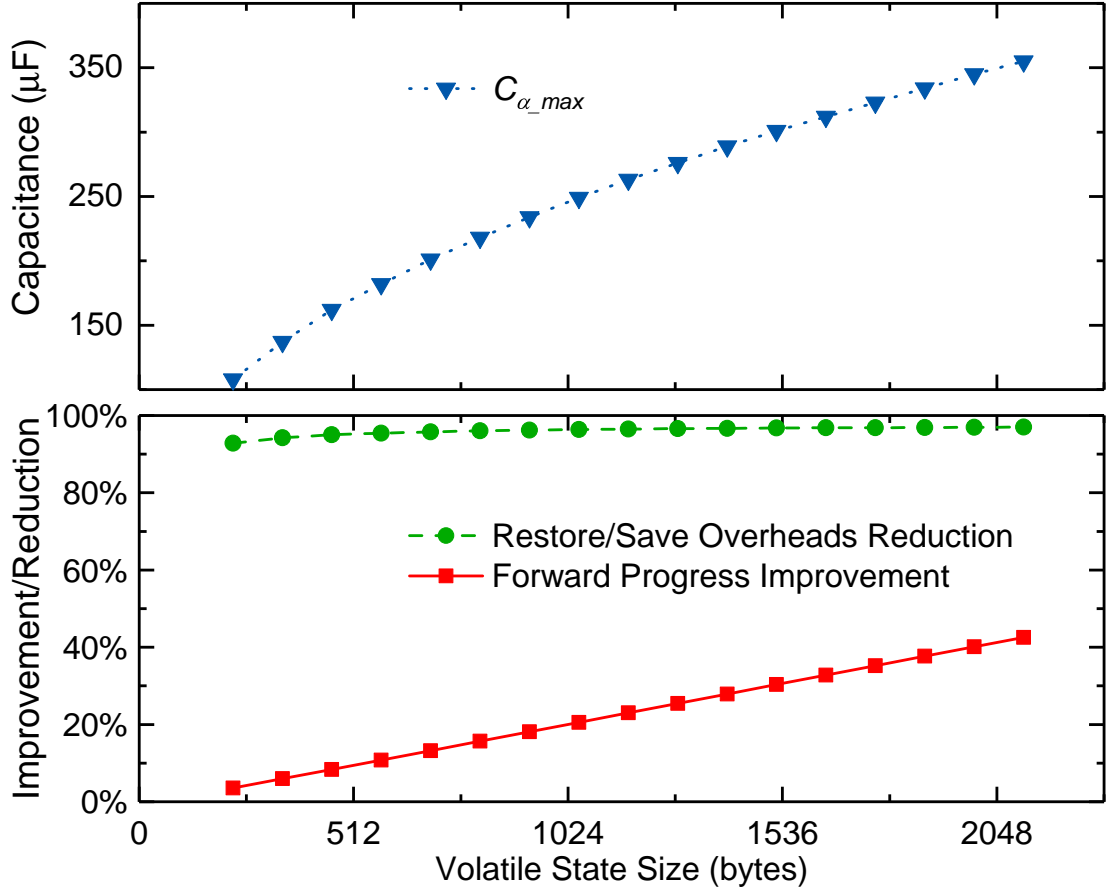


FIGURE 3.5: Impact of RAM usage (linear to restore/save overheads) on sizing energy storage with 0.4 mA current supply. Improvement and reduction are normalised by the minimum capacitance case.

case (64B register data and a 160B stack) and the maximum case (64B register data and a full 2048B RAM) respectively as shown in Table 3.3. As these time overheads are expected to be linear to the state size [94], the model can be tuned for various volatile state sizes by linearly scaling the profiled values.

An example of this is plotted in Figure 3.5. The forward progress improvement by sizing energy storage increases with the volatile state size, and  $C_{\alpha_{max}}$  grows accordingly. The improvement becomes insignificant when the volatile state size is small because the restore and save overheads are already negligible. For example, when the workload uses the least volatile state (the leftmost point), the maximum progress improvement is only 3.6% although the restore and save overheads are reduced by 93%.

Where the size of the volatile state may vary at run time, a different capacitor size within the range 108–355  $\mu\text{F}$  may have been recommended (Figure 3.5). However, as can be seen from Figure 3.3, there is a minimal difference in forward progress across this range. In the worst case, a 2.7% reduction results from setting  $C_{\alpha_{\max}}$  for the minimum state size, while running with the largest state size.

### 3.3 Experimental Validation

This section compares experimental forward progress with the modelled one to validate the proposed reactive IPS model and the presented energy storage sizing effects.

#### 3.3.1 Experiment Setup

We validated our model on the IPS system that we parameterised for exploration (Section 3.2), so its IPS method, voltage thresholds, current draws, and workload are as mentioned. The on-board decoupling capacitance was measured as 10.0  $\mu\text{F}$ , and hence was the minimum capacitance that could be tested. Further capacitance was added to provide extra energy storage up to a maximum of 43  $\mu\text{F}$ , as forward progress with this capacitance can approximate  $\alpha_{\text{exe\_ideal}}$  (an upper bound), which is linear to supply current  $I_{\text{in}}$  when  $I_{\text{ipm}} < I_{\text{in}} < I_{\text{exe}}$  (mentioned in Section 3.1.2).

In the experiment, the task completion rate, i.e. the number of tasks completed per second, is used as the metric of forward progress rather than the effective execution time ratio. To gain the task completion rate from the model, we multiply the normalised forward progress (execution time ratio) generated from our model by the completion rate when the system executes constantly.

#### 3.3.2 Model Validation

To validate the accuracy of our model, we powered the device with a range of supply currents (0–0.9 mA) to operate the device in *Intermittent* mode, and repeated the tests with three energy storage capacities: a) 10.0  $\mu\text{F}$  decoupling capacitance; b) 21.5  $\mu\text{F}$  (11.5  $\mu\text{F}$  added); c) 43.0  $\mu\text{F}$  (33.0  $\mu\text{F}$  added). We compared the actual forward progress against predictions generated from our model. As shown in Figure 3.6, the model-generated forward progress matches closely with the experimental results with only 0.5% mean absolute percentage error across all the results. Hence, the proposed model is able to accurately estimate forward progress for design exploration.



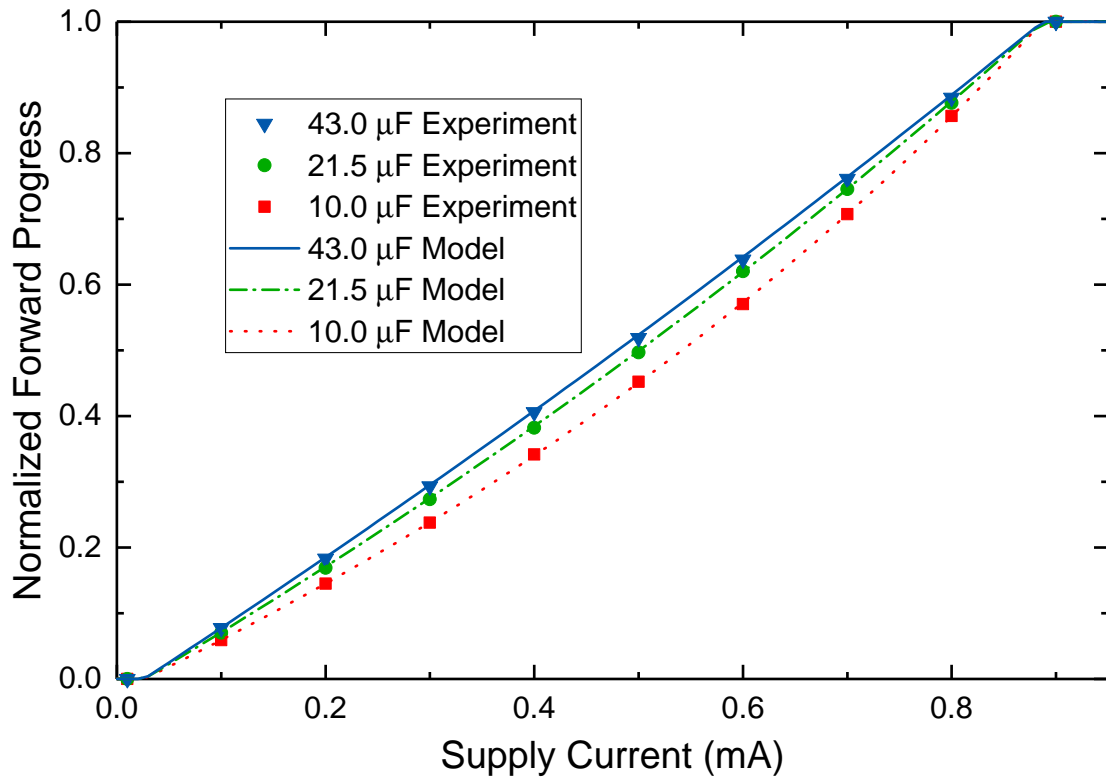


FIGURE 3.6: Model validation with experimental and modelled forward progress.

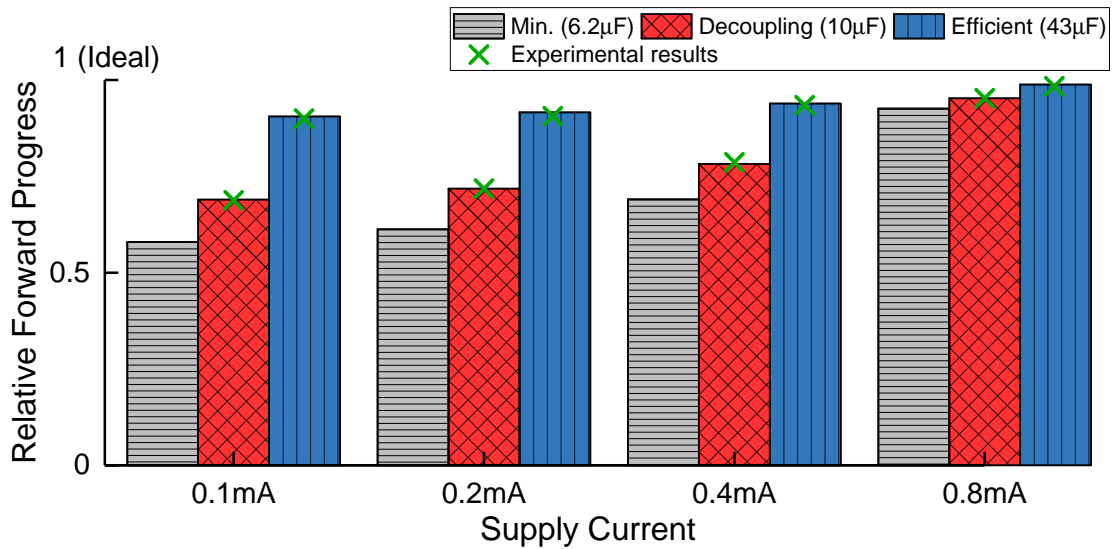


FIGURE 3.7: The relationship between energy storage capacitance and IPS forward progress, for various supply currents.

### 3.3.3 Validation of Sizing Effects

As shown with modelled and experimental results in Figure 3.7, the efficiently-sized energy storage capacitance ( $43\text{ }\mu\text{F}$ ) improves forward progress by up to 55% and 30% compared against using the minimum and decoupling capacitance respectively. We notice that this improvement becomes significant when the supply current attenuates because the save and restore overheads consume a larger proportion of the available energy. Also, the efficiently-sized capacitor achieves at least 90% of the ideal forward progress across the tested supply currents. The ideal case only switches between LPM and execution, without restoring and saving overheads (explained in Section 3.1.2). These results illustrate the importance of this technique, in particular for conditions where the supply current is low.

A bit more discussion on the results?

## 3.4 Summary

While conventional IPSs have used minimal levels of capacitance, this chapter explored the energy storage sizing effect on IPS's forward progress. A model of reactive IPSs was proposed to facilitate the understanding and design exploration of IPSs, explaining a mathematical relationship between forward progress and system parameters, e.g. energy storage capacitance and supply current. We then configured the proposed model with an experimentally-profiled IPS platform, and utilised it to explore the energy storage sizing effect. The exploration results showed that sizing energy storage can improve forward progress by up to 65%. We also found that this improvement becomes significant when the supply current attenuates, which implies the importance of sizing energy storage in energy harvesting conditions where the supply current is low. The model was experimentally validated across a range of supply current and energy storage capacitance, showing a mean absolute percentage error of 0.5%. We conclude that adding a relatively small amount of energy storage can significantly improve forward progress.

The proposed model has demonstrated its potential for design exploration of IPSs. In the next chapter, we will incorporate the model in a simulation framework that recommends an appropriate energy storage size in real-world energy conditions.

## Chapter 4

# Energy Storage Sizing Approach for Deploying IPSs

Having analysed the sizing effect of energy storage on IPS performance, this chapter focusses on the energy storage sizing effect when deploying IPSs under real-world energy conditions, and providing an approach that recommends an energy storage size.

As presented in Chapter 3, providing more energy storage than the minimum can improve forward progress. However, it was also revealed in Section 3.2.2 that to obtain the maximum forward progress improvement with  $C_{\alpha_{\max}}$  can take  $3.2\times$  capacitance compared to the one that achieves 95% of the maximum improvement. A larger capacitor typically occupies more physical space, which may contradict with some IPS applications that require miniaturised size, e.g. implantable medical devices [95]. Also, a larger capacitor takes longer to recharge, hence prolonging the period of power interruption and compromising reactivity. A systematic method is in need to decide the energy storage size for deploying IPSs, considering a trade-off of multiple design factors.

However, current tools for IPSs (reviewed in Section 4.1) are not practical for fast estimation of forward progress in a long-term deployment, and lack a method of sizing energy storage to improve forward progress while moderating the physical size and interruption periods. This chapter presents an approach for sizing energy storage in IPSs, quantifying and trading off forward progress, capacitor volume, and interruption periods. With the model in Section 3 integrated, the proposed sizing approach is able to fast explore the relationship between the energy storage size and forward progress with long-term real-world energy conditions. An example cost function is also provided to trade off multiple design factors so as to recommend an energy storage size. The main contributions in this chapter are as follows:

- A model-based sizing approach that recommends appropriate energy storage capacitance in IPSs (Section 4.2).
- An evaluation of the impact of sizing in real-world conditions using real energy availability data (Section 4.3). This includes a cost function-based method for trading off parameters. In an example, this reduced capacitor volume and interruption periods by 83% and 91% respectively, while sacrificing 7% of forward progress, compared to solely maximising forward progress.



The associated simulation tool, coded in C, is available open-source <sup>1</sup>.

The remainder of this chapter is organised as follows. Section 4.1 reviews the current tools and models for IPSs. Section 4.2 proposes an approach for sizing energy storage in IPS deployment. Section 4.3 configures and demonstrates the proposed sizing approach with real-world energy source data, with forward progress, capacitor volume, and interruption periods being estimated and traded off. Finally, Section 4.4 summarises this chapter.

## 4.1 Related Work

To explore forward progress of IPSs, simulation tools need to represent transient operation (timescales of  $\mu\text{s}$ -ms) as well as long-term overall performance (from days up to years). A number of models have been proposed for exploring system designs and parameters in IPSs.

Su *et al.* [96] modelled a dual-channel solar-powered nonvolatile sensor node, and Jackson *et al.* [97] provided a model to explore battery usage in IPSs. Both were configured for long-term simulations and large energy storage (from mF-scale supercapacitors to batteries), thus cannot respond to frequent power interruptions and accurately estimate forward progress when using minimized energy storage (e.g. 4.7  $\mu\text{F}$  [32]).

In contrast, a set of fine-grained models have been proposed to accurately simulate the frequent micro-operations in IPSs. NVPsim [98] is a gem5-based simulator for non-volatile processors. Fused [99] is a closed-loop simulator which allows interaction between power consumption, power supply, and forward progress. EH model [100] can compare a range of IPS approaches in a single active period with the same energy budget, quantifying forward progress by the energy spent on effective execution. These fine-grained models are inefficient for processing long-term energy data, especially when iterative tests are needed for various system configurations.

Besides models and simulators, hardware emulators of energy harvesters [101, 102] can provide repeatable power profiles recorded from energy harvesters for experimental

<sup>1</sup><https://git.soton.ac.uk/energy-driven/energy-storage-sizing>

comparisons. Though they provide practical results, hardware emulations are limited by hardware options and are generally impractical for performing long-term trials.

To address the above problem, we provide a reactive IPS model to estimate forward progress, as well as a simulation tool that enables fast exploration with long-term real-world environmental conditions. Further, we provide a sizing approach which recommends appropriate energy storage capacitance for deploying IPSs.

## 4.2 Energy Storage Sizing Approach

As mentioned, previous IPS designs typically adopt a minimised capacitor size so as to minimise device dimensions and interruption periods, but this can also reduce forward progress. An appropriate capacitor size instead may balance the three factors.

We propose a sizing approach which recommends appropriate energy storage capacitance for an IPS, trading off forward progress against capacitor volume and interruption periods. We present a system model which accepts real long-term data on environmental energy conditions. The three inputs can be swept for design exploration, but we focus on energy storage in this chapter. The model outputs forward progress, capacitor volume, and interruption periods (defined in Section 4.3.2). These are subsequently traded off in a cost function to obtain the appropriate energy storage capacitance. This process is summarised Figure 4.1 with details explained as follows.

### 4.2.1 Input

A time trace of representative environmental energy conditions in the intended deployment location is provided as an input, along with the energy harvester size. For design exploration, assuming the energy source is equally distributed in the deployed space, these can optionally be changed to explore variations and scales of harvested power. A pre-defined set of energy storage capacitance values are swept through.

### 4.2.2 System Model

This contains three modules, i.e. *Energy Harvester and Conversion Circuits*, *Energy Storage*, and *Intermittent Load*. The three modules communicate by their voltage and current flows. The current production  $I_{\text{harv}}$  and consumption  $I_{\text{load}}$  are buffered in the energy storage, which then calculates  $V_{\text{cc}}$  for the load and the harvester output. Due to the variety in each module, they should be individually specified to represent the target platform according to the techniques implemented.

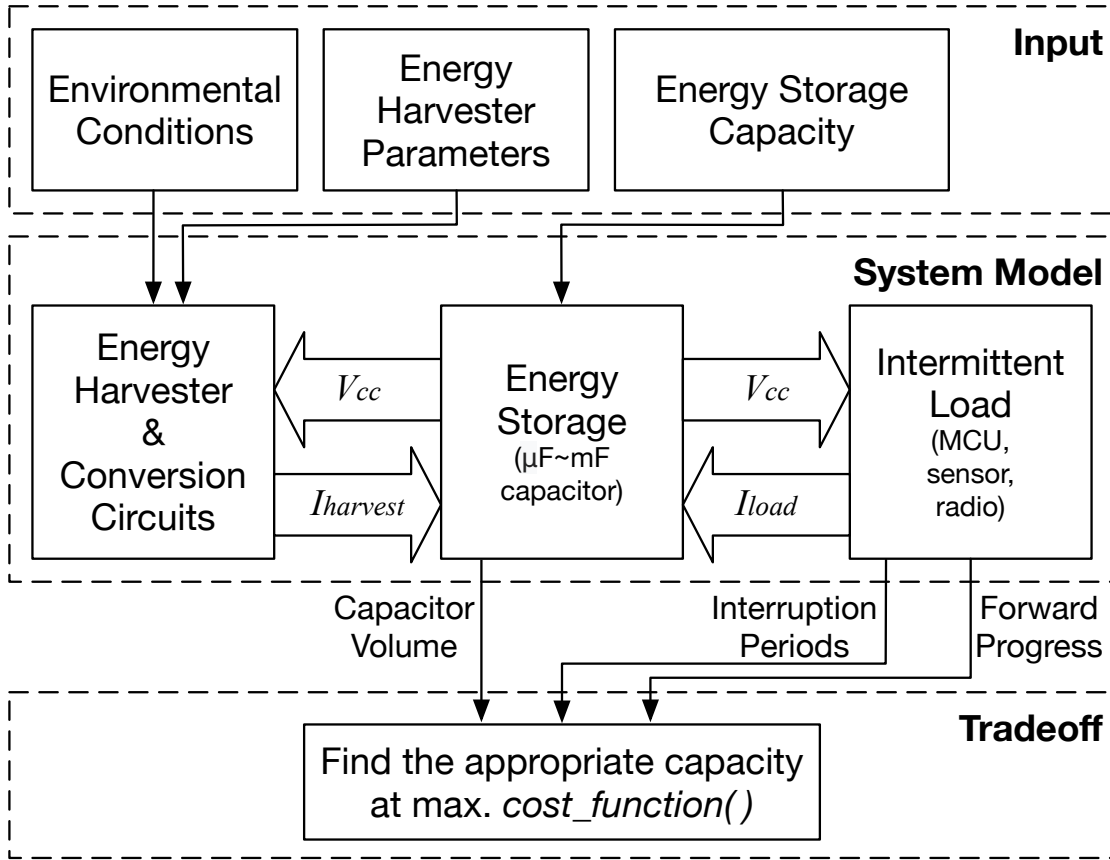


FIGURE 4.1: Structure of the proposed system model and sizing approach.

- *Energy Harvester and Conversion Circuits:* The energy harvester module transduces environmental energy into electricity. The harvested power is typically conditioned to provide a suitable voltage for charging the energy storage and supplying the load efficiently. In IPSs, conversion circuits may simply be a diode to inhibit backflow of current. The energy harvester and conversion circuits can be modelled together as a module because they are usually coupled or integrated.
- *Energy Storage:* Energy storage in IPSs is usually in the form of a  $\mu F$ - to  $mF$ -scale capacitor. It must be sufficient to complete the most energy-expensive atomic operation, and may be formed only of the decoupling capacitor(s). This also includes an empirical model relating capacitance to capacitor volume (discussed in Section 4.3.3).
- *Intermittent Load:* It includes all the power consumers in an IPS, such as a microcontroller, sensors, and a radio. This module outputs forward progress and interruption periods using the model presented in Section 3.1.

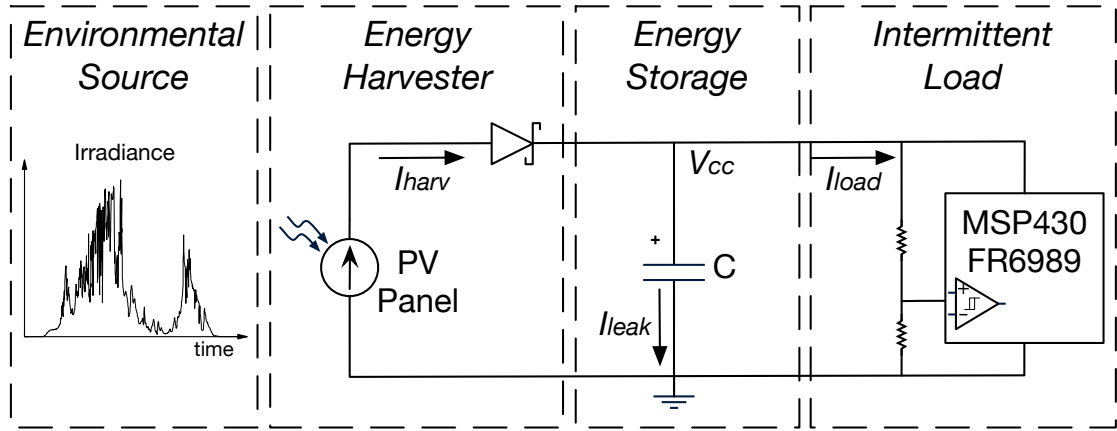


FIGURE 4.2: System model of a PV-based IPS.

### 4.2.3 Trade-off

The appropriate capacitance is then found through a cost function (an example of which is presented in Section 4.3.3). This may trade-off forward progress against capacitor volume and interruption periods.

## 4.3 Sizing under Real-World Energy Conditions

In this section, we model an IPS with a PV energy harvester to explore the energy storage sizing effect in real-world energy conditions, and demonstrate use of the proposed sizing approach.

### 4.3.1 Simulation Configuration

We integrate the validated reactive IPS model into a system model with a PV energy-harvesting supply as shown in Figure 4.2. The energy storage model and the intermittent load model are as presented in Section 3.2.

We use a converter-less supply circuit where only a Schottky diode is connected to the energy harvester output in order to prevent current backflow. The energy source conditions are imported from NREL outdoor solar irradiance data [103] and EnHANTs indoor irradiance data [104]. Four sets of light conditions are used to encompass different energy environments. To convert irradiance into harvested power, we adopt a PV cell model [105] which uses the parameters available in common datasheets, so it can easily be reconfigured to suit various devices. The output current  $I_o$  of the PV cell model can then be described as:

$$I_o = \frac{G}{G_{\text{ref}}} I_{\text{sc}} \left( 1 - \left( 1 - \frac{I_{\text{mpp}}}{I_{\text{sc}}} \right)^{\frac{V_o - V_{\text{oc}}}{V_{\text{mpp}} - V_{\text{oc}}}} \right) \quad (4.1)$$

TABLE 4.1: PV cell properties under a  $1000 \text{ W/cm}^2$ , AM-1.5 light source

Parameter	Value
Open-Circuit Voltage	0.89 V/cell
Short-Circuit Current	14.8 mA/cm <sup>2</sup>
Maximum Power Voltage	0.65 V/cell
Maximum Power Current	12.1 mA/cm <sup>2</sup>

where  $V_o$  is the output voltage of the PV cell,  $G$  is the ambient irradiance,  $G_{\text{ref}}$  is the reference irradiance (normally  $1000 \text{ W/cm}^2$ ), and  $I_{\text{sc}}$ ,  $V_{\text{oc}}$ ,  $I_{\text{mpp}}$ ,  $V_{\text{mpp}}$  are respectively short-circuit current, open-circuit voltage, and the current and voltage at maximum power point (MPP) given the reference irradiance.  $V_o$  and  $G$  are dynamic at run time, while other parameters in this model are constant. We refer to Panasonic Amorton glass type solar cells [106] for PV cell properties as shown in Table 4.1. We set four cells in series (with  $V_{\text{oc}} = 3.56\text{V}$ ) to match the operating voltage of the MCU (maximum 3.6V), and model energy harvester sizing by scaling the cell area.

Our simulation tool can perform two simulation processes: (a) sort and process the time distribution of environmental conditions, and (b) simulate system state chronologically with a fine-grained time step. Process (a) reduces simulation time significantly, e.g. from hours to seconds, but ignores the restore operation after a brownout reset, hence overestimating forward progress, and it overestimates more with smaller capacitance and lower supply current. In the following results, Figure 4.3 comes from Process (a) for fast exploration, and Figure 4.5 and Figure 4.7 come from Process (b) for accurate records of interruption periods.

### 4.3.2 Exploration with Real-World Energy Source Conditions

In real-world deployments, ambient energy source conditions are dependent on time and location. The energy harvester and storage need to be sized to achieve the desired forward progress across the range of expected conditions.

#### 4.3.2.1 Sizing the Energy Harvester

For the purposes of this exploration, three levels of baseline mean forward progress ( $\alpha_{\text{exe}}$ ) are set as 0.1, 0.2, and 0.3. We use the system model to find the PV panel area that achieves the expected forward progress under the different energy source conditions with minimum energy storage. We scale the PV panel area to find that which achieves each baseline  $\alpha_{\text{exe}}$ . As shown in Figure 4.3, the energy harvester sizes that achieve the desired  $\alpha_{\text{exe}}$  may span orders of magnitude given different energy source conditions from  $\text{mm}^2$  for outdoor sources ((c) and (d)) to  $\text{cm}^2$  for indoor sources ((a) and (b)).



#### 4.3.2.2 Sizing the Energy Storage

Having obtained the energy harvester sizes for the baseline forward progress, we then use the modelling approach to size energy storage. We analyse the sizing effect of energy storage on forward progress given real-world energy conditions. Figure 4.3 shows a 7.8-43.3% improvement in forward progress by sizing energy storage under the given real-world energy conditions and baseline energy harvester sizes. It can also be inferred that optimising energy storage can either improve forward progress for a given energy harvester size, or reduce the energy harvester size that achieves the target forward progress. Given higher-power energy sources (e.g. Denver 2018 and Hawaii 2018 outdoor solar), increasing the harvester size efficiently improves forward progress with minor dimensional overheads, e.g. tens of  $\text{mm}^2$ ; however, given lower-power sources (e.g. EnHANTs Setup A and Setup D indoor light), optimising energy storage capacitance can save tens of  $\text{cm}^2$  of PV panel area to achieve the same forward progress.

Also, the progress improvement by sizing energy storage varies accordingly with energy source conditions. As mentioned in Chapter 3, this improvement stems from the reduction of restore and save overheads when the supply current is low and the device work in the *Intermittent* mode. Thus, the results of EnHANTs Setup A and Setup D show a higher progress improvement from sizing energy storage than those of Denver 2018 and Hawaii 2018.

The mean forward progress given target  $\alpha_{\text{exe}} = 0.1$  is plotted in Figure 4.4, with the 60th and 90th time percentiles of forward progress. In all the above datasets, the energy source is absent and the system is off for around 55 % of time, so we plot the percentiles from the 60th. The mean progress during the energy-available periods is averaged over the energy-absent periods, so the actual mean forward progress during the energy-available periods is nearly double the annual mean.

#### 4.3.2.3 Interruption Period

Besides forward progress, we also explore how the capacitance can change the interruption periods. When interrupted by insufficient power supply, an IPS enters an interruption period where it saves its volatile state, waits for supply voltage to recover, and restores the state to resume execution, without making any forward progress. Applications that require frequent sensing may be negatively affected by long interruption periods. We measure an interruption period as *the period between two successive execution periods*, e.g. a consecutive ‘SLR’ period in Figure 3.2 forms an interruption period. We record all the interruption periods during a one-year simulation with 10–50  $\mu\text{F}$  capacitors, the Denver 2018 dataset, and an 80  $\text{mm}^2$  PV panel. Figure 4.5 presents the

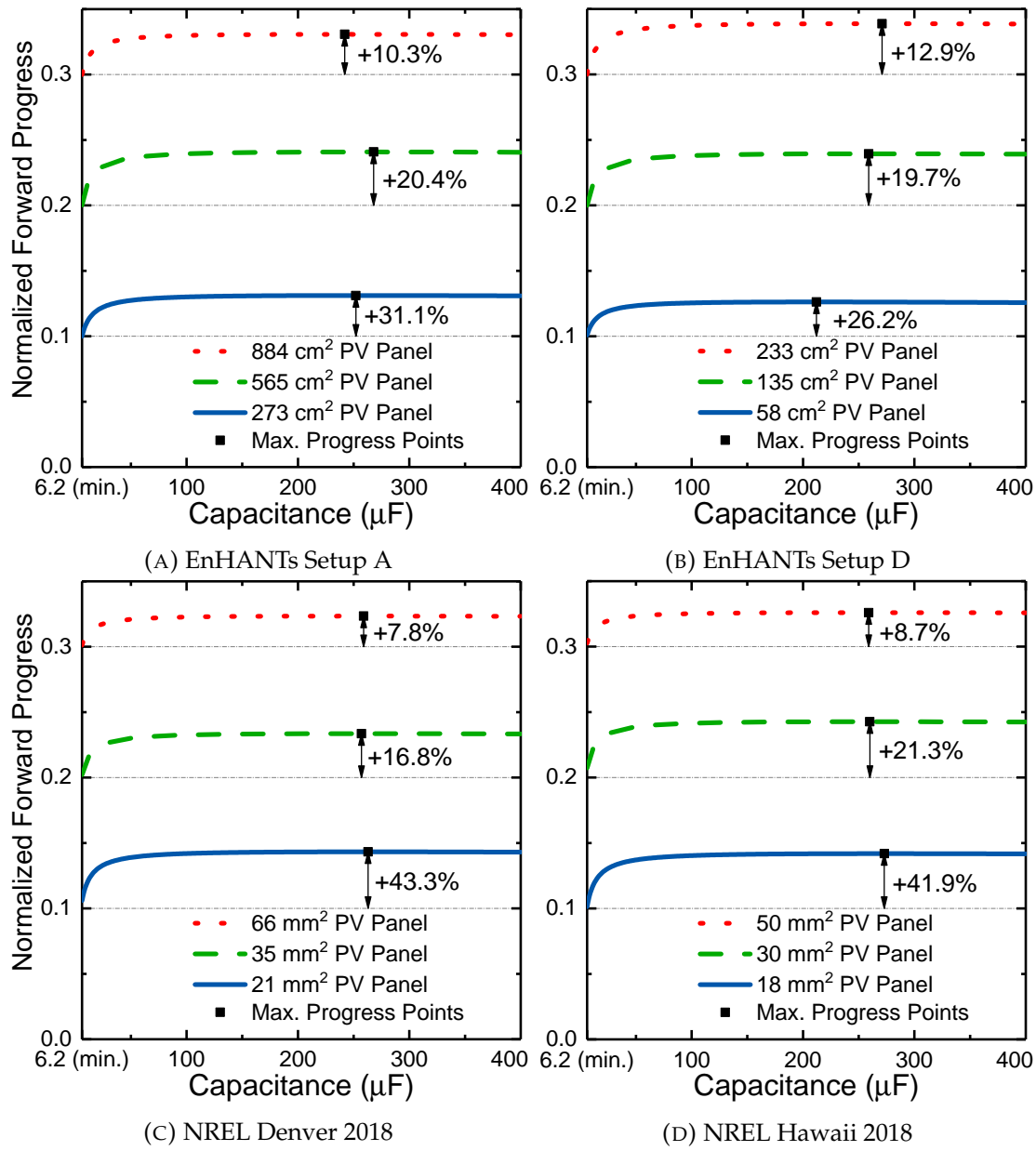


FIGURE 4.3: Improvement of average forward progress by sizing energy storage given different PV panel areas under real-world energy source conditions. The model is able to find the PV panel area required for achieving the target mean forward progress.

distribution of all the interruption periods. With increased energy storage, the interruption period is prolonged. For example, the 90th percentile of interruption periods increases from 32.2 ms at  $10 \mu\text{F}$  to 123.4 ms at  $50 \mu\text{F}$  at an approximate rate of 23 ms per  $10 \mu\text{F}$ . Facilitated by the simulator, developers are enabled to estimate whether the distribution of interruption periods meet their application requirement.

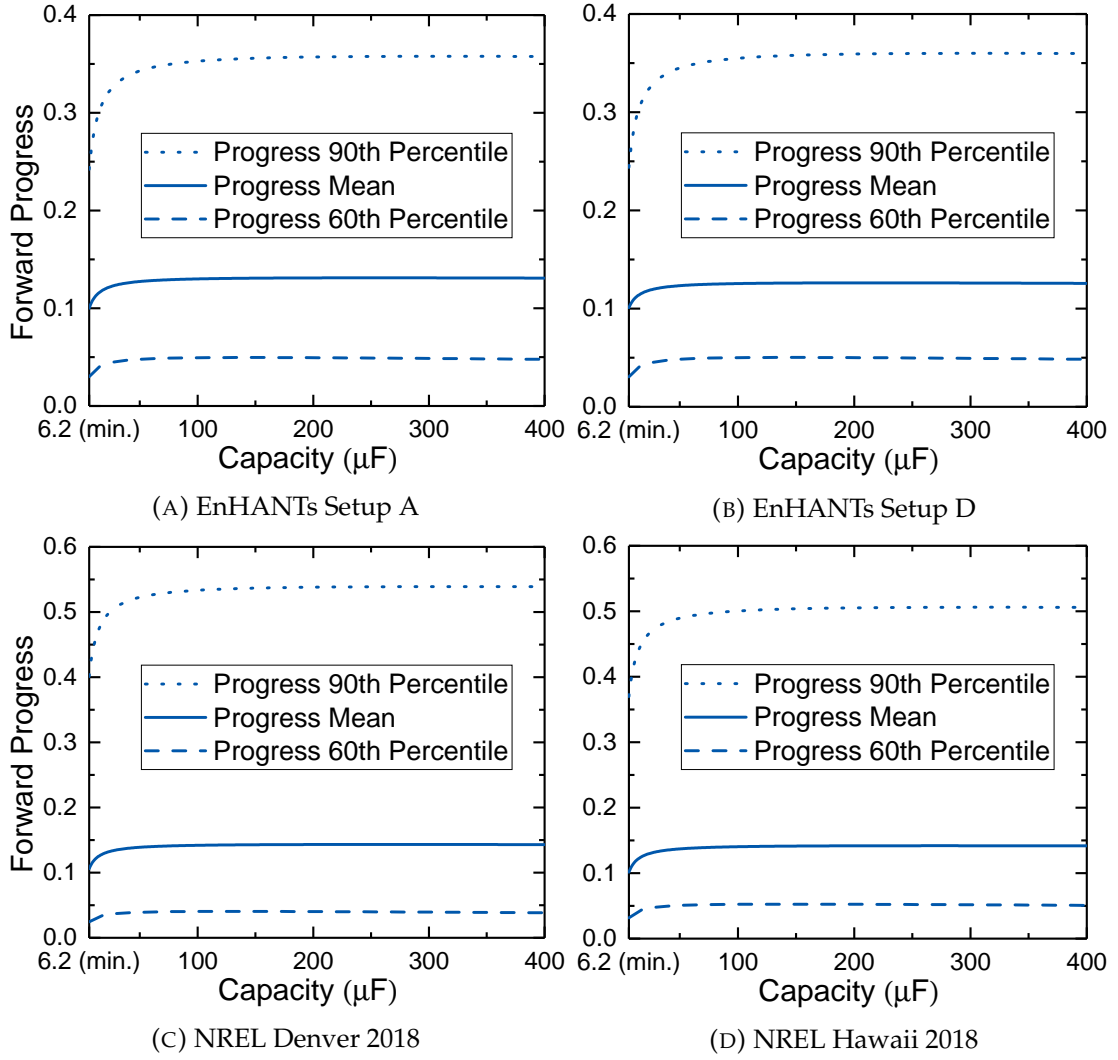


FIGURE 4.4: Time percentiles of forward progress by sizing energy storage with target  $\alpha_{\text{exe}} = 0.1$  and the corresponding PV panel area listed in Figure 4.3. The percentiles start from the 60th as the system is off for around 55% of time due to insufficient energy source.

### 4.3.3 Trading Forward Progress, Dimensions, and Interruption Period

Although increasing energy storage capacitance improves forward progress, larger capacitance increases both dimensions and interruption periods. We evaluate the overheads of increased capacitor dimensions and interruption periods, and then trade them off against forward progress using a cost function to suggest an optimal capacitance value.

#### 4.3.3.1 Metric of Dimensions

The overhead of capacitor dimensions is evaluated by characteristics of off-the-shelf tantalum capacitors. We narrow down the range of sample capacitors within a set of

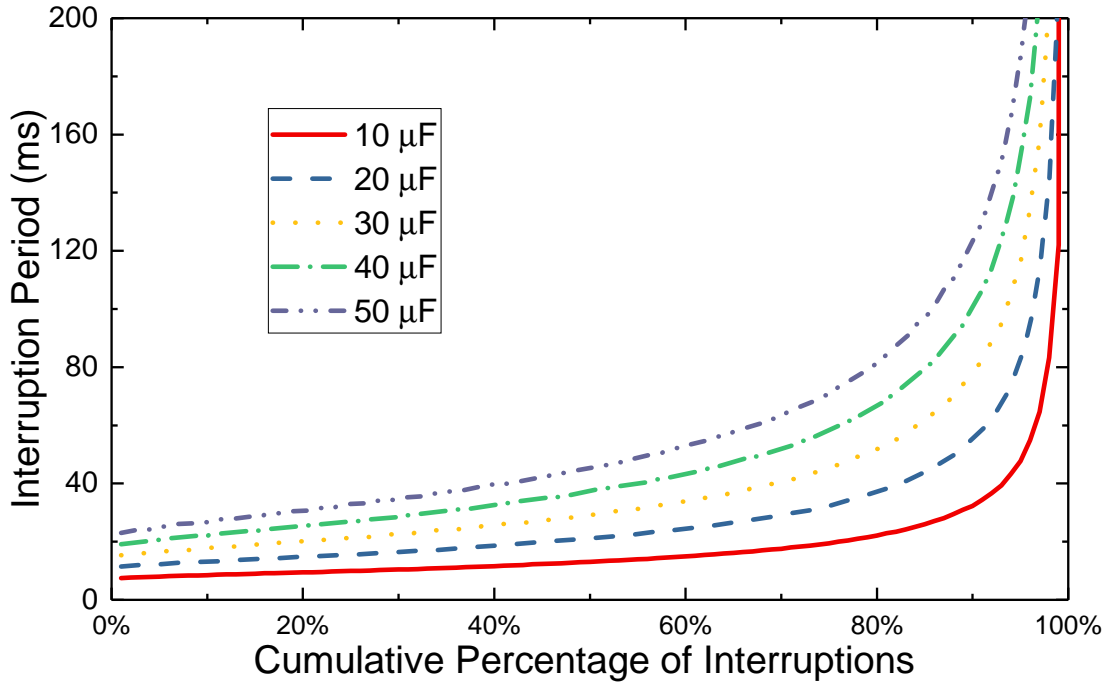


FIGURE 4.5: Distribution of interruption periods.

characteristics: low-profile, 10V rated voltage, and surface-mount package, and select six series of capacitors<sup>2</sup>. The volume and capacitance of these devices are plotted in Figure 4.6. We use the regression of these data to approximate a capacitance-volume relationship.

#### 4.3.3.2 Metric of Interruption Periods

Applications may have various requirements on interruption periods. To demonstrate the usage of our sizing approach, we consider a designer requests the 90th percentile of all interruption periods as an example metric of interruption periods, denoted as  $T_{\text{int}}$ . This metric indicates 90% of interruption periods are shorter than  $T_{\text{int}}$ . This metric can be adapted for particular application requirements.

#### 4.3.3.3 Cost Function

From the previous observations (Figure 3.4) we can see that achieving the optimal progress improvement costs much more capacitance (mean  $3.2\times$ ) than to achieve 95% improvement. A trade-off is necessary to improve forward progress while restricting the overheads of increased capacitor volume and interruption periods. This involves a problem of multi-criteria decision making [107], which is outside the scope of this

<sup>2</sup>The series of capacitor considered were: AVX TAJ, AVX TACmicrochip, AVX F92, Vishay 572D, Vishay 591D, and Vishay 592D.

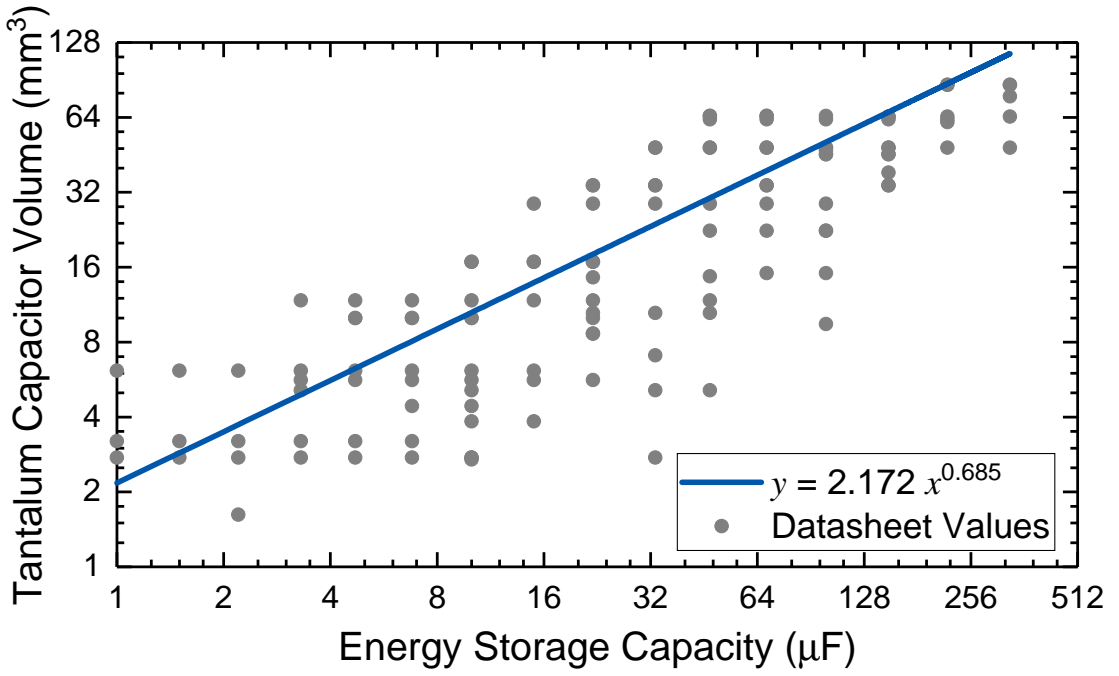


FIGURE 4.6: Tantalum capacitor volume against capacitance for the six series of capacitors analysed.

work. Nevertheless, we provide a cost function in (4.2) as an example to illustrate how these three factors could be traded-off, but designers are expected to customise a cost function with parameters of importance to specific application requirements. Note that the function (4.2) is to be maximised to find the recommended capacitance.

$$f = \frac{\alpha_{\text{exe}}}{k_1} - \left( \frac{v_{\text{cap}}}{k_2} \right)^2 - \left( \frac{T_{\text{int}}}{k_3} \right)^2 \quad (4.2)$$

$\alpha_{\text{exe}}$  denotes normalised forward progress,  $v_{\text{cap}}$  denotes capacitor volume, and  $T_{\text{int}}$  denotes application interruption periods as mentioned in Section 4.3.3.2.  $\alpha_{\text{exe}}$ ,  $v_{\text{cap}}$ , and  $T_{\text{int}}$  can be generated from the simulation tool given  $C$  as an input.  $k_1$ ,  $k_2$ , and  $k_3$  are coefficients for normalising each metric, and they are empirically determined according to applications. In this example, the undesirable parameters are expressed as quadratic and negative terms to give an increasing cost to higher values. While only three parameters are considered here, others (such as the energy harvester size) could be included for a system-wise sizing scenario. As an example to demonstrate its usage, we arbitrarily configure the function by setting  $k_1 = 0.2$ ,  $k_2 = 200 \text{ mm}^3$ , and  $k_3 = 500 \text{ ms}$ .

#### 4.3.3.4 Results

The effect of the trade-off is plotted in Figure 4.7 using the Denver 2018 energy source dataset. Compared to the capacitor size that solely maximises forward progress, on average, an appropriately-sized capacitor achieves 93% of the maximum forward progress,

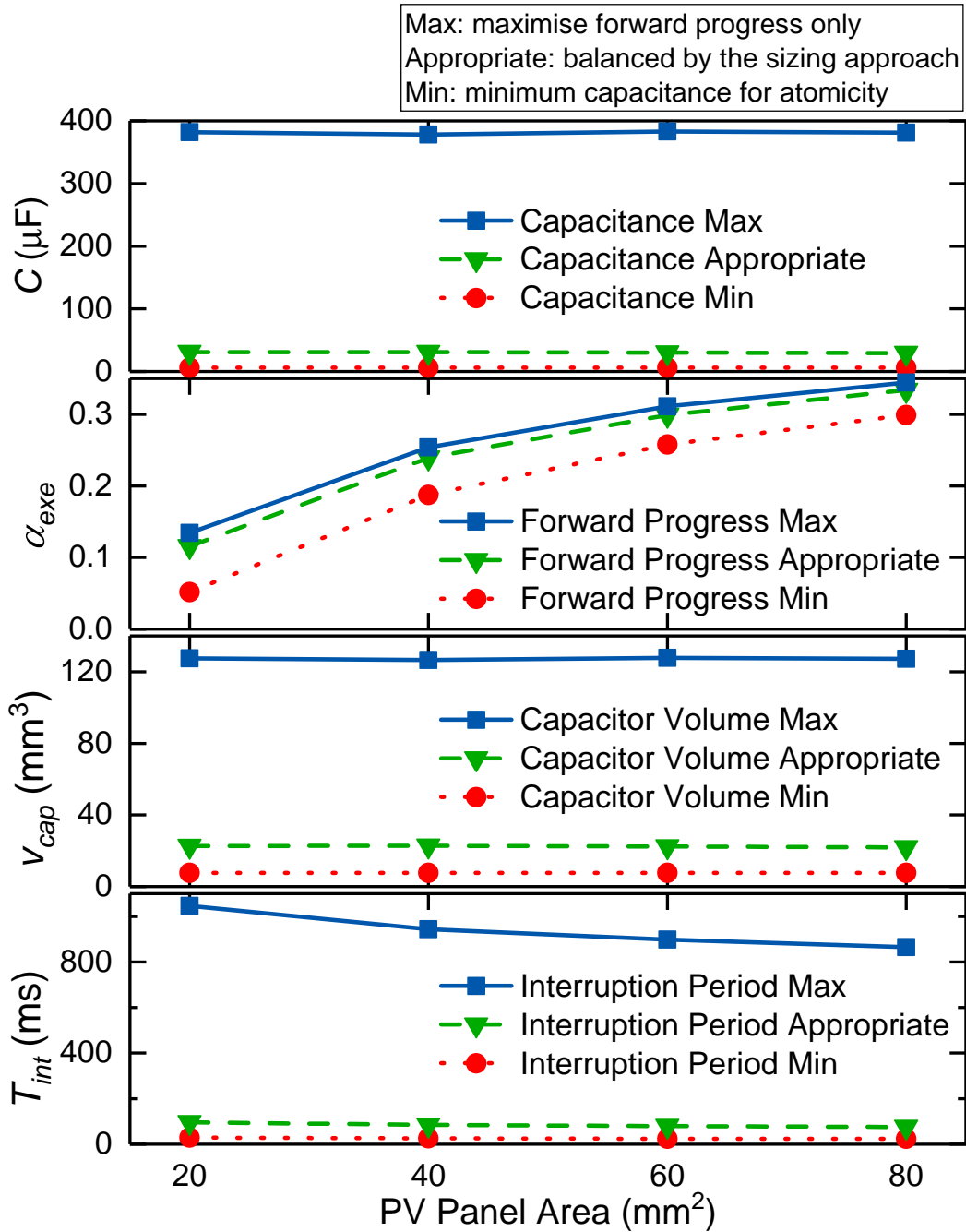


FIGURE 4.7: The sizing approach trades off forward progress, capacitor volume, and interruption periods. The results are plotted against a range of PV panel area, given Denver 2018 energy source dataset.

while saving 83% of capacitor volume and 91% of interruption periods. This also demonstrates the efficacy of the cost function and the chosen coefficients. Compared to the minimum storage case, the appropriately-sized capacitor improves forward progress by 12-124% with energy storage increased from 6.2  $\mu\text{F}$  to 30  $\mu\text{F}$ .

As shown in Figure 4.6, the closest available capacitance that satisfies the 6.2  $\mu\text{F}$  minimum capacitance is 6.8  $\mu\text{F}$ , whereas the closest available capacitance to the appropriate

30  $\mu\text{F}$  is 33  $\mu\text{F}$ . The minimum volumes of 6.8  $\mu\text{F}$  and 33  $\mu\text{F}$  capacitors are both 2.75  $\text{mm}^3$ , which means using the appropriate capacitance, instead of the minimum one, may not incur dimensional overhead. The regressed volume of the above two capacitance values are 8.1  $\text{mm}^3$  and 23.8  $\text{mm}^3$  respectively. However, the selection of capacitors can be dependent on factors other than physical volume, such as reliability, operation temperature, and more specific application needs. These factors can also be added into the cost function if necessary.

## 4.4 Summary

This chapter has presented an approach for sizing energy storage when deploying IPSs, trading off forward progress against capacitor volume and interruption periods. The work includes a simulation tool which is available to download, enabling researchers to experiment with energy storage sizes to optimise IPS designs. The approach was configured and demonstrated with an experimentally-profiled IPS and real-world data of PV sources, showing up to a 43% annual forward progress gain by sizing energy storage. A cost function can be incorporated, allowing various properties of the system to be traded-off. The results showed that the suggested energy storage capacitance achieves 93% of the maximum forward progress while saving 83% capacitor volume and 91% interruption periods. Our conclusion is that energy storage should be carefully designed, rather than minimised or indiscriminately picked, to efficiently operate IPSs.





## Chapter 5

# Runtime Energy Profiling and Adaptation for IPSs

Apart from computational workloads, embedded sensing systems need to utilise peripherals, such as sensors, computational accelerators, and radios, which typically require *atomicity* [108]. In the context of IPSs, an atomic operation should not be checkpointed during execution; if interrupted by power failures, it should restart rather than checkpoint and resume. A peripheral operation is considered atomic because it is usually problematic to checkpoint and restore the operation later, even if the intermediate peripheral state is also checkpointed. For example, checkpointing during a sensor reading and resuming it later can cause incorrect results or an infinite wait as the initialisation is lost, and violate timeliness as the sensor does not render the latest and consecutive results [24]. Prior works on intermittent peripheral operations either customise a design-time calibrated energy budget for each peripheral operation individually [35], or allocate a universal and large energy budget that ensure the most energy-hungry operation can finish in one active cycle [24].

However, in this chapter **we** argue that manually profiling each peripheral operation and customising energy thresholds is impractical due to variability in IPSs, where we have considered the variability in the data amount to process, peripheral configurations, devices, and energy buffering capacitance (detailed in Section 5.2.1). A fixed threshold can be violated if any of the above cases happen, and lead to non-termination<sup>1</sup>. In practical deployment, considering the complexity and labour effort, it is unrealistic to profile every atomic operation for every device under every runtime scenario at design time and customise the energy budgets accordingly.

---

<sup>1</sup>Non-termination happens when the pre-defined energy budget is less than how much the operation consumes and the supply is not strong enough to fill the energy gap. It is one of the main causes for failures in intermittent systems.

On the other hand, using only one high voltage threshold, though probably avoids non-termination, can affect system energy efficiency. IPSs typically minimise operating voltage in order to lower quiescent power consumption from power conversion loss and system leakage [35]. Also, a high operating voltage can decrease the output current of energy harvesters, making it harder to charge up the buffering capacitor [109]. Hence, setting a high wake-up voltage threshold results in a longer charging time than a linear scale of the voltage threshold, which therefore slows down the system execution or even leave the system in an infinite wait under poor energy conditions.

To address the above issue, we propose OPTIC<sup>2</sup>, a methodology that profiles energy consumption of operations at runtime and dynamically adapts energy thresholds based on newly profiled consumption and user-defined parameters. A naive approach of runtime energy profiling can be disconnecting the power supply during profiling and taking two readings of supply voltage before and after an operation [2], but this can waste the harvested energy during the operation. In contrast, OPTIC profiles the maximum drop of supply voltage that an operation can cause while the energy harvesting supply is connected. The profiling strategy is to measure the input current in the charging cycle so as to calculate the maximum drop of supply voltage in the discharging cycle. The runtime profiled energy budget can thus, compared to a design-time profiled one, closely match with the latest energy consumption. Based on the profiling results, OPTIC dynamically adapts the threshold for each atomic operation, with an option of scaling thresholds by user-defined parameters, e.g. a variable data size. Therefore, OPTIC enables IPSs to allocate a barely sufficient energy budget despite runtime energy variations, and hence mitigates non-termination while achieves high energy efficiency, eventually improving the workload throughput.

The main contributions of this chapter can be summarised as follows:

1. An exploration of the runtime variations of energy consumption in IPSs that compromise existing approaches in comparison with an adaptive thresholding scheme.
2. A method of runtime energy profiling of tasks for IPSs without disconnecting supply, showing a high accuracy within 5 mV.
3. An adaptive thresholding scheme that, utilising the runtime energy profiling method, dynamically allocates barely sufficient energy budgets for tasks, with an optional scaling based on user-defined parameters. The proposed scheme enables a system to survive with 67.5% less energy buffering capacitance than the initially allocated amount and presents up to a 98% speedup with variable data sizes, compared to SoA approaches.

---

<sup>2</sup>OPTIC: One Energy Profiling and Threshold Adaptation for Intermittent Computers.

4. Implementation of the proposed runtime energy profiling and threshold adaptation method, with an efficient supply voltage monitor.

The rest of this chapter is organised as follows. Section 5.1 reviews existing IPS work on peripheral operation and their method of energy provision. Runtime energy variations of workloads are explored in Section 5.2, with simulated performance of an adaptive thresholding scheme compared against SoA approaches given the variations. OPTIC's runtime energy profiling method and runtime energy adaption routine are proposed in Section 5.3 and Section 5.4 respectively. An implementation of OPTIC is presented in Section 5.5. Experimental evaluation is shown in Section 5.6. Finally, Section 5.7 summarises the main findings in this chapter.

## 5.1 Related Work

Several existing designs have been able to handle atomic peripheral operations in IPSs, where energy profiling of workloads is an inherent part of their methodologies.

DEBS [35] experimentally profiles the energy consumption of each task at design time, and designates a threshold to each task individually. After completing an operation, DEBS enters a low-power mode (LPM) and waits for energy to be replenished to the next threshold.

Samoyed [24] utilises a custom design-time *energy profiler* to identify an energy storage size that suffices to run an adequate number (hundreds, as suggested) of peripheral operations in one active cycle. At runtime, Samoyed starts execution when energy is refilled to a certain threshold, and keeps executing until energy is depleted. Samoyed differs from proactive intermittent computing approaches, e.g. Alpaca [77], mainly on handling computational workloads where it reactively checkpoints when the buffered energy is below a threshold, and supports user-customised subdivision of peripheral operations when the operation cannot complete in one active cycle.

RESTOP [92] provides programmer-configurable rules that track the instructions issued to peripherals through serial interfaces in a history table. On power recovery, RESTOP re-issues instructions saved in the history table and then resumes the interrupted operation. At design time, RESTOP needs to profile the worst-case energy consumption for restoring peripheral state to identify the minimum (most-efficient) restore threshold.

As reviewed above, prior work profiles the energy consumption of atomic peripheral operations at design time to determine a voltage threshold or a capacitor size that avoids non-termination. However, this does not actually guarantee the completion of every atomic operation because energy consumption can change with any runtime

conditions different to the profiling setup (demonstrated in Section 5.2.1). Hence, to tolerate dynamic variations, previous designs should usually leave an inefficiently large margin when allocating energy budgets. If this large margin is not given, they can cause either non-termination or high overheads of tracking and restoring state, where DEBS fails, Samoyed undo-logs the NVM data, and RESTOP re-issues peripheral instructions.

## 5.2 Design Exploration

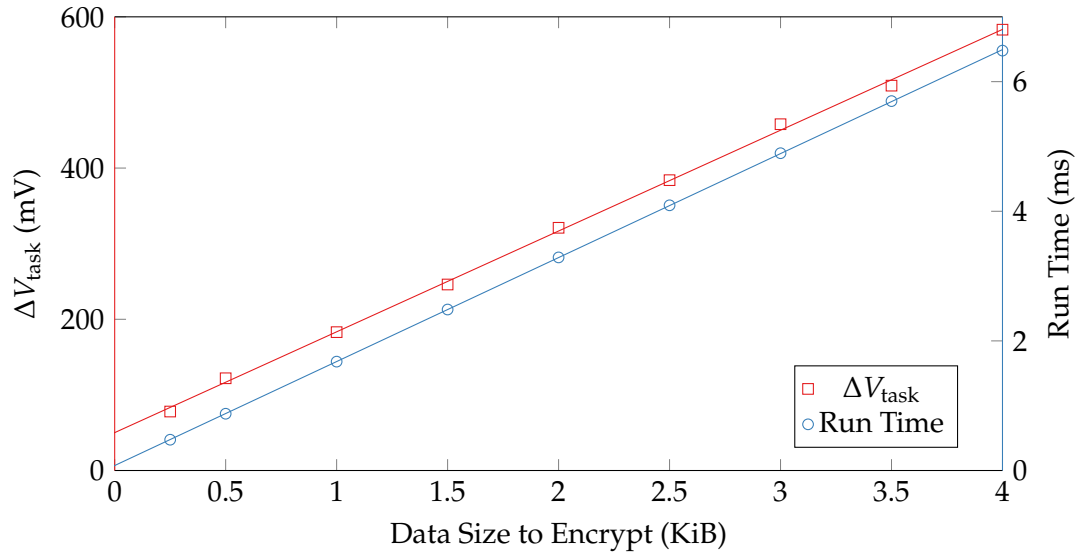
In this section, we study the variability in IPSs that can violate a predefined fixed threshold. We then investigate how existing approaches fail or become inefficient under this variability, and explore the potential of an adaptive thresholding scheme.

### 5.2.1 Variability in Intermittent Systems

Design-time profiling of workloads' energy consumption in the prior work can be potentially violated by the variability of IPSs. To study and demonstrate the variability, we chose the built-in AES accelerator on the TI MSP430FR5994 microcontroller unit (MCU) as an example peripheral workload. The example AES function encrypts data in the cypher block chain mode, and can process up to 4KB data with a 128-, 192-, or 256-bit key length. In the following experiments, we measured  $\Delta V_{\text{task}}$ , *the drop of supply voltage caused by an operation without any incoming energy meanwhile*, which directly determines the minimum voltage threshold that safely guarantees the completion of an atomic operation. We used Device 1 in Table 5.2, which has 11.5  $\mu\text{F}$  energy buffering capacitance, for the tests for variable data sizes and peripheral configurations, whereas in the device variability test we tested 3 devices. We explored four factors that can possibly change  $\Delta V_{\text{task}}$ , which are variable data amounts, variable peripheral configurations, devices variability, and capacitor degradation and tolerance. Besides the above four, energy consumption can also change with other factors, such as temperature, clock frequency, and silicon ageing, but we have found them either insignificant or hard to validate on our experimental platform.

#### 5.2.1.1 Variable Data Sizes

A peripheral function can accept a runtime variable amount of data, such as a variable data size to encrypt or different lengths of packets for a radio to transmit. An example of this is plotted in Figure 5.1, where the size of the square dots represent a 5 mV precision error of the scope and the lines represent linear regression. We observed that  $\Delta V_{\text{task}}$  has a linear relationship with the data size, with an offset energy consumption

FIGURE 5.1:  $\Delta V_{\text{task}}$  varying linearly with the data size in AES 128-bit encryption.TABLE 5.1:  $\Delta V_{\text{task}}$  Varying with Configurations in AES 4KB Encryption

Configuration	$\Delta V_{\text{task}}$	Run Time
128-bit key	583 mV	6.479 ms
192-bit key	690 mV	7.638 ms
256-bit key	736 mV	8.606 ms

that accounts for the initialisation. In this case, the linearly scaled  $\Delta V_{\text{task}}$  comes from linearly scaled run time.

### 5.2.1.2 Variability in Peripheral Configurations

A peripheral can run with variable configurations at runtime, and demonstrate variable performance and energy consumption. For example, as shown in Table 5.1, an AES accelerator can encrypt data with 128-, 192-, or 256-bit keys. A longer key provides higher security, but also takes more time and energy to complete. The dynamic range of configuration variability in this case can be a 26% increase in  $\Delta V_{\text{task}}$  and a 33% increase in run time.

### 5.2.1.3 Device Variability

Devices have their variation in power consumption, even with the same part number. A threshold profiled on one device can be inadequate on another. We did a test on three developments boards of the same MCU, where it runs 128-bit AES encryption on 4KB data. As listed in Table 5.2, the effect of device variability on  $\Delta V_{\text{task}}$  is up to 9% among the three devices, though with almost the same run time (0.5% variation). It should be

TABLE 5.2:  $\Delta V_{\text{task}}$  Varying among Devices in AES 128-bit 4KB Encryption

Device No.	$\Delta V_{\text{task}}$	Run Time
1	583 mV	6.479 ms
2	555 mV	6.444 ms
3	535 mV	6.462 ms

noticed that device variability can also present across platforms that can run the same or similar code.

#### 5.2.1.4 Capacitor Ageing and Tolerance

As the component for buffering energy in IPSs, capacitors typically present a  $\pm 10\text{-}20\%$  tolerance on rated capacitance as reported in many commercial capacitors. Capacitors also age over time. It is shown that capacitance can decrease by 7.2% in 3000 hours (125 days) under a 25 °C ambient temperature in experiments [110], and by 50% within 10 years under 40 °C as manufacturers stated [111]. A degraded capacitor does not change the load consumption, but can increase  $\Delta V_{\text{task}}$ , and hence makes the pre-defined voltage threshold unsafe or inefficient.

The above four examples present that the variability in IPSs can potentially make a predefined  $\Delta V_{\text{task}}$  insufficient. It is unrealistic to profile the  $\Delta V_{\text{task}}$  in each scenario at design time in practice considering the complexity of the variations, and still cannot encompass unexpected situations, necessitating a runtime energy profiling approach.

### 5.2.2 Performance Improvement with Adaptive Thresholds

Having presented the variability in IPSs, we explore in modelling and simulation the potential of adaptive thresholds on coping with such variability, as opposed to existing fixed-threshold approaches, which may fail or run inefficiently under such variability.

#### 5.2.2.1 Power Analysis

As suggested in prior work, operating at a lower voltage can improve system energy efficiency due to a higher charging efficiency and a lower power consumption.

To validate this, we analysed the charging characteristic of a glass-type amorphous PV panel in an white LED lighting environment. We used the PV panel to charge a 103  $\mu\text{F}$  capacitor from 0 V to 3.05 V where the capacitor cannot be charged up anymore. The voltage-time charging trace is then differentiated to gain an I-V curve that represents the PV panel (Figure 5.2). To model this curve, we did a linear regression for the data

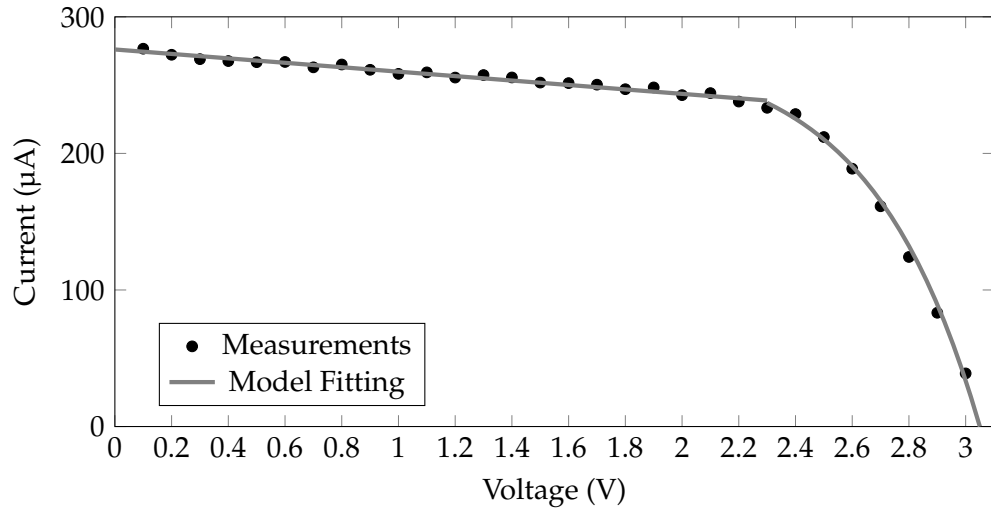


FIGURE 5.2: An I-V curve of a glass-type amorphous PV panel (Sanyo AM-1417CA, 35 mm×13.9 mm) under a white LED lighting condition.

in 0–2.3 V, and adapted a published PV panel model [105] to represent the curve in 2.3–3.05 V. The model function of this I-V curve is then expressed as:

$$I_{in} = \begin{cases} -16.25V_{in} + 276.10 & , \quad 0 \text{ V} < V_{in} \leq 2.3 \text{ V} \\ I_{sc} \left( 1 - e^{\ln(1 - \frac{I_{mpp}}{I_{sc}}) \frac{V_{in} - V_{oc}}{V_{mpp} - V_{oc}}} \right) & , \quad 2.3 \text{ V} < V_{in} \leq 3.05 \text{ V} \end{cases} \quad (\mu\text{A}) \quad (5.1)$$

where we set  $I_{sc} = 276 \mu\text{A}$ ,  $V_{oc} = 3.05 \text{ V}$ ,  $I_{mpp} = 237 \mu\text{A}$ , and  $V_{mpp} = 2.3 \text{ V}$ .

In the MSP430FR5994 platform, we did not observe a significant change in current consumption with supply voltage (up to 2%). This is majorly due to an on-chip LDO that droops down the external supply voltage to a constant internal supply voltage, and hence maintaining a relatively stable current draw as the external supply voltage changes. Hence, we omitted the voltage effect on current consumption in this simulation.

We used the energy and time overheads of AES encryption presented in Section 5.2.1 to simulate the workload characteristics. In simulation, the current draw remains constant during one operation, but changes with dynamic data sizes and configurations due to the variable charge consumption and run time.

### 5.2.2.2 Runtime Control Models

We modelled an ideal adaptive threshold scheme against two SoA fixed-threshold schemes. We focussed on modelling the control logic and threshold settings, and omitted the state management overhead as it can be dependent on the actual implementation.

In the ideal adaptive scheme, the system knows exactly how much energy is needed for the next operation and sets the lowest threshold that suffices the energy budget.

DEBS sets a minimum threshold for a fixed operation. We explored two cases of DEBS, labelled as DEBS Low and DEBS High. We firstly modelled DEBS Low, which does not foresee any possible changes in data sizes and configurations. DEBS Low's threshold was profiled with 1KB data and a 128-bit key length without considering any variability. We then modelled DEBS High in a case where it foresees the possible dynamic increase in workload consumption due to variable data sizes and configurations and sets its threshold based on the most energy-hungry setup, while it does not consider further capacitor ageing.

Samoyed differs from DEBS and the adaptive scheme in its control, where, when completing an operation, it keeps executing until it dies rather than sleeps and waits for the next threshold. Samoyed suggests allocating an abundant energy budget, so its threshold is also set to the highest possible operating voltage.

### 5.2.2.3 Simulation Setup

In simulation, the system has 10  $\mu\text{F}$  system capacitance without charge at the start. The shutdown threshold is 1.8 V, against which DEBS and the adaptive scheme set their threshold, with a 10 mV small margin. The system consumes 10  $\mu\text{A}$  when it is inactive. To evaluate the performance of the three schemes, we conducted two tests that simulate a variable workload and capacitance reduction respectively. The variable workload test runs a random data amount from 16B to 4080B (1 to 255 blocks of data, 16B per block), and also a random 128-, 192-, or 256-bit key length, both uniformly distributed. The energy harvesting characteristics presented in Figure 5.2 is used as the supply for this test. All the schemes take the same random series of data sizes and configurations. The capacitance reduction test runs with 0-60% reduced capacitance, in line with the maximum possible reduction shown in Section 5.2.1.4. The system in this test is supplied with a 50  $\mu\text{A}$  constant current and runs only the most energy-hungry operation, in order to examine whether the system can avoid non-termination even under the worst case. We ran 10 rounds of simulations for each setup, and each round simulates for 10 s.

### 5.2.2.4 Results

Figure 5.3 shows the mean, maximum, and minimum numbers of completed and failed operations in the variable workload test. DEBS Low cannot terminate once it encounters an operation that consumes more than what it is profiled for and the supply is too weak to provide the energy gap. DEBS Low can only occasionally get progress on



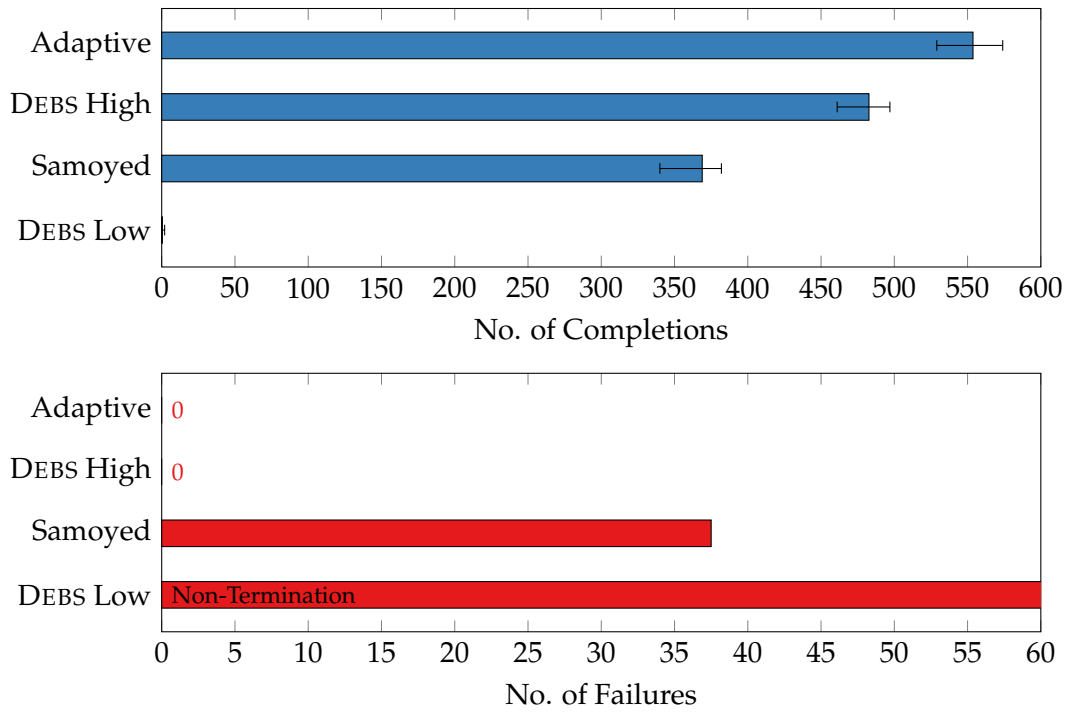


FIGURE 5.3: Numbers of completed and failed operations of DEBS Low, Samoyed, DEBS High, and Adaptive given random data sizes and configurations and a PV supply in a 10 s simulation.

lightweight operations before non-termination. Samoyed also suffers performance loss from waiting for a high energy threshold (2.9 V in this case), and failing an operation at the end of an active cycle. DEBS High is relatively efficient because it does not usually fail due to a sufficient energy budget and a sleep-after-completion control. The adaptive scheme runs the most efficiently among these four. It runs at reduced operating voltage that improves system energy efficiency, and also guarantees the completion of every task by setting a minimised but safe threshold. As an example voltage trace shown in Figure 5.4, the adaptive scheme runs with 2.11 V mean voltage, while the ones for Samoyed and DEBS High are 2.36 V and 2.40 V respectively. Due to the above reasons, the adaptive scheme completes more operations over Samoyed by 50% and DEBS High by 15% on average.

Figure 5.5 shows the results of the capacitance reduction test, where we have omitted DEBS Low as it has already failed in non-termination with origin capacitance (so will still fail with reduced capacitance). With the capacitance decreased, DEBS High also falls into non-termination like DEBS Low. Samoyed, where its threshold is set to 3.6 V in this case, can still progress until a 60% reduction of capacitance because its abundant energy budget can support at least one or a few operations in one active cycle. The adaptive scheme still maintains the highest forward progress among these control scheme.

The above exploration presents that using a fixed low threshold can leave the system

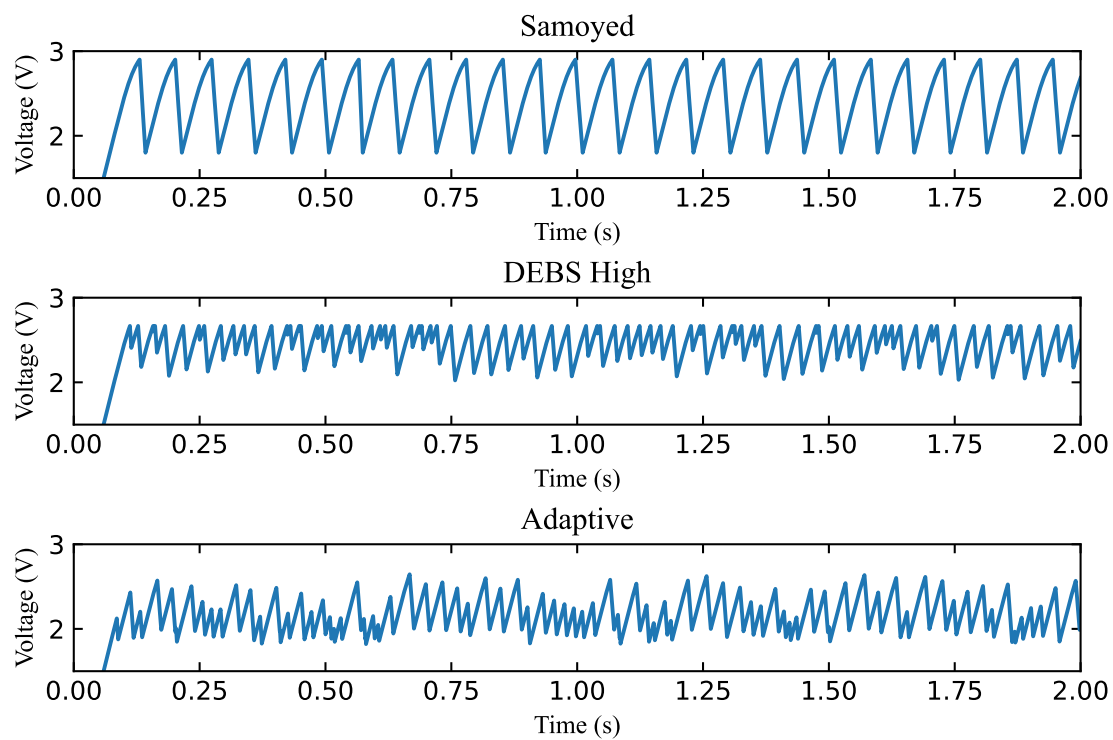


FIGURE 5.4: An instance of supply voltage traces in simulation.

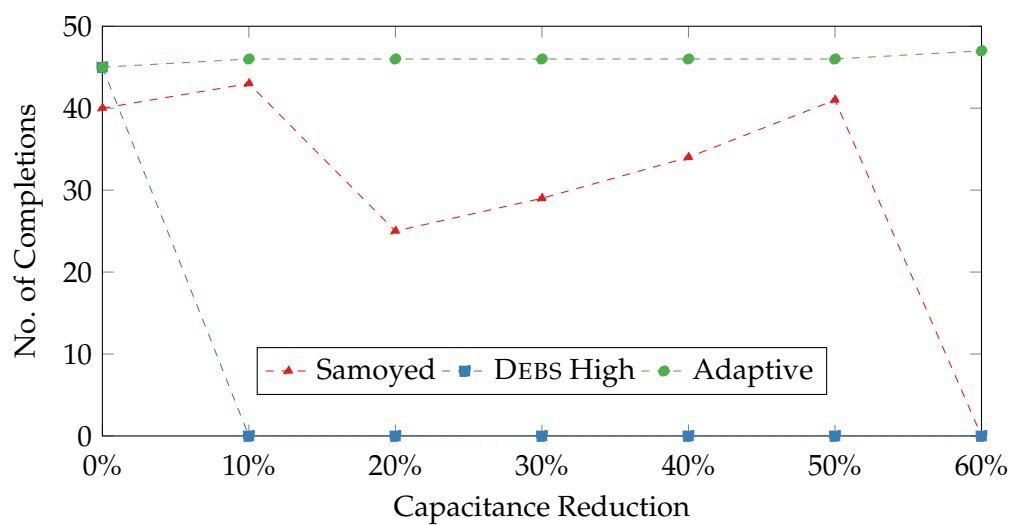


FIGURE 5.5: Number of completed operations of Samoyed, DEBS High, and the Adaptive scheme with capacitance reduction.

in non-termination (e.g. DEBS Low and DEBS High) but allocating an abundant energy budget compromises system efficiency (DEBS High and Samoyed). An adaptive threshold can potentially overcome both problems.

Motivated by the previous examples of variable energy consumption and the benefit of an adaptive threshold, we propose OPTIC, a new methodology for profiling energy consumption of tasks at runtime and adapting energy budgets to the variable energy consumption of tasks.

### 5.3 OPTIC Runtime Energy Profiling

OPTIC's runtime energy profiling method efficiently profiles the maximum drop of supply voltage that a task can cause, i.e. the aforementioned  $\Delta V_{\text{task}}$ . Unlike the previous disconnecting-supply method, OPTIC's performs energy profiling with the supply connected, so as to reserve energy input during profiling. When the supply is connected,  $\Delta V_{\text{task}}$  cannot be measured simply by two voltage measurements at the beginning and the end of a task because the supply keeps charging the system during execution. Instead, OPTIC analyses the supply current in the charge cycle, and uses it to derive  $\Delta V_{\text{task}}$  in the discharge cycle.

OPTIC's runtime energy profiling method assumes an IPS is able to measure the supply voltage and to record time when asleep and active. Usually, these two functions can be achieved with efficient on-chip ADCs and timers on common off-the-shelf MCUs, e.g. MSP430FR series (an example platform used in IPS literature).

#### 5.3.1 A disconnecting-supply approach

Before introducing OPTIC's energy profiling method, a naive method for runtime energy profiling is disconnecting the supply and measure the supply voltage at the beginning ( $V_1$ ) and the end ( $V_2$ ) of a task, hence  $\Delta V_{\text{task}}$  can be calculated as:

$$\Delta V_{\text{task}} = V_1 - V_2 \quad (5.2)$$

However, this can waste the energy input during the task execution. The total wasted charge is:

$$Q_{\text{waste}} = I_{\text{in}} T_{\text{task}} \quad (5.3)$$

which increases linearly with the current input and the time length of a task.

An example circuit to achieve this method is shown in Figure 5.6. It utilises an N-channel FET to short-circuit the energy harvesting supply during calibration, with a pull-down resistor to keep the gate low when MCU is not powered. The supply is

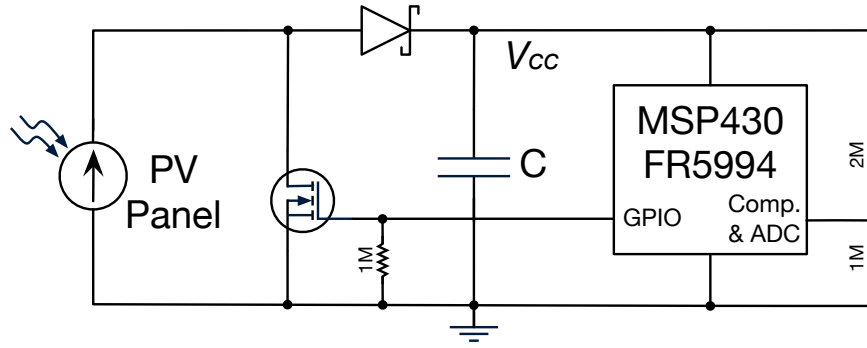


FIGURE 5.6: Experimental schematic.

TABLE 5.3: Definitions of Mathematical Symbols

Symbol	Definition
$\Delta V_{\text{task}}$	Maximum voltage decrease of a task
$\Delta V_{\text{charge}}$	Voltage increase of a charge cycle
$\Delta V_{\text{discharge}}$	Voltage decrease of a discharge cycle
$C$	System energy storage capacitance
$I_{\text{in}}$	Input current from energy harvester
$I_{\text{sleep}}$	System sleep current draw
$I_{\text{task}}$	System execution current draw during a task
$T_{\text{charge}}$	Time length of a charge cycle
$T_{\text{task}}$	Time length of a task execution cycle

decoupled by a diode to prevent current backflow. The MSP430FR5994 MCU uses its internal comparator and ADC to monitor and measure a divided supply voltage  $\frac{1}{3}V_{cc}$ .

### 5.3.2 Principles

To obtain  $\Delta V_{\text{task}}$ , OPTIC's runtime energy profiling method compensates the voltage difference before and after an operation by an estimated voltage gain brought by the supply during the operation. The estimated voltage gain is calculated by measuring the charging ability in the last charge cycle and scaling it with the duration of the discharge cycle. Thus, OPTIC takes three voltage readings and two timer readings to perform one energy profiling.

To focus on the profiling rationale in the following illustration, we temporarily assume the mean supply current in a charge cycle remains the same in the next discharge cycle, both denoted as  $I_{\text{in}}$ . We will discuss the effect of volatile supply current shortly. We also omit the overhead of ADC voltage reading here.

Figure 5.7 to be replaced with a more 'academic' look.

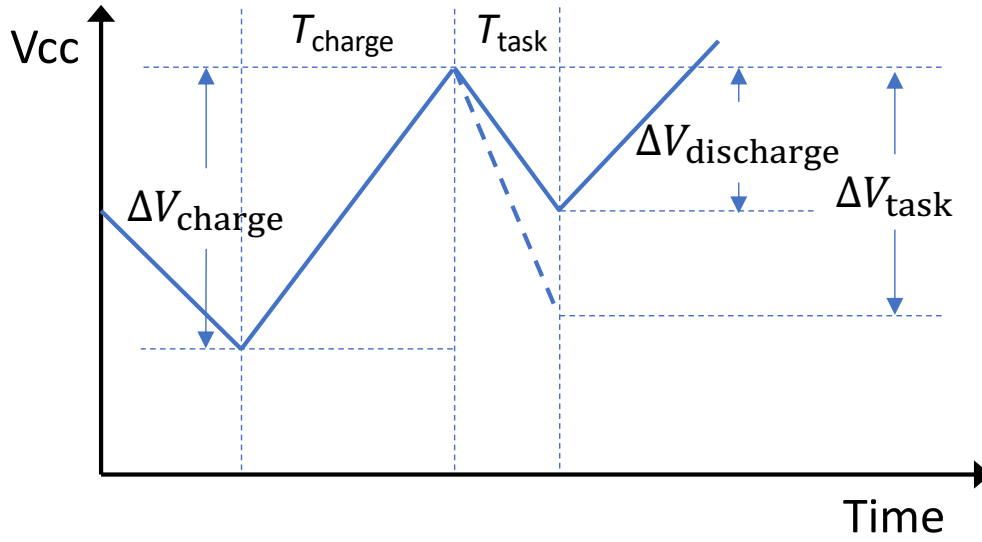


FIGURE 5.7: An illustrative supply voltage trace for explaining OPTIC's runtime energy profiling method.

We show an illustrative trace of supply voltage across a charge-discharge cycle in Figure 5.7 with the symbols listed in Table 5.3.

The system charge increase in the charging cycle can be described as

$$\Delta V_{\text{charge}} C = (I_{\text{in}} - I_{\text{sleep}}) T_{\text{charge}} \quad (5.4)$$

where  $I_{\text{sleep}}$  is the current draw of the whole system when it sleeps and waits for energy refilling, including the current consumption for voltage monitoring, time recording, and other quiescent or leakage current.

The system charge reduction in the discharging cycle can be described as

$$\Delta V_{\text{discharge}} C = (I_{\text{task}} - I_{\text{in}}) T_{\text{task}} \quad (5.5)$$

where  $I_{\text{task}}$  consists of the current draw of the main workload, voltage monitoring, time recording, and other quiescent or leakage current.

The actual charge consumption of a task comes from the consumer part in Equation 5.5, which is

$$\Delta V_{\text{task}} C = I_{\text{task}} T_{\text{task}} \quad (5.6)$$

Hence, combining and rearranging Equation 5.4, Equation 5.5, and Equation 5.6, we can get the expression of  $\Delta V_{\text{task}}$  as

$$\Delta V_{\text{task}} = \Delta V_{\text{discharge}} + \Delta V_{\text{charge}} \frac{T_{\text{task}}}{T_{\text{charge}}} + \frac{I_{\text{sleep}} T_{\text{task}}}{C} \quad (5.7)$$

$\Delta V_{\text{task}}$  is the actual voltage drop that a task can cause, and directly determines the voltage threshold a system should set for the task to safely complete. In Equation 5.7,  $\Delta V_{\text{charge}}$ ,  $\Delta V_{\text{discharge}}$ ,  $T_{\text{task}}$ , and  $T_{\text{charge}}$  are all perceivable values.  $\Delta V_{\text{charge}}$  and  $\Delta V_{\text{discharge}}$  can be measured by three voltage readings at the transition points of charge and discharge cycles.  $T_{\text{task}}$  and  $T_{\text{charge}}$  can be measured with an on-chip timer.

$\frac{I_{\text{sleep}} T_{\text{task}}}{C}$  is a theoretical profiling error of this approach. If it is negligible or compensable,  $\Delta V_{\text{task}}$  can be derived at runtime with all perceivable values.

### 5.3.3 Minimising and Compensating Theoretical Profiling Error

As the profiling method ignores the last term  $\frac{I_{\text{sleep}} T_{\text{task}}}{C}$  in Equation 5.7, the profiled value can be theoretically smaller than the actual one. However, the empirical values of  $I_{\text{sleep}}$ ,  $T_{\text{task}}$ , and  $C$  in IPSs indicate that this error is relatively small. The system sleep current  $I_{\text{sleep}}$  is a key property that is to be minimised in IPSs, and can be down to even sub- $\mu\text{A}$  with modern low power techniques. The system's energy buffering capacitance  $C$  is typically in the  $\mu\text{F}$  level in IPSs. The execution time of a task  $T_{\text{task}}$  is typically a few or tens of ms as the energy buffering capacitor cannot afford a long, energy-hungry task. Hence,  $\frac{I_{\text{sleep}} T_{\text{task}}}{C}$  should be typically under 10 mV. This is insignificant compared to the voltage drop of a task (potentially hundreds of mV), and can be easily or intrinsically compensated by margins in implementation. For example, a voltage comparator may not have such resolution and precision, and thus may over-provision a small energy budget that compensate this error. Manually adding a small software offset to the profiling results can also overcome this error. Therefore, this theoretical profiling error is insignificant in implementation and can be easily compensated.

### 5.3.4 Effect of Volatile Supply Current

The profiling method uses the average current input in the charge cycle as the current input in the next discharge cycle to derive the actual charge consumption. A charge-discharge cycle can be typically from tens to hundreds of ms, considering the capacitor size and the supply power in IPSs. From our practical observation on some types of energy harvesters (e.g. PV cells), OPTIC's profiling method performs stably (results presented in Section 5.6) as the supply current pattern complies with the assumption on supply current. However, we still anticipate there can be more volatile energy sources and discuss the consequent effect.

We denote the the mean current in charge and discharge cycles as  $I_{\text{in.charge}}$  and  $I_{\text{in.discharge}}$  respectively. When  $I_{\text{in.charge}} > I_{\text{in.discharge}}$ , the system over-profiles  $\Delta V_{\text{task}}$  by  $(I_{\text{in.charge}} - I_{\text{in.discharge}})T_{\text{task}}/C$  higher. When  $I_{\text{in.charge}} < I_{\text{in.discharge}}$ , the system under-profiles  $\Delta V_{\text{task}}$  by  $(I_{\text{in.discharge}} - I_{\text{in.charge}})T_{\text{task}}/C$  lower. While the over-profiled energy budget should

be safe, the under-profiled energy budget could be inadequate, making the following task failed. An unfortunate case is when the system first under-profiles a task with a rapidly increasing supply current, and then executes the task again using the newly profiled budget while no further energy is harvested during the execution. This can lead to a task failure, where the system needs the existing approaches in IPSs to maintain atomic progress, e.g. disabling checkpoints during atomic sections. The over- or under-profiled results can be corrected when  $I_{\text{in.charge}}$  and  $I_{\text{in.discharge}}$  match again.

As discussed, it is indicated that OPTIC's profiling method is suitable for energy sources that are not liable to change significantly across a charge-discharge cycle. If the energy source is too volatile to obtain reliable profiling results, a disconnecting-supply profiling method could be adopted as a workaround.

## 5.4 OPTIC Runtime Energy Adaptation

OPTIC runtime energy adaptation utilises the presented runtime energy profiling to dynamically adapts the voltage threshold to the latest energy consumption of a task. The adaptation method assumes the system is able to monitor the supply voltage and signal the MCU to wake up or sleep when a high or low threshold is hit, and the threshold is configurable by the MCU at runtime. In practice, this voltage monitoring ability is widely adopted by IPSs in the forms of a voltage comparator [29, 112], an energy management unit [24, 35], or a periodic ADC polling [94].

The fundamental goal of the runtime energy adaptation is to allocate a barely sufficient energy budget for each task. Utilising the presented runtime energy profiling method, OPTIC is able to obtain the latest  $\Delta V_{\text{task}}$  of a task and update its threshold accordingly. The voltage threshold  $V_{\text{th}}$  of a barely sufficient energy budget is defined as:

$$V_{\text{th}} = \Delta V_{\text{task}} + V_{\text{end}} \quad (5.8)$$

where  $V_{\text{end}}$  is the target end voltage below which the whole or part of system's hardware cannot function correctly.  $V_{\text{end}}$  can be higher than the MCU shutdown voltage, e.g. a peripheral that has a higher operating voltage. Besides allocating the lowest  $V_{\text{th}}$ , an ideal adaptation scheme is also expected to have low overheads, run energy profiling only when necessary, and react to energy variations immediately.

Based on the above aims, we design OPTIC's runtime adaptation scheme. It consists of a basic adaptation routine for a fixed workload and an optional linear adaptation method for workloads that has a linearly-scaled  $\Delta V_{\text{task}}$  with dynamic parameters. OPTIC's runtime energy adaptation is decoupled with the energy profiling method. The adaptation scheme allows the energy profiling method to be integrated in the routine

but only requires an interface which allows it to trigger an instance of profiling and return a profiling result.

### 5.4.1 Adaptation Routine

A flowchart of OPTIC's adaptation routine is shown in Figure 5.8. The routine operates at the entry and the exit of a task. Checkpoints are disabled during the atomic task, so the program rolls back to a point before the task entry if a power interruption happens between the entry and the exit. The system executes the task body when  $V_{cc}$  is above  $V_{th}$ . If  $V_{cc}$  is below  $V_{th}$ , the system sleeps and waits until  $V_{th}$  is reached.

A non-volatile flag, "failed", is assigned for each task in order to monitor whether  $V_{end}$  is met with the current  $V_{th}$ . The "failed" flag is set when a power interruption happens in the task body or when  $V_{cc}$  falls below  $V_{end}$  after the task body finishes. At the entry of a task, OPTIC checks whether "failed" is set, i.e. whether  $V_{th}$  fails to meet  $V_{end}$  last time, and increment  $V_{th}$  if it is set. The increment amount can be dependent on volatility of energy consumption and the resolution of the adopted voltage monitor. In practice (Section 5.5), we found that incrementing one unit step of the voltage monitor, which corresponds to about 30 mV in our implementation, suffices both stability and reactivity.

Following the failure check, the routine has a control of when to trigger energy profiling (blue blocks in Figure 5.8), such that energy profiling is not performed every time that the task is run so as to save the energy and time overheads on unnecessary profiling. The control logic can be configured as per the requirements of users or applications. We have exemplified this with a delay counter, where the energy profiling is enabled every a number of completions. Alternatively, persistent timekeepers [113–115] can also be used to trigger energy profiling once a period of real time passes.

If energy profiling is enabled, the dashed purple blocks in Figure 5.8 are performed in the routine. The particular operations involved can be dependent on the profiling method, while we have illustrated this in the flowchart with OPTIC's profiling method. As explained, OPTIC's energy profiling operates at three points when the charge cycle starts, when the charge cycle ends and the discharge cycle starts, and when the discharge cycle ends.  $V_{th}$  is then updated after a new  $\Delta V_{task}$  is profiled following Equation 5.8. If a charge cycle is not needed, i.e. the energy stored is already sufficient for the task, the profiling is skipped and performed next time as this contradicts the design of OPTIC's profiling method.



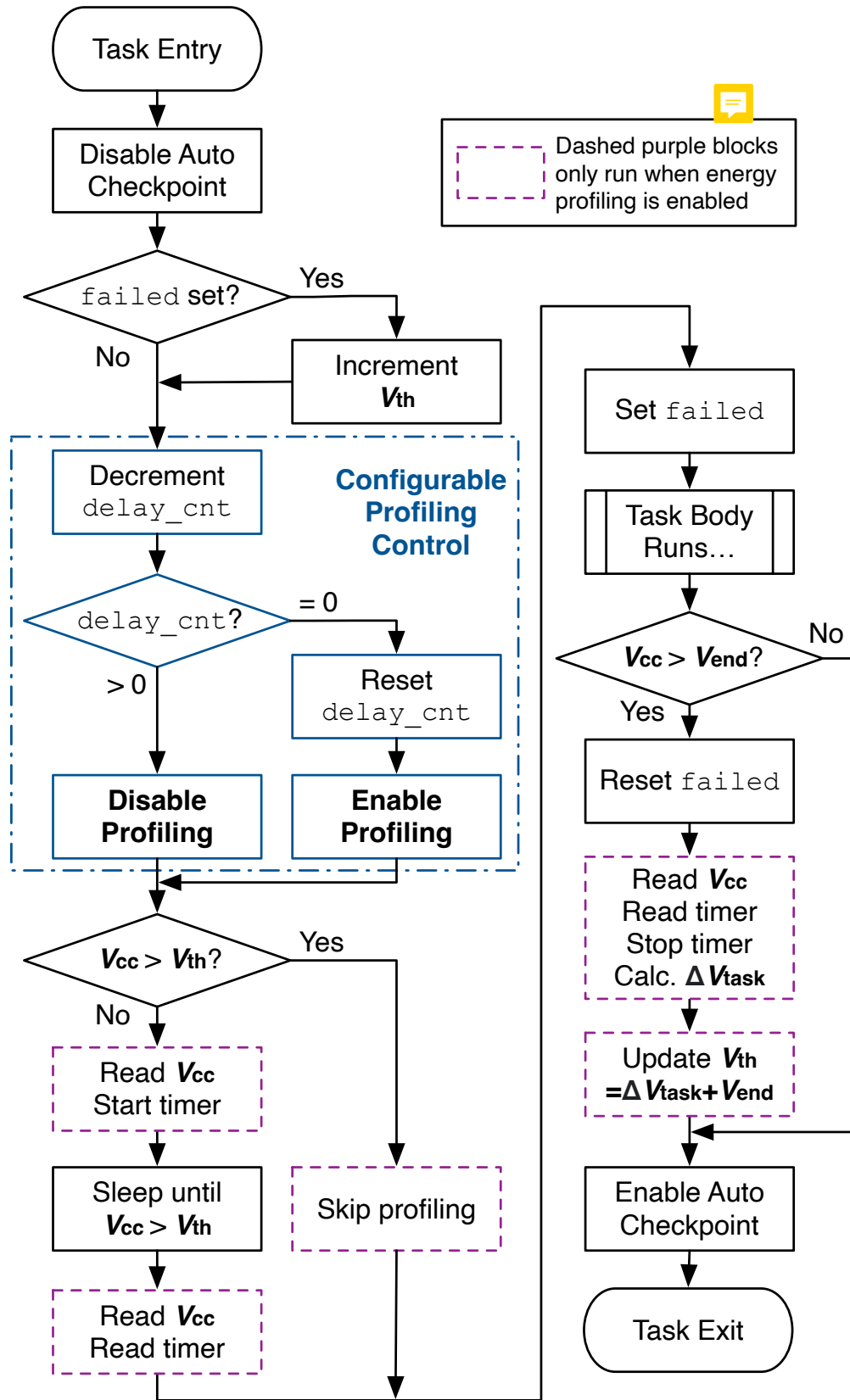


FIGURE 5.8: Flowchart of OPTIC's runtime energy adaptation routine. The blue blocks represent a configurable control logic to decide when to perform energy profiling. The dashed purple blocks are only run when the profiling is enabled, and represent OPTIC's energy profiling with the last block updating  $V_{th}$  with the new  $\Delta V_{task}$ .

### 5.4.2 Linear Adaptation

The above threshold adaptation is design for workloads that have a fixed amount of computational work and a determined configuration, the  $\Delta V_{\text{task}}$  variation of which can change slowly with non-computational factors, e.g. capacitor ageing or temperature variations. For workloads that have runtime changeable parameters that scale energy consumption significantly, e.g. data sizes and peripheral configurations, the above adaptation can cost a number of failures before adapting to the new threshold. While dynamic configurations can be solved with multiple thresholds that switched by the configuration, data sizes can be fine-grained and can introduce a high memory overhead considering the number of thresholds needed. Hence, we propose a linear adaptation method as an option for workloads that have linearly-scaled energy consumption with its parameter.

Thus, a linearly-scaled  $\Delta V_{\text{task}}$  can be represented as:

$$\Delta V_{\text{task}} = \theta_1 x + \theta_0 \quad (5.9)$$

where  $x$  is the parameter that is supposed to scale  $\Delta V_{\text{task}}$ .  $\theta_1$  and  $\theta_0$  are the slope and y-intercept of the linear relationship between  $\Delta V_{\text{task}}$  and  $x$ . Hence,  $V_{\text{th}}$  for the task should be set as:

$$V_{\text{th}} = \theta_1 x + \theta_0 + V_{\text{end}} \quad (5.10)$$

A straightforward solution to obtain  $\theta_1$  and  $\theta_0$  can be taking a series of profiling results and calculating the regression function. Though viable, this can introduce relatively high overheads on sampling and calculation.

To lower the overheads, we adopt an efficient method where energy profiling is performed to update  $\theta_1$  and  $\theta_0$  when  $x$  reaches its minimum or maximum values.  $\theta_1$  and  $\theta_0$  can then be calculated with less computation than linear regression. When the task is run with a  $x$  value other than the minimum or maximum, the energy profiling is disabled and  $\theta_0$  is incremented when necessary, e.g. a  $x$  value that causes a higher  $\Delta V_{\text{task}}$  than what the equation predicts.

The routine of the linear adaptation method is then similar to the one shown in Figure 5.8, with modifications on the profiling control and the increment and update of  $V_{\text{th}}$ , where it controls whether to profile based on  $x$ , increments  $\theta_0$ , and updates  $\theta_1$  and  $\theta_0$  rather than  $V_{\text{th}}$ .

Discussion on e.g. adaptation to other non-linear relationship, the ability to fall back differentiates it from a "simply-incrementing-threshold" approach?

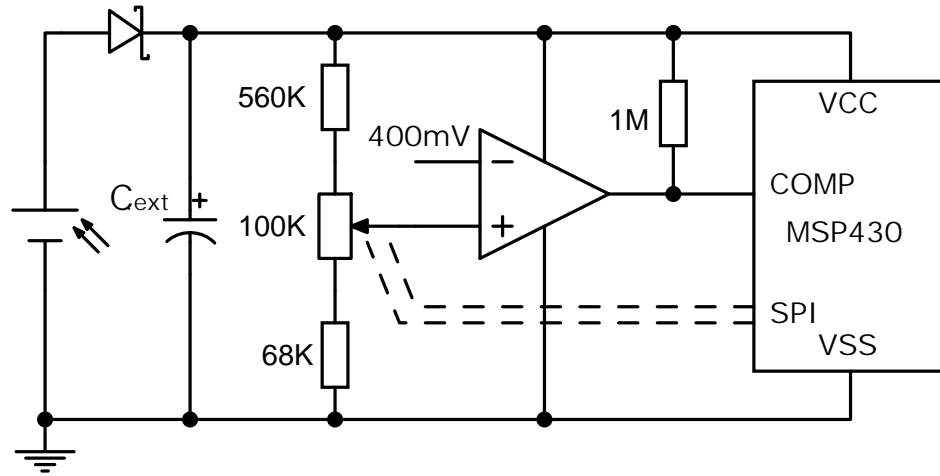


FIGURE 5.9: OPTIC system schematic.

## 5.5 Implementation

OPTIC was implemented based on an MSP430FR5994 development board. Its runtime is implemented as a C library and used with function calls. OPTIC is available open-source at <https://git.soton.ac.uk/jz8u17/atom-energy>, along with the simulation program of design exploration, comparisons of runtime (Samoyed and DEBS), and benchmarks.

Check the git repo later.

The system schematic is shown in Figure 5.9. To reduce power consumption, the system utilises the MCU's on-chip ADC, timer, and voltage reference to perform energy profiling, and an external voltage monitor to monitor and control the threshold. The energy harvester is decoupled from the rest of the system by a diode to prevent the backflow of current when the harvester's power output drops off. The harvested energy is then buffered in a  $10\text{ }\mu\text{F}$  capacitor ( $C_{\text{ext}}$ ). Together with  $1.5\text{ }\mu\text{F}$  on-board decoupling capacitance, the system has an energy buffering capacity of  $11.5\text{ }\mu\text{F}$  in total.

The energy profiling is achieved through the on-chip modules. The ADC reads voltage from a built-in  $1/2 V_{\text{CC}}$  channel, and thus an external voltage divider is not needed. A  $2\text{ V}$  voltage reference is used by the ADC to convert the voltage reading, hence providing a  $0\text{--}4\text{ V}$  reading range. A timer, driven by a  $10\text{ kHz}$  low-power clock, records the charge and discharge cycle for OPTIC's energy profiling.

### 5.5.1 External Voltage Monitor

As shown in Figure 5.9, we built an external voltage monitor to control the threshold that signals the MCU to wake up or sleep. The voltage monitor consists of a 100 k $\Omega$  129-step digital potentiometer (MCP4131-104) controlled through SPI, a voltage comparator (LT6703HVIS5-3) with 400 mV internal reference. Two resistors, 560 k $\Omega$  and 68 k $\Omega$ , were connected with the digital potentiometer to provide a detection range of 1.73–4.28 V, which covers the operating voltage range of the system. A 1 M $\Omega$  pull-up resistor was added at the comparator's open-collector output. Hence, the detected voltage threshold of  $V_{cc}$  is:

$$V_{th} = \frac{560 + 100 + 68}{\frac{N_{wiper}}{128} * 100 + 68} \times 0.4 \quad (V) \quad (5.11)$$

where  $N_{wiper}$  is the wiper step of the potentiometer, ranged in 0-128 inclusively. Also, the profiling result of  $\Delta V_{task}$  is stored as  $N_{profiling}$  in a digital ADC-scale format:

$$\Delta V_{task} = \frac{N_{profiling}}{N_{adcmax}} \times V_{adcmax} \quad (5.12)$$

where  $\Delta V_{task}$  is as defined in Equation 5.8.  $N_{adcmax}$  and  $V_{adcmax}$  are the maximum digital ADC reading and its corresponding voltage, which are 4095 and 4 V respectively in our implementation. Combining Equation 5.8, Equation 5.11, and Equation 5.12, we can obtain the relationship between  $N_{profiling}$  and  $N_{wiper}$  as:

$$\frac{N_{profiling}}{N_{adcmax}} \times V_{adcmax} + V_{end} = \frac{560 + 100 + 68}{\frac{N_{wiper}}{128} * 100 + 68} \times 0.4 \quad (5.13)$$

where  $V_{end}$  is the target end voltage, which we set at 2 V because the energy profiling uses the 2 V voltage reference for ADC reading such that the energy profiling can correctly work above  $V_{end}$ .

In order to speed up the threshold setting from this non-linear relationship (Equation 5.13), We generated a look-up table to efficiently convert a profiling result  $N_{profiling}$  into the corresponding voltage threshold setting  $N_{wiper}$ . To avoid unnecessarily fine-grained steps, we equally divide  $N_{profiling}$  by a step of  $N_{step}$ . We recommend setting  $N_{step}$  as a power of 2 for an efficient threshold conversion, and we set  $N_{step}$  as 32, which translates to a voltage step of about 31 mV. We traversed  $N_{wiper}$  to find the closest  $V_{th}$  for each step of  $N_{profiling}$ , and the look-up table is then formed by the array of  $N_{wiper}$ . We also shifted the look-up table by one step higher so that the look-up table can inherently round up the threshold. Therefore, the corresponding threshold setting  $N_{wiper}$  of a profiling result  $N_{profiling}$  can be found in the look-up table with a computation-efficient

index of  $\frac{N_{\text{profiling}}}{N_{\text{step}}}$  as shown in Equation 5.14.

$$N_{\text{wiper}} = \text{lookup\_table}\left(\frac{N_{\text{profiling}}}{N_{\text{step}}}\right) \quad (5.14)$$

### 5.5.2 Software

OPTIC's software is implemented as a library that accounts for the bootstrap configuration, function interfaces, memory mapping, and state retention. The bootstrap performs necessary system initialisation, such as configuring clocks, GPIOs, essential peripherals, and loading RAM data. OPTIC's software interface is implemented as two function calls at the entry and exit of an atomic task. Each atomic task should be assigned with a function ID such that its state is independent from other atomic tasks. The state of an atomic task consists of a minimum of 2 bytes non-volatile data that accounts for a failure check and an adaptive threshold, with optional data for a user-defined control logic (e.g. a delay counter) or linear adaptation. The state retention mechanism is implemented as a style of reactive intermittent computing as in [34, 73]. The usage of OPTIC's software is straightforward by assigning an ID to an atomic task in the library's header and calling the functions with the ID at the entry and exit of the atomic task.

## 5.6 Experimental Evaluation

We experimentally evaluated OPTIC, showing its ability to run with an adaptive minimum threshold that mitigate non-termination and improve energy efficiency. OPTIC's runtime energy profiling presents a low and relatively consistent error across different task scales. We show that, despite with reduced capacitance, OPTIC is able to adapt  $V_{\text{th}}$  to meet a target end voltage  $V_{\text{end}}$  until the highest threshold is reached, while the fixed-threshold comparison DEBS fails. We also show that OPTIC improves performance over DEBS and Samoyed with a PV panel supply owing to its reduced operating voltage.

### 5.6.1 Experimental Setup and Benchmarks

A PV panel (Sanyo AM-1417CA) provided the sole power supply for the system. It is covered in a black box with a white LED light as the only energy source, producing a consistent supply characteristic (as shown in Figure 5.2) during the experiments. For the experiment on capacitance reduction only, we instead use a constant low-current supply so as to examine whether the system is able to survive with little energy income during task execution.

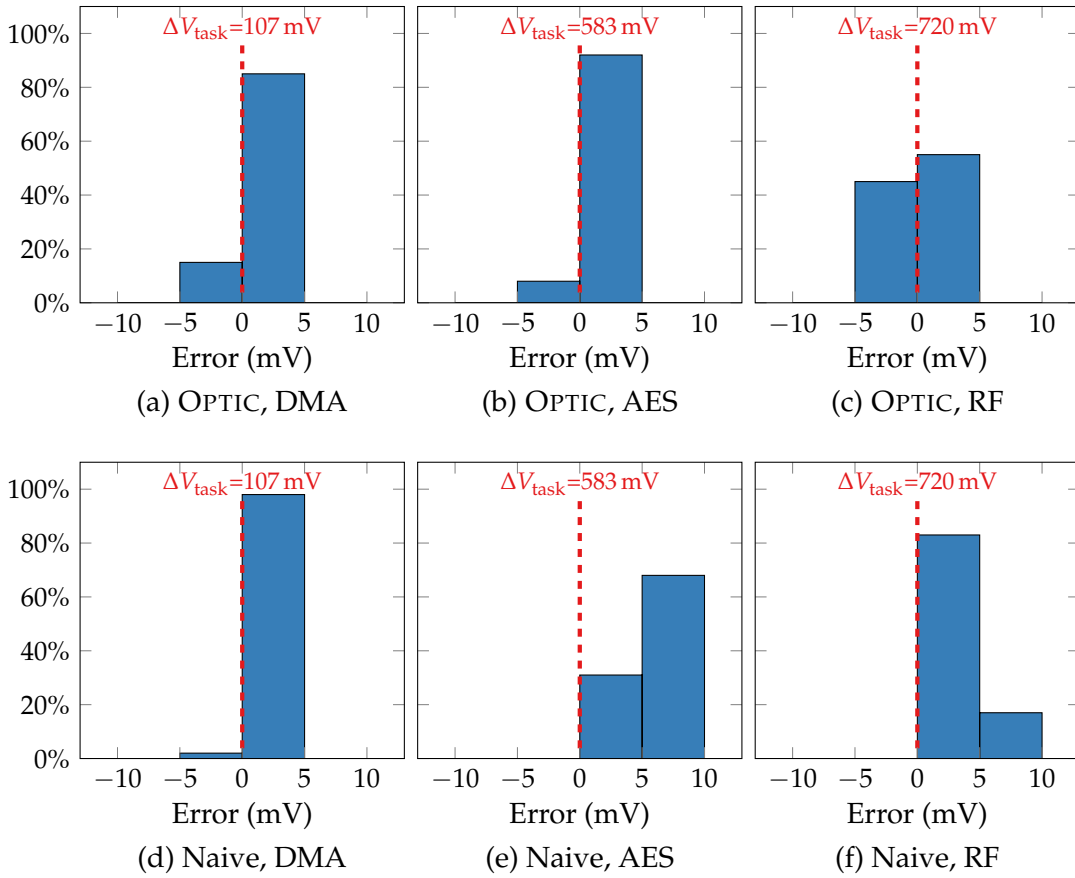


FIGURE 5.10: Error Distribution of OPTIC's Runtime Energy Profiling given a PV supply, compared to the "Naive" disconnecting-supply method.

Three common peripheral tasks in IoT sensors were used as the benchmarks for evaluation.

- **DMA:** Data transfer using an on-chip DMA module, frequently used in data logging.
- **AES:** AES encryption using an on-chip AES accelerator processing up to 4KB data at a time for secure communication.
- **RF:** Wireless communication through an external nRF24L01 radio module, transmitting a payload up to 96B at a time, configured as a 2Mbps air data rate and a 0 dBm output power. The radio module is connected through an LDO with a 2 V output voltage to lower the quiescent current consumption, with a 10  $\mu\text{F}$  at the LDO's low side.

### 5.6.2 Profiling Accuracy

We first measured the profiling accuracy of OPTIC's runtime energy profiling ability. A hundred profiling results were obtained for each workload. Manual profiling was

also conducted by disconnecting the power supply during task execution and reading  $\Delta V_{\text{task}}$  from a scope, and used as a reference that we evaluate the profiling results against. The results are divided in a 5 mV step because the resolution of our scope is 5 mV, below which the manual profiled reference is not even accurate.

As shown in Figure 5.10, the profiling errors are low and relatively consistent (mostly within 5 mV) across the three workload with different levels of energy consumption. The error becomes insignificant with energy-hungry tasks, e.g. RF. Compared to the step of voltage thresholds in our implementation (around 30 mV), this 5 mV error is acceptable as it can convert to a relatively stable threshold assuming a fixed energy consumption.

Additionally, the average profiling results are shown to be a slightly higher than the reference, which seems to contradict the theoretical error that is supposed to make the profiling undershoot. This is majorly due to a positive error in the MCU's internal  $1/2 V_{\text{cc}}$  divider from an observation that the Naive approach produced a higher reading. This also evidences that the theoretical error is insignificant and easily compensated by other factors.

### 5.6.3 Reliability with Dynamic Energy Consumption

We evaluated whether OPTIC can adapt to variability in IPSs and keep making forward progress. We classified the variability in three categories according to the frequency of these changes:

- **Changing once**, such as new workloads, devices, and components.
- **Changing infrequently**, such as capacitor ageing, device ageing, temperature changes, and configurations that last for a long term.
- **Changing frequently**, such as variable data sizes and peripheral configurations that can frequently change.

To reduce similar results, we show one example in each category to illustrate OPTIC's adaptation to variability.

#### 5.6.3.1 Changing once

Figure 5.11 shows an example of how OPTIC adapts its threshold to a new workload and a new device. The system runs an AES-128 encryption on 1KB data repetitively. The algorithm does not have any knowledge on the energy consumption of the platform or the workload. The system first waits for the initial profiling threshold, which

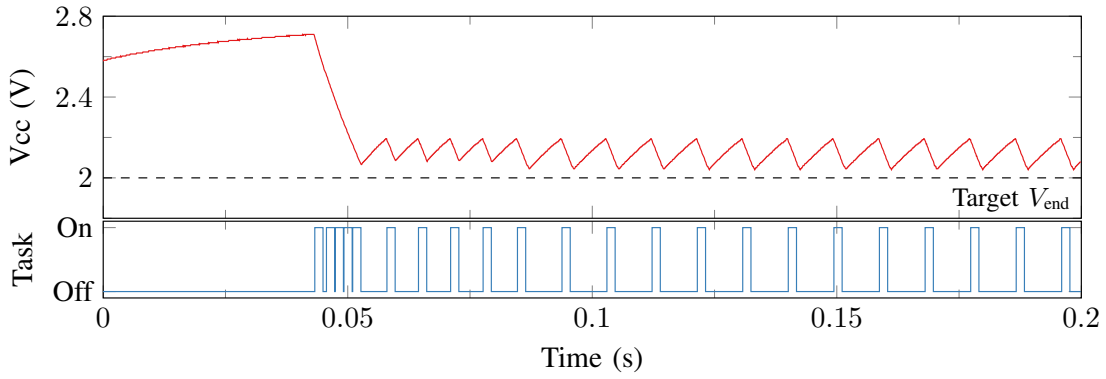


FIGURE 5.11: A voltage trace of OPTIC adapting to a new operation on a new device.

is set at 2.7 V in this case. Then it performs energy profiling as this is the first time it executes this task. The next threshold for the task is then adapted to a lower one. In the following execution, the system is able to maintain the same threshold that guarantees the completion of the task. The end voltage after completing a task matches closely with the target  $V_{\text{end}}$ , with a small margin that comes from both the round-up threshold and the energy harvested during the task execution. The above example shows OPTIC's ability to adapt to a new workload or device, obviating the need for manual energy profiling for various scenarios, e.g. updating workloads or deploying new devices.

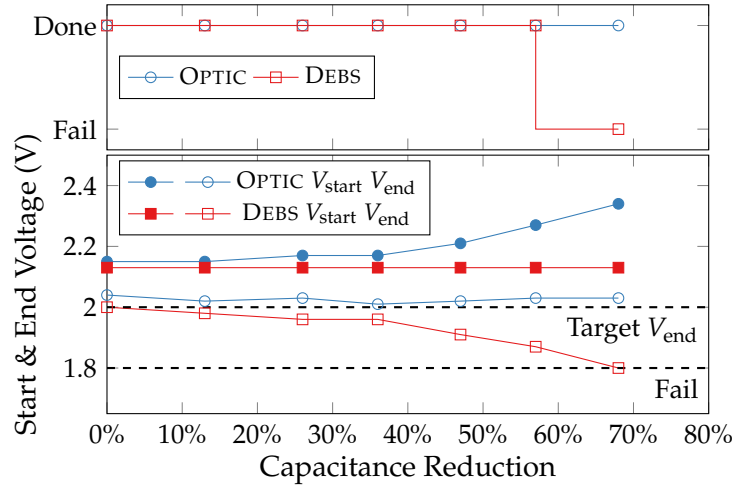
### 5.6.3.2 Changing infrequently

We then evaluated OPTIC's adaptation on infrequently or slowly changing  $\Delta V_{\text{task}}$ . We took capacitor ageing as an example for this category of changes. The capacitor ageing was emulated with a capacitor bank consisting of 1  $\mu\text{F}$  capacitors. The capacitor bank replaced the 10  $\mu\text{F}$   $C_{\text{ext}}$  in Figure 5.9, and hence the system capacitance could then be tuned in the range of 1.5–11.7  $\mu\text{F}$  with 1.2–1.5  $\mu\text{F}$  per step as measured.

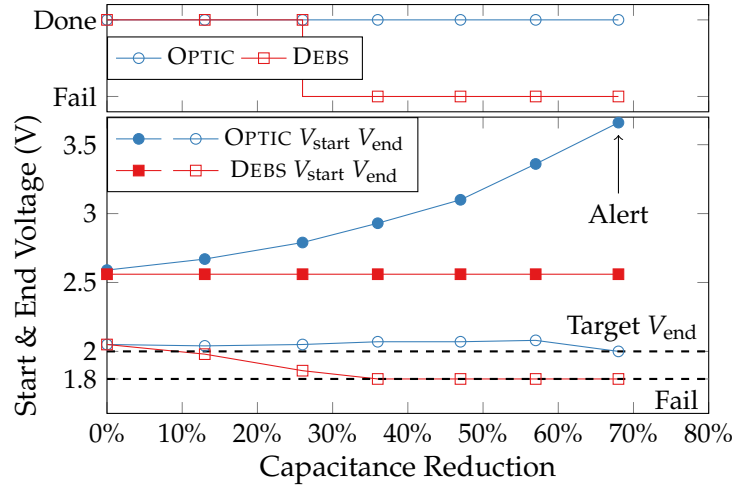
In this experiment, the initial system capacitance was 11.7  $\mu\text{F}$ , and was reduced step by step to test the system's ability against capacitor ageing. We compared OPTIC against DEBS in terms of whether it may fail. As the target end voltage for OPTIC in this implementation is 2 V, we configured the thresholds of DEBS against 2 V as well for a fair comparison, allowing additional energy before the shutdown threshold (1.8 V) is reached. We omitted the results of Samoyed as it assumes an abundant energy budget and the simulation results in Figure 5.5 indicate it is resilient to reduction of capacitance though with performance loss.

Figure 5.12 shows whether OPTIC and DEBS can safely complete the tasks with their threshold settings, along with their start and end voltages. In terms of meeting the target  $V_{\text{end}}$ , OPTIC is able to increase its threshold to prevent its end voltage dropping below the target  $V_{\text{end}}$ , while DEBS fails to do so with reduced capacitance as its

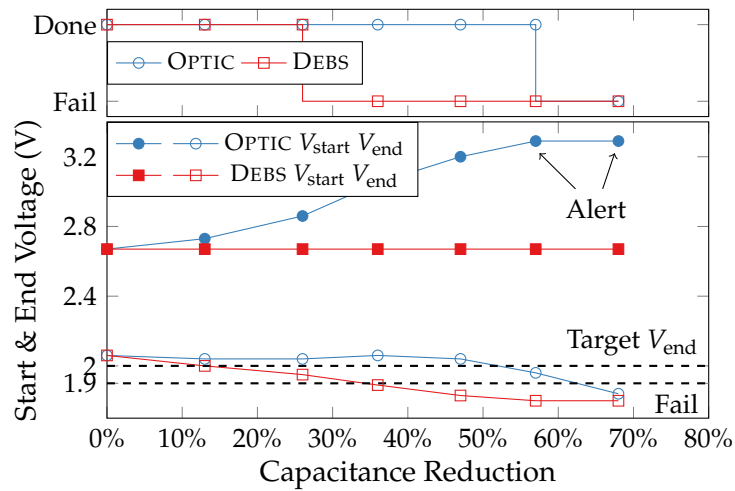




(A) DMA



(B) AES



(C) RF

FIGURE 5.12: Effect of Capacitor Degradation on OPTIC and DEBS.

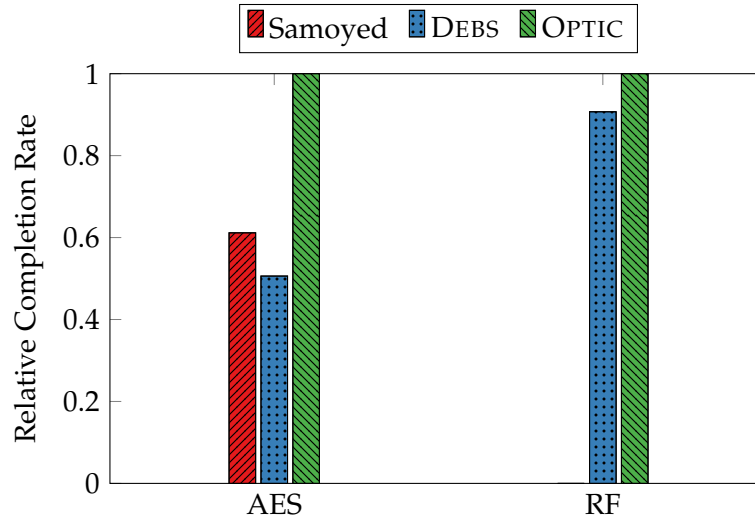


FIGURE 5.13: Relative Completion Rates of Samoyed, DEBS, and OPTIC with variable data sizes and a PV supply.

threshold is fixed. The increase of OPTIC's threshold has a limit, where we set with the maximum operating voltage (3.6 V) for DMA and AES, and 3.3 V for RF beyond which the system's quiescent current draw becomes larger than the supply. OPTIC's threshold is increased with reduced capacitance until the upper limit is met, where it signals an alert. In a practical scenario, the alert could be sent to maintainers and indicate further actions needed. Owing to the threshold adaptation, OPTIC can still survive with much lower capacitance, only failing the RF task with the lowest capacitance (67.5% reduction).

### 5.6.3.3 Changing frequently

A task may have runtime variable data sizes and configurations, which frequently change  $\Delta V_{\text{task}}$ . While DEBS and Samoyed can set a high threshold that suffices the most energy-hungry task, OPTIC can also adapt its threshold to frequently changing  $\Delta V_{\text{task}}$  so as to lower operating voltage and increase forward progress.

We demonstrate OPTIC's linear threshold adaptation on workloads that have variable data sizes, where AES encrypts 512B to 4KB data with a 256-bit key length, and RF sends 16B to 96B data. An array of randomised numbers was generated to switch the data sizes. The average completion rate in a 30s window was recorded as a performance metric. As shown in Figure 5.13, OPTIC managed to make 64% and 98% more progress compared to Samoyed and DEBS respectively on the AES workload. On the RF workload, the improvement compared to DEBS is 10% while Samoyed failed because the radio cannot reset to the correct state after a power failure and draws large current. The improvement of OPTIC comes from a lower threshold from which the system can harvest more energy and save the time on waiting for unnecessary energy.

## 5.7 Summary

Though previous IPS designs adopt fixed energy thresholds profiled at design time for atom tasks, this chapter has shown that this can cause non-termination or reduce system energy efficiency. We found that the variability in IPSs can significantly change energy consumption. We presented four examples of such variability, i.e. variable data sizes, variable peripheral configurations, device variability, and capacitor ageing, all of which can violate a predefined energy threshold at runtime.

To address this issue, we proposed OPTIC, a runtime energy profiling and adaptation method. We proposed two methods of runtime energy profiling. A disconnecting-supply method measures the supply voltage difference before and after executing a task while short-circuiting the supply. While this is straight forward, it wastes the energy input during the task execution. A connecting-supply method for runtime energy profiling is also proposed, where it estimates the energy input during the task execution by measuring the current input before the task and compensating the supply voltage difference of execution. Experimental results has shown the proposed profiling method has a high accuracy of less than 5 mV. This enables IPSs to profile tasks' energy consumption at runtime and alleviates manual profiling efforts in development. We also proposed a runtime energy adaptation routine that adapts the voltage threshold for a task utilising the proposed runtime energy profiling, with an option of linearly scaling the threshold by user-defined parameters.

We implemented OPTIC on a TI MSP430FR5994 MCU, with an external supply voltage monitor that can be efficiently configured and wake up the MCU when a threshold is hit. The experimental results showed that OPTIC can reliably adapt its threshold for a new task on a new device. OPTIC can also adapt to an increased  $\Delta V_{\text{task}}$  caused by increased energy consumption or device ageing, e.g. up to 67.5% capacitance reduction that emulates an ageing capacitor, while the SoA fails, making IPSs possible to operate beyond capacitor lifetime. Finally, with variable data sizes or configurations, OPTIC is able to efficiently set barely sufficient energy thresholds that lowers operating voltage and improves energy efficiency, thus improving up to 98% progress over the SoA.



## Chapter 6

# Conclusions and Future Work

Enabled by energy harvesting and low-power computing techniques, IPSs are expected to be a promising system paradigm for numerous IoT sensors in the near future, with forecasts of hundreds of billions being installed [116]. IPSs adapt to the intrinsically variable and uncontrollable power input of energy harvesters, and thus, circumvent large volume, environmental impact, and limited lifespan of large energy buffers, i.e. batteries and supercapacitors, that contradict with the requirements of future IoT sensors.

While existing IPS technology has mainly focussed on the computing part, i.e. efficiently and correctly retaining the system state across power interruptions, this thesis has explored energy budgeting in IPSs. The energy budget in an IPS is represented as the energy of an active cycle when the load wakes up and executes program. As the energy budget is determined by the energy storage size and the voltage threshold that wakes up the load, we have conducted the research following the two aspects, where Chapter 3 and Chapter 4 explored the energy storage sizing effect and Chapter 5 proposed runtime profiling and adaptation of voltage thresholds.

To minimise device dimensions and interruption periods, most IPSs have adopted only a minimum amount of energy storage. However, in Chapter 3, we have found that this can be energy inefficient as the system has to frequently save and restore the state. Hence, we have proposed a reactive IPS model to explore the sizing effect of energy storage on forward progress. Derived from the pattern of operating cycles in IPSs, the proposed model can fast and accurately estimates forward progress given supply current and energy storage capacitance, facilitating exploration and understanding of IPSs. We configured the proposed model with experimentally profiled parameters on a reactive IPS platform. The model was experimentally validated with a 0.5% mean error across multiple conditions of supply current and energy storage capacitance. We then explored the energy storage sizing effect with respect to supply current and volatile

state size, showing a forward progress improvement of up to 65% compared to using minimised energy storage. We also found that the forward progress improvement from sizing energy storage becomes significant when supply current is low and when volatile state size is large. Additionally, we also found that the energy storage capacitance that achieves the maximum forward progress improvement (i.e.  $C_{\alpha_{\max}}$  as denoted in Chapter 3) can be  $3.2\times$  as large as the one that gains a 95% improvement. With considerations on volume and charging time of a large capacitor, this indicates that we need an energy storage sizing approach that comprehends multiple design factors in IPSs instead of maximising forward progress only.

Extended from Chapter 3, an energy storage sizing approach for deploying IPSs was proposed in Chapter 4. Following a modelling and simulation process, the sizing approach is able to output forward progress, capacitor volume, and interruption periods given long-term energy source data, energy harvester configurations, and energy storage capacitance. Through iterations with different capacitance values, the sizing approach trades off various properties of the system with a cost function and recommends an appropriate energy storage size. We have configured and demonstrated the sizing approach with parameters profiled on an IPS and real-world data of indoor and outdoor PV sources. The results showed up to a 43% annual forward progress gain by sizing energy storage. Corresponding to Chapter 3, this improvement is more significant with weaker power input, e.g. a smaller PV panel size. With an example cost functions, the results showed that the suggested energy storage capacitance achieves 93% of the maximum forward progress while saving 83% capacitor volume and 91% interruption periods, compared to the one that solely maximises forward progress. Combining the findings in Chapter 3 and Chapter 4, we conclude that energy storage should be carefully designed, rather than minimised or indiscriminately picked, to efficiently operate IPSs.

While the energy storage size studied, Chapter 5 has focussed on the voltage thresholds of an energy budget. We found that, with the runtime variability of energy consumption, the prior SoA approaches can cause non-termination or reduce system energy efficiency. We have exemplified the variable energy consumption in four cases, which are variable data sizes, variable peripheral configurations, device variability, and capacitor ageing. Motivated by this, we proposed OPTIC, a runtime energy profiling and adaptation method. OPTIC's runtime energy profiling measured  $\Delta V_{\text{task}}$  (as explained in Section 5.2) with supply connected to save the input energy during profiling. To obtain  $\Delta V_{\text{task}}$ , it measures the input current before the task and compensates the supply voltage difference of executing a task by the input current. Utilising the runtime energy profiling method, OPTIC's runtime energy adaptation adapts the voltage threshold for a task, efficiently allocating a barely sufficient threshold according to its runtime energy consumption. OPTIC's runtime energy adaptation also provides an option of linearly

scaling the threshold by user-defined parameters, allowing a fast switching of thresholds without excessive profiling. We implemented OPTIC on a TI MSP430FR5994 MCU with an external supply voltage monitor. The experimental results has shown multiple findings as follows. OPTIC's runtime energy profiling has a low error within 5 mV, enabling IPSs to perform energy profiling at runtime and alleviating manual profiling efforts. OPTIC can adapt its threshold for a new task or on a new device. OPTIC is also able to cope with an increased  $\Delta V_{\text{task}}$  from increased energy consumption or capacitor ageing, where it survived with up to 68% capacitance reduction while the SoA failed, allowing IPSs to operate beyond capacitor lifetime. Finally, OPTIC efficiently adjusts to a barely sufficient threshold with variable data sizes, which lowers operating voltage and improves energy efficiency, thus improving up to 98% progress over the SoA approaches.

Answers to research questions?

## 6.1 Future Work

Can the threshold go even lower?

Can IPS change from a MCU-centred system to an EMU-centred system, i.e powering the load modules in turn?





## References

- [1] Jie Zhan, Geoff V. Merrett, and Alex S. Weddell. Exploring the effect of energy storage sizing on intermittent computing system performance. *IEEE Transactions on Computer-Aided Design of Integrated Circuits and Systems*, pages 1–10, 2021.
- [2] Jie Zhan, Alex S. Weddell, and Geoff V. Merrett. Adaptive energy budgeting for atomic operations in intermittently-powered systems. In *Proceedings of the 8th International Workshop on Energy Harvesting and Energy-Neutral Sensing Systems, ENSys '20*, page 82–83, New York, NY, USA, 2020. Association for Computing Machinery.
- [3] Oliver Hahm, Emmanuel Baccelli, Hauke Petersen, and Nicolas Tsiftes. Operating systems for low-end devices in the internet of things: a survey. *IEEE Internet of Things Journal*, 3(5):720–734, 2016.
- [4] Luca Mainetti, Luigi Patrono, and Antonio Vilei. Evolution of wireless sensor networks towards the internet of things: A survey. In *Software, Telecommunications and Computer Networks (SoftCOM), 2011 19th International Conference on*, pages 1–6. IEEE, 2011.
- [5] Tosiron Adegbiya, Anita Rogacs, Chandrakant Patel, and Ann Gordon-Ross. Microprocessor optimizations for the internet of things: A survey. *IEEE Transactions on Computer-Aided Design of Integrated Circuits and Systems*, 37(1):7–20, 2017.
- [6] Weisong Shi, Jie Cao, Quan Zhang, Youhuizi Li, and Lanyu Xu. Edge computing: Vision and challenges. *IEEE Internet of Things Journal*, 3(5):637–646, 2016.
- [7] Jan M Rabaey, M Josie Ammer, Julio L Da Silva, Danny Patel, and Shad Roundy. Picoradio supports ad hoc ultra-low power wireless networking. *Computer*, 33(7):42–48, 2000.
- [8] Paul D Mitcheson, Eric M Yeatman, G Kondala Rao, Andrew S Holmes, and Tim C Green. Energy harvesting from human and machine motion for wireless electronic devices. *Proceedings of the IEEE*, 96(9):1457–1486, 2008.
- [9] Sravanthi Chalasani and James M Conrad. A survey of energy harvesting sources for embedded systems. In *Southeastcon, 2008. IEEE*, pages 442–447. IEEE, 2008.

- [10] Sujesha Sudevalayam and Purushottam Kulkarni. Energy harvesting sensor nodes: Survey and implications. *IEEE Communications Surveys & Tutorials*, 13(3):443–461, 2011.
- [11] Aman Kansal, Jason Hsu, Sadaf Zahedi, and Mani B Srivastava. Power management in energy harvesting sensor networks. *ACM Transactions on Embedded Computing Systems (TECS)*, 6(4):32, 2007.
- [12] Bernhard Buchli, Felix Sutton, Jan Beutel, and Lothar Thiele. Dynamic power management for long-term energy neutral operation of solar energy harvesting systems. In *Proceedings of the 12th ACM Conference on Embedded Network Sensor Systems*, pages 31–45. ACM, 2014.
- [13] Trong Nhan Le, Olivier Sentieys, Olivier Berder, Alain Pegatoquet, and Cecile Belleudy. Power manager with pid controller in energy harvesting wireless sensor networks. In *Green Computing and Communications (GreenCom), 2012 IEEE International Conference on*, pages 668–670. IEEE, 2012.
- [14] Antonio Caruso, Stefano Chessa, Soledad Escolar, Xavier del Toro, and Juan Carlos López. A dynamic programming algorithm for high-level task scheduling in energy harvesting iot. *IEEE Internet of Things Journal*, 2018.
- [15] Peter Wägemann, Tobias Distler, Heiko Janker, Phillip Raffeck, Volkmar Sieh, and Wolfgang Schröder-Preikschat. Operating energy-neutral real-time systems. *ACM Transactions on Embedded Computing Systems (TECS)*, 17(1):11, 2018.
- [16] Fayaz Akhtar and Mubashir Husain Rehmani. Energy replenishment using renewable and traditional energy resources for sustainable wireless sensor networks: A review. *Renewable and Sustainable Energy Reviews*, 45:769–784, 2015.
- [17] Daler Rakhmatov, Sarma Vrudhula, and Deborah A Wallach. Battery lifetime prediction for energy-aware computing. In *Proceedings of the 2002 international symposium on Low power electronics and design*, pages 154–159. ACM, 2002.
- [18] Geoff V Merrett and Alex S Weddell. Supercapacitor leakage in energy-harvesting sensor nodes: Fact or fiction? In *Networked Sensing Systems (INSS), 2012 Ninth International Conference on*, pages 1–5. IEEE, 2012.
- [19] Farhan I Simjee and Pai H Chou. Efficient charging of supercapacitors for extended lifetime of wireless sensor nodes. *IEEE Transactions on power electronics*, 23(3):1526–1536, 2008.
- [20] Xiaofan Jiang, Joseph Polastre, and David Culler. Perpetual environmentally powered sensor networks. In *Proceedings of the 4th international symposium on Information processing in sensor networks*, page 65. IEEE Press, 2005.

- [21] Farhan Simjee and Pai H Chou. Everlast: long-life, supercapacitor-operated wireless sensor node. In *Proceedings of the 2006 international symposium on Low power electronics and design*, pages 197–202. ACM, 2006.
- [22] Ian F Akyildiz, Weilian Su, Yogesh Sankarasubramaniam, and Erdal Cayirci. Wireless sensor networks: a survey. *Computer networks*, 38(4):393–422, 2002.
- [23] Daniele Miorandi, Sabrina Sicari, Francesco De Pellegrini, and Imrich Chlamtac. Internet of things: Vision, applications and research challenges. *Ad hoc networks*, 10(7):1497–1516, 2012.
- [24] Kiwan Maeng and Brandon Lucia. Supporting peripherals in intermittent systems with just-in-time checkpoints. In *Proceedings of the 40th ACM SIGPLAN Conference on Programming Language Design and Implementation*, pages 1101–1116. ACM, 2019.
- [25] Alexei Colin, Emily Ruppel, and Brandon Lucia. A reconfigurable energy storage architecture for energy-harvesting devices. In *Proceedings of the Twenty-Third International Conference on Architectural Support for Programming Languages and Operating Systems*, pages 767–781. ACM, 2018.
- [26] Samuel Wong Chang Bing, Domenico Balsamo, and Geoff V Merrett. An energy-driven wireless bicycle trip counter with zero energy storage. In *Proceedings of the 16th ACM Conference on Embedded Networked Sensor Systems*, pages 404–405. ACM, 2018.
- [27] Samuel DeBruin, Bradford Campbell, and Prabal Dutta. Monjolo: An energy-harvesting energy meter architecture. In *Proceedings of the 11th ACM Conference on Embedded Networked Sensor Systems*, page 18. ACM, 2013.
- [28] K. Ma, X. Li, K. Swaminathan, Y. Zheng, S. Li, Y. Liu, Y. Xie, J. J. Sampson, and V. Narayanan. Nonvolatile processor architectures: Efficient, reliable progress with unstable power. *IEEE Micro*, 36(3):72–83, May 2016.
- [29] Domenico Balsamo, Alex S. Weddell, Anup Das, Alberto Rodriguez Arreola, Davide Brunelli, Bashir M. Al-Hashimi, Geoff V. Merrett, and Luca Benini. Hibernus++: A self-calibrating and adaptive system for transiently-powered embedded devices. *IEEE Transactions on Computer-Aided Design of Integrated Circuits and Systems*, 35(12):1968–1980, 2016.
- [30] Hrishikesh Jayakumar, Arnab Raha, Woo Suk Lee, and Vijay Raghunathan. Quickrecall: A HW/SW approach for computing across power cycles in transiently powered computers. *J. Emerg. Technol. Comput. Syst.*, 12(1), August 2015.
- [31] Josiah Hester, Lanny Sitanayah, and Jacob Sorber. Tragedy of the coulombs: Federating energy storage for tiny, intermittently-powered sensors. In *Proc. 13th SenSys*, page 5–16, Seoul, South Korea, 2015.

- [32] Domenico Balsamo, Benjamin J. Fletcher, Alex S. Weddell, Giorgos Karatzias, Bashir M. Al-Hashimi, and Geoff V. Merrett. Momentum: Power-neutral performance scaling with intrinsic mppt for energy harvesting computing systems. *ACM Trans. Embed. Comput. Syst.*, 17(6), January 2019.
- [33] Kiwan Maeng and Brandon Lucia. Adaptive dynamic checkpointing for safe efficient intermittent computing. In *Proc. 13th OSDI*, pages 129–144, Carlsbad, CA, October 2018.
- [34] D. Balsamo, A. S. Weddell, G. V. Merrett, B. M. Al-Hashimi, D. Brunelli, and L. Benini. Hibernus: Sustaining computation during intermittent supply for energy-harvesting systems. *IEEE Embedded Systems Letters*, 7(1):15–18, March 2015.
- [35] Andres Gomez, Lukas Sigrist, Michele Magno, Luca Benini, and Lothar Thiele. Dynamic energy burst scaling for transiently powered systems. In *2016 Design, Automation & Test in Europe Conference & Exhibition (DATE)*, pages 349–354. IEEE, 2016.
- [36] Faisal Karim Shaikh and Sherali Zeadally. Energy harvesting in wireless sensor networks: A comprehensive review. *Renewable and Sustainable Energy Reviews*, 55:1041–1054, 2016.
- [37] Scott D Moss, Owen R Payne, Genevieve A Hart, and Chandarin Ung. Scaling and power density metrics of electromagnetic vibration energy harvesting devices. *Smart Materials and Structures*, 24(2):023001, 2015.
- [38] Vijay Raghunathan, Aman Kansal, Jason Hsu, Jonathan Friedman, and Mani Srivastava. Design considerations for solar energy harvesting wireless embedded systems. In *Information Processing in Sensor Networks, 2005. IPSN 2005. Fourth International Symposium on*, pages 457–462. IEEE, 2005.
- [39] Winston KG Seah, Zhi Ang Eu, and Hwee-Pink Tan. Wireless sensor networks powered by ambient energy harvesting (wsn-heap)-survey and challenges. In *Wireless Communication, Vehicular Technology, Information Theory and Aerospace & Electronic Systems Technology, 2009. Wireless VITAE 2009. 1st International Conference on*, pages 1–5. IEEE, 2009.
- [40] Weidong Xiao, William G Dunford, and Antoine Capel. A novel modeling method for photovoltaic cells. In *Power Electronics Specialists Conference, 2004. PESC 04. 2004 IEEE 35th Annual*, volume 3, pages 1950–1956. IEEE, 2004.
- [41] Oscar López-Lapeña, Maria Teresa Penella, and Manel Gasulla. A new mppt method for low-power solar energy harvesting. *IEEE Transactions on Industrial Electronics*, 57(9):3129–3138, 2010.

- [42] Francisco Paz and Martin Ordonez. High-performance solar mppt using switching ripple identification based on a lock-in amplifier. *IEEE Transactions on Industrial Electronics*, 63(6):3595–3604, 2016.
- [43] Deepak Verma, Savita Nema, AM Shandilya, and Soubhagya K Dash. Maximum power point tracking (mppt) techniques: Recapitulation in solar photovoltaic systems. *Renewable and Sustainable Energy Reviews*, 54:1018–1034, 2016.
- [44] Shad Roundy, Dan Steingart, Luc Frechette, Paul Wright, and Jan Rabaey. Power sources for wireless sensor networks. In *European workshop on wireless sensor networks*, pages 1–17. Springer, 2004.
- [45] Cian O Mathuna, Terence O’Donnell, Rafael V Martinez-Catala, James Rohan, and Brendan O’Flynn. Energy scavenging for long-term deployable wireless sensor networks. *Talanta*, 75(3):613–623, 2008.
- [46] Detlev Heinemann, Elke Lorenz, and Marco Girodo. Forecasting of solar radiation. *Solar energy resource management for electricity generation from local level to global scale*. Nova Science Publishers, New York, 2006.
- [47] National solar radiation database data viewer. <https://maps.nrel.gov/nsrdb-viewer/>.
- [48] Solrmap loyola marymount university (rsr). <http://midcdmz.nrel.gov/apps/daily.pl?site=LMU&start=20100406&yr=2016&mo=05&dy=05>.
- [49] Peter Corke, Philip Valencia, Pavan Sikka, Tim Wark, and Les Overs. Long-duration solar-powered wireless sensor networks. In *Proceedings of the 4th workshop on Embedded networked sensors*, pages 33–37. ACM, 2007.
- [50] Aaron N Parks, Alanson P Sample, Yi Zhao, and Joshua R Smith. A wireless sensing platform utilizing ambient rf energy. In *Power Amplifiers for Wireless and Radio Applications (PAWR), 2013 IEEE Topical Conference on*, pages 160–162. IEEE, 2013.
- [51] Alanson P Sample, Daniel J Yeager, Pauline S Powledge, Alexander V Mamishev, and Joshua R Smith. Design of an rfid-based battery-free programmable sensing platform. *IEEE transactions on instrumentation and measurement*, 57(11):2608–2615, 2008.
- [52] Saman Naderiparizi, Aaron N Parks, Zerina Kapetanovic, Benjamin Ransford, and Joshua R Smith. Wispcam: A battery-free rfid camera. In *RFID (RFID), 2015 IEEE International Conference on*, pages 166–173. IEEE, 2015.
- [53] Domenico Balsamo, Anup Das, Alex S Weddell, Davide Brunelli, Bashir M Al-Hashimi, Geoff V Merrett, and Luca Benini. Graceful performance modulation

- for power-neutral transient computing systems. *IEEE Transactions on Computer-Aided Design of Integrated Circuits and Systems*, 35(5):738–749, 2016.
- [54] Navin Sharma, Jeremy Gummesson, David Irwin, and Prashant Shenoy. Cloudy computing: Leveraging weather forecasts in energy harvesting sensor systems. In *Sensor Mesh and Ad Hoc Communications and Networks (SECON), 2010 7th Annual IEEE Communications Society Conference on*, pages 1–9. IEEE, 2010.
- [55] Alessandro Cammarano, Chiara Petrioli, and Dora Spenza. Pro-energy: A novel energy prediction model for solar and wind energy-harvesting wireless sensor networks. In *Mobile Adhoc and Sensor Systems (MASS), 2012 IEEE 9th International Conference on*, pages 75–83. IEEE, 2012.
- [56] Raul Morais, Samuel G Matos, Miguel A Fernandes, António LG Valente, Salvariano FSP Soares, PJSG Ferreira, and MJCS Reis. Sun, wind and water flow as energy supply for small stationary data acquisition platforms. *Computers and electronics in agriculture*, 64(2):120–132, 2008.
- [57] Jay Taneja, Jaein Jeong, and David Culler. Design, modeling, and capacity planning for micro-solar power sensor networks. In *Proceedings of the 7th international conference on Information processing in sensor networks*, pages 407–418. IEEE Computer Society, 2008.
- [58] Michal Prauzek, Jaromir Konecny, Monika Borova, Karolina Janosova, Jakub Hlavica, and Petr Musilek. Energy harvesting sources, storage devices and system topologies for environmental wireless sensor networks: A review. *Sensors*, 18(8):2446, 2018.
- [59] Paulo R Bueno. Nanoscale origins of super-capacitance phenomena. *Journal of Power Sources*, 414:420–434, 2019.
- [60] Jiří Libich, Josef Máca, Jiří Vondrák, Ondřej Čech, and Marie Sedlaříková. Supercapacitors: Properties and applications. *Journal of Energy Storage*, 17:224–227, 2018.
- [61] Christian Renner, Jürgen Jessen, and Volker Turau. Lifetime prediction for supercapacitor-powered wireless sensor nodes. *Proceedings of FGSN*, pages 1–6, 2009.
- [62] Chulsung Park and Pai H Chou. Ambimax: Autonomous energy harvesting platform for multi-supply wireless sensor nodes. In *2006 3rd annual IEEE communications society on sensor and ad hoc communications and networks*, volume 1, pages 168–177. IEEE, 2006.
- [63] Geoff V Merrett and Bashir M Al-Hashimi. Energy-driven computing: Rethinking the design of energy harvesting systems. In *Proceedings of the Conference on*

- Design, Automation & Test in Europe*, pages 960–965. European Design and Automation Association, 2017.
- [64] Soledad Escolar, Stefano Chessa, and Jesús Carretero. Energy-neutral networked wireless sensors. *Simulation Modelling Practice and Theory*, 43:1–15, 2014.
- [65] Christopher M Vigorito, Deepak Ganesan, and Andrew G Barto. Adaptive control of duty cycling in energy-harvesting wireless sensor networks. In *Sensor, Mesh and Ad Hoc Communications and Networks, 2007. SECON'07. 4th Annual IEEE Communications Society Conference on*, pages 21–30. IEEE, 2007.
- [66] Joaquin Recas Piorno, Carlo Bergonzini, David Atienza, and Tajana Simunic Rosing. Prediction and management in energy harvested wireless sensor nodes. In *Wireless Communication, Vehicular Technology, Information Theory and Aerospace & Electronic Systems Technology, 2009. Wireless VITAE 2009. 1st International Conference on*, pages 6–10. IEEE, 2009.
- [67] Matthew J Walker, Stephan Diestelhorst, Andreas Hansson, Domenico Balsamo, Geoff V Merrett, and Bashir M Al-Hashimi. Thermally-aware composite run-time cpu power models. In *Power and Timing Modeling, Optimization and Simulation (PATMOS), 2016 26th International Workshop on*, pages 17–24. IEEE, 2016.
- [68] Benjamin Ransford, Jacob Sorber, and Kevin Fu. Mementos: System support for long-running computation on rfid-scale devices. *Acm Sigplan Notices*, 47(4):159–170, 2012.
- [69] Sivert T Sliper, Domenico Balsamo, Alex S Weddell, and Geoff V Merrett. Enabling intermittent computing on high-performance out-of-order processors. In *Proceedings of the 6th International Workshop on Energy Harvesting & Energy-Neutral Sensing Systems*, pages 19–25. ACM, 2018.
- [70] Naveed Anwar Bhatti and Luca Mottola. Harvos: Efficient code instrumentation for transiently-powered embedded sensing. In *Proceedings of the 16th ACM/IEEE International Conference on Information Processing in Sensor Networks*, pages 209–219. ACM, 2017.
- [71] Kiwan Maeng and Brandon Lucia. Adaptive dynamic checkpointing for safe efficient intermittent computing. In *13th {USENIX} Symposium on Operating Systems Design and Implementation ({OSDI} 18)*, pages 129–144, 2018.
- [72] Brandon Lucia and Benjamin Ransford. A simpler, safer programming and execution model for intermittent systems. In *Proceedings of the 36th ACM SIGPLAN Conference on Programming Language Design and Implementation, PLDI '15*, pages 575–585, New York, NY, USA, 2015. ACM.

- [73] Hrishikesh Jayakumar, Arnab Raha, and Vijay Raghunathan. Quickrecall: A low overhead hw/sw approach for enabling computations across power cycles in transiently powered computers. In *2014 27th International Conference on VLSI Design and 2014 13th International Conference on Embedded Systems*, pages 330–335. IEEE, 2014.
- [74] Alberto Rodriguez Arreola, Domenico Balsamo, Anup K Das, Alex S Weddell, Davide Brunelli, Bashir M Al-Hashimi, and Geoff V Merrett. Approaches to transient computing for energy harvesting systems: A quantitative evaluation. In *Proceedings of the 3rd International Workshop on Energy Harvesting & Energy Neutral Sensing Systems*, pages 3–8. ACM, 2015.
- [75] Josiah David Hester and Jacob Sorber. New directions: The future of sensing is batteryless, intermittent, and awesome. In *15th ACM Conference on Embedded Networked Sensor Systems (SenSys’ 17)*, 2017.
- [76] Alexei Colin and Brandon Lucia. Chain: tasks and channels for reliable intermittent programs. *ACM SIGPLAN Notices*, 51(10):514–530, 2016.
- [77] Kiwan Maeng, Alexei Colin, and Brandon Lucia. Alpaca: Intermittent execution without checkpoints. *Proc. ACM Program. Lang.*, 1(OOPSLA), October 2017.
- [78] Alexei Colin and Brandon Lucia. Termination checking and task decomposition for task-based intermittent programs. In *Proceedings of the 27th International Conference on Compiler Construction*, pages 116–127. ACM, 2018.
- [79] Yongpan Liu, Zewei Li, Hehe Li, Yiqun Wang, Xueqing Li, Kaisheng Ma, Shuangchen Li, Meng-Fan Chang, Sampson John, Yuan Xie, et al. Ambient energy harvesting nonvolatile processors: from circuit to system. In *Proceedings of the 52nd Annual Design Automation Conference*, page 150. ACM, 2015.
- [80] Yiqun Wang, Yongpan Liu, Shuangchen Li, Daming Zhang, Bo Zhao, Mei-Fang Chiang, Yanxin Yan, Baiko Sai, and Huazhong Yang. A 3 $\mu$ s wake-up time non-volatile processor based on ferroelectric flip-flops. In *ESSCIRC (ESSCIRC), 2012 Proceedings of the*, pages 149–152. IEEE, 2012.
- [81] Fang Su, Yongpan Liu, Yiqun Wang, and Huazhong Yang. A ferroelectric non-volatile processor with 46 $\mu$ s system-level wake-up time and 14 $\mu$ s sleep time for energy harvesting applications. *IEEE Transactions on Circuits and Systems I: Regular Papers*, 64(3):596–607, 2017.
- [82] Yongpan Liu, Fang Su, Yixiong Yang, Zhibo Wang, Yiqun Wang, Zewei Li, Xueqing Li, Ryuji Yoshimura, Takashi Naiki, Takashi Tsuwa, et al. A 130-nm ferroelectric nonvolatile system-on-chip with direct peripheral restore architecture for transient computing system. *IEEE Journal of Solid-State Circuits*, 2019.



- [83] Kaisheng Ma, Yang Zheng, Shuangchen Li, Karthik Swaminathan, Xueqing Li, Yongpan Liu, Jack Sampson, Yuan Xie, and Vijaykrishnan Narayanan. Architecture exploration for ambient energy harvesting nonvolatile processors. In *High Performance Computer Architecture (HPCA), 2015 IEEE 21st International Symposium on*, pages 526–537. IEEE, 2015.
- [84] Kaisheng Ma, Xueqing Li, Jinyang Li, Yongpan Liu, Yuan Xie, Jack Sampson, Mahmut Taylan Kandemir, and Vijaykrishnan Narayanan. Incidental computing on iot nonvolatile processors. In *Proceedings of the 50th Annual IEEE/ACM International Symposium on Microarchitecture*, pages 204–218. ACM, 2017.
- [85] Kaisheng Ma, Xueqing Li, Karthik Swaminathan, Yang Zheng, Shuangchen Li, Yongpan Liu, Yuan Xie, John Jack Sampson, and Vijaykrishnan Narayanan. Non-volatile processor architectures: Efficient, reliable progress with unstable power. *IEEE Micro*, 36(3):72–83, 2016.
- [86] Fang Su, Kaisheng Ma, Xueqing Li, Tongda Wu, Yongpan Liu, and Vijaykrishnan Narayanan. Nonvolatile processors: Why is it trending? In *2017 Design, Automation & Test in Europe Conference & Exhibition (DATE)*, pages 966–971. IEEE, 2017.
- [87] Benjamin J Fletcher, Domenico Balsamo, and Geoff V Merrett. Power neutral performance scaling for energy harvesting mp-socs. In *Proceedings of the Conference on Design, Automation & Test in Europe*, pages 1520–1525. European Design and Automation Association, 2017.
- [88] Yiqun Wang, Yongpan Liu, Cong Wang, Zewei Li, Xiao Sheng, Hyung Gyu Lee, Naehyuck Chang, and Huazhong Yang. Storage-less and converter-less photovoltaic energy harvesting with maximum power point tracking for internet of things. *IEEE Transactions on Computer-Aided Design of Integrated Circuits and Systems*, 35(2):173–186, 2016.
- [89] Yung-Hsiang Lu, Luca Benini, and Giovanni De Micheli. Low-power task scheduling for multiple devices. In *Hardware/Software Codesign, 2000. CODES 2000. Proceedings of the Eighth International Workshop on*, pages 39–43. IEEE, 2000.
- [90] D. Balsamo, A. Das, A. S. Weddell, D. Brunelli, B. M. Al-Hashimi, G. V. Merrett, and L. Benini. Graceful performance modulation for power-neutral transient computing systems. *IEEE Transactions on Computer-Aided Design of Integrated Circuits and Systems*, 35(5):738–749, May 2016.
- [91] Radovan Faltus. Low leakage current aspect of designing with tantalum and niobium oxide capacitors. Technical report, AVX, 2012.
- [92] Alberto Rodriguez Arreola, Domenico Balsamo, Geoff V. Merrett, and Alex S. Weddell. Restop: Retaining external peripheral state in intermittently-powered sensor systems. *Sensors*, 18(1), 2018.

- [93] Kiwan Maeng and Brandon Lucia. Supporting peripherals in intermittent systems with just-in-time checkpoints. In *Proc. 40th PLDI*, pages 1101–1116, Phoenix, AZ, USA, 2019.
- [94] Sivert T. Sliper, Domenico Balsamo, Nikos Nikoleris, William Wang, Alex S. Weddell, and Geoff V. Merrett. Efficient state retention through paged memory management for reactive transient computing. In *Proc. 56th DAC*, pages 26:1–26:6, June 2019.
- [95] Achraf Ben Amar, Ammar B. Kouki, and Hung Cao. Power approaches for implantable medical devices. *Sensors*, 15(11):28889–28914, 2015.
- [96] Fang Su, Yongpan Liu, Xiao Sheng, Hyung Gyu Lee, Naehyuck Chang, and Huazhong Yang. A task failure rate aware dual-channel solar power system for nonvolatile sensor nodes. *ACM Trans. Embed. Comput. Syst.*, 18(4), July 2019.
- [97] Neal Jackson, Joshua Adkins, and Prabal Dutta. Capacity over capacitance for reliable energy harvesting sensors. In *Proceedings of the 18th International Conference on Information Processing in Sensor Networks, IPSN '19*, pages 193–204, New York, NY, USA, 2019. ACM.
- [98] Yizi Gu, Y. Liu, Y. Wang, H. Li, and H. Yang. NVPsim: A simulator for architecture explorations of nonvolatile processors. In *Proc. 21st ASP-DAC*, pages 147–152, January 2016.
- [99] Sivert T Sliper, William Wang, Nikos Nikoleris, Alexander Weddell, and Geoff Merrett. Fused: closed-loop performance and energy simulation of embedded systems. In *Proc. ISPASS*, Boston, MA, USA, 2020.
- [100] J. San Miguel, K. Ganesan, M. Badr, C. Xia, R. Li, H. Hsiao, and N. Enright Jerger. The EH model: Early design space exploration of intermittent processor architectures. In *Proc. 51st IEEE/ACM MICRO*, pages 600–612, Fukuoka, Japan, Oct 2018.
- [101] Josiah Hester, Timothy Scott, and Jacob Sorber. Ekho: Realistic and repeatable experimentation for tiny energy-harvesting sensors. In *Proc. 12th SenSys*, page 1–15, Memphis, Tennessee, 2014.
- [102] Kai Geissdoerfer, Mikołaj Chwalisz, and Marco Zimmerling. Shepherd: A portable testbed for the batteryless iot. In *Proc. 17th SenSys*, page 83–95, New York, NY, USA, 2019.
- [103] A Andreas and T Stoffel. Nrel solar radiation research laboratory (srsl): Baseline measurement system (bms); golden, colorado (data). *NREL Report NO.DA-5500-56488*, 1981.

- [104] M. Gorlatova, A. Wallwater, and G. Zussman. Networking low-power energy harvesting devices: Measurements and algorithms. *IEEE Trans. Mobile Comput.*, 12(9):1853–1865, September 2013.
- [105] Silvano Vergura. A complete and simplified datasheet-based model of pv cells in variable environmental conditions for circuit simulation. *Energies*, 9(5), 2016.
- [106] Panasonic. Amorphous silicon solar cells. [https://www.panasonic-electric-works.com/cps/rde/xbcr/pew\\_eu\\_en/ca\\_amorton\\_solar\\_cells\\_2018\\_en.pdf](https://www.panasonic-electric-works.com/cps/rde/xbcr/pew_eu_en/ca_amorton_solar_cells_2018_en.pdf). Last accessed: 23 June, 2019.
- [107] Evangelos Triantaphyllou. *Multi-criteria decision making methods: A comparative study*. Springer, 2000.
- [108] Gautier Berthou, Pierre-Évariste Dagand, Delphine Demange, Rémi Oudin, and Tanguy Risset. Intermittent computing with peripherals, formally verified. In *The 21st ACM SIGPLAN/SIGBED Conference on Languages, Compilers, and Tools for Embedded Systems, LCTES '20*, page 85–96, New York, NY, USA, 2020. Association for Computing Machinery.
- [109] Chen Pan, Mimi Xie, and Jingtong Hu. Maximize energy utilization for ultra-low energy harvesting powered embedded systems. In *2017 IEEE 23rd International Conference on Embedded and Real-Time Computing Systems and Applications (RTCSA)*, pages 1–6, 2017.
- [110] Chetan Kulkarni, Gautam Biswas, Xenofon Koutsoukos, Jose Celaya, and Kai Goebel. Experimental studies of ageing in electrolytic capacitors. Technical report, VANDERBILT UNIV NASHVILLE TN DEPT OF ELECTRICAL ENGINEERING AND COMPUTER SCIENCE, 2010.
- [111] Vishay. *Aluminum Electrolytic Capacitors Radial Low Leakage Current*, 2016.
- [112] Chih-Kai Kang, Chun-Han Lin, Pi-Cheng Hsiu, and Ming-Syan Chen. Homerun: Hw/sw co-design for program atomicity on self-powered intermittent systems. In *Proceedings of the International Symposium on Low Power Electronics and Design, ISLPED '18*, New York, NY, USA, 2018. Association for Computing Machinery.
- [113] Jasper de Winkel, Carlo Delle Donne, Kasim Sinan Yildirim, Przemysław Pawełczak, and Josiah Hester. Reliable timekeeping for intermittent computing. In *Proceedings of the Twenty-Fifth International Conference on Architectural Support for Programming Languages and Operating Systems, ASPLOS '20*, page 53–67, New York, NY, USA, 2020. Association for Computing Machinery.
- [114] Vishal Deep, Vishak Narayanan, Mathew Wymore, Daji Qiao, and Henry Duwe. Harc: A heterogeneous array of redundant persistent clocks for batteryless, intermittently-powered systems. In *2020 IEEE Real-Time Systems Symposium (RTSS)*, pages 270–282, 2020.

- [115] Josiah Hester, Nicole Tobias, Amir Rahmati, Lanny Sitanayah, Daniel Holcomb, Kevin Fu, Wayne P. Burleson, and Jacob Sorber. Persistent clocks for batteryless sensing devices. *ACM Trans. Embed. Comput. Syst.*, 15(4), aug 2016.
- [116] Philip Sparks. The route to a trillion devices. Technical report, ARM Ltd., 2017.